(2)

DOT/FAA/CT-86/25 -I

FAA TECHNICAL CENTER
Atlantic City Airport
N.J. 08405

Computer Simulation of a Transport Aircraft Seat and Occupant(s) in a Crash Environment Volume 1 - Technical Report

Akif O. Bolukbasi
David H. Laananen

FINAL REPORT

August 1986

U.S. Department of Transportation
Federal Aviation Administration

NOTICE

This document is disseminated under the sponsorship of the Department of Transportation in the interest of information exchange. The United States Government assumes no liability for the contents or use thereof.

The United States Government does not endorse products or manufacturers. Trade or manufacturer's names appear herein solely because they are considered essential to the object of this report.

Technical Report Document Page

1. Report No.	2. Government Accession No.	3. Recipient's Catalog No.
DOT/FAA/CT-86/25-I	ADA175953	

4. Title and Subtitle	5. Report Date
COMPUTER SIMULATION OF A TRANSPORT AIRCRAFT SEAT AND OCCUPANT(S) IN A CRASH ENVIRONMENT, VOLUME I - TECHNICAL REPORT	August 1986
	6. Performing Organization Code
	8. Performing Organization Report No. TR-84430
7. Author(s) A. O. Bolukbasi and D. H. Laananen	10. Work Unit No. (TRAIS)
9. Performing Organization Name and Address Simula Inc. 10016 S. 51st Street Phoenix, AZ 85044	11. Contract or Grant No. DTFA03-83-00036
	13. Type of Report and Period Covered FINAL REPORT June 1983 - March 1986
12. Sponsoring Agency Name and Address Federal Aviation Administration Technical Center Atlantic City Airport, NJ 08405	14. Sponsoring Agency Code ACT-330

15. Supplementary Notes

FAA Technical Monitor - L. M. Neri, ACT-330

16. Abstract

A mathematical model of a transport aircraft seat, occupants, and restraint system has been developed for use in analysis of transport aircraft crashworthiness. Because of the significant role played by the seat in overall system crashworthiness, a finite element model of the seat structure is included. The seat model can accommodate large plastic deformations and includes the capability for simulation of local buckling of bending members. Because the program has been written for use primarily by engineers concerned with the design and analysis of seat and restraint systems, an effort has been made to minimize the input data required to describe the occupant. This report is Volume I of a two-volume document. Volume I discusses development of the mathematical model of the occupants, the finite element seat analysis, validation, and organization of the computer program. Volume II contains instructions for preparing input data and operating the program.

17. Key Words	18. Distribution Statement
Aircraft Computer Simulation Crashworthiness Restraint Systems Seats	Document is available to the U.S. public through the National Technical Information Service, Springfield, Virginia 22161.

19. Security Classif. (of this report)	20. Security Classif. (of this page)	21. No. of Pages	22. Price
Unclassified	Unclassified	136	

Form DOT F 1700.7 (8-72)

FOREWORD

This report was prepared by Simula Inc. under Contract No. DTFA03-83-C-00036 with the Federal Aviation Administration (FAA) Technical Center, where L. M. Neri acted as Technical Monitor. Under the same contract, computer simulation program SOM-TA (Seat/Occupant Simulation Model for Transport Aircraft) was developed.

The Simula Inc. Project Engineer was Mr. Akif O. Bolukbasi. Dr. David H. Laananen of Arizona State University provided consulting services during the development and validation of program SOM-TA, and the preparation of this report. Data for model validation were provided by the Protection and Survival Laboratory of the FAA Civil Aeromedical Institute, where the tests were conducted under the leadership of Mr. R. F. Chandler.

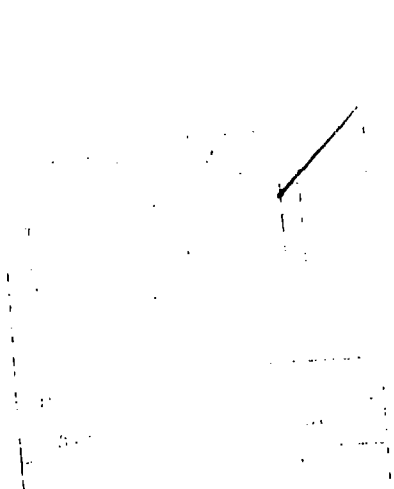

TABLE OF CONTENTS

TABLE OF CONTENTS (CONTD)

TABLE OF CONTENTS (CONTD)

LIST OF ILLUSTRATIONS

LIST OF ILLUSTRATIONS (CONTD)

LIST OF ILLUSTRATIONS (CONTD)

LIST OF TABLES

EXECUTIVE SUMMARY

Program SOM-TA (Seat/Occupant Model - Transport Aircraft) has been developed for use in evaluating the crashworthiness of transport aircraft seats and restraint systems. It combines a three-dimensional dynamic model of the human body with a finite element model of the seat structure. The program allows simulation of one, two, or three passengers of the same or different sizes. It is intended to provide the design engineer a tool with which he can analyze the structural elements of the seat as well as evaluate the dynamic response of the passengers during a crash.

The program is documented in two volumes. Volume I discusses development of the seat and occupant models, validation, and organization of the computer program. Volume II contains instructions for preparing input data and operating the program.

The occupant model consists of 12 masses that represent the upper and lower torso, neck, head, and two segments for each of the arms and legs. An optional model of the human body includes beam elements in the spine and neck, but is restricted to two-dimensional motion.

External forces are applied to the occupant by the cushions, floor, and restraint system. Interface between the occupant and seat is provided by the seat bottom cushion, back cushion, and an optional headrest. Contact between the occupant(s) and the back of the seat row in front can also be simulated. The restraint system can consist of a lap belt alone or combined with a single shoulder belt, over either shoulder, or a double-strap shoulder harness. Each component of the restraint system can be attached to either the seat or the aircraft structure.

The seat structure is modeled using the finite element method of analysis, selected because it is not dependent on previous testing, and it has the flexibility to deal with a wide range of design concepts. The SOM-TA seat analysis uses three-dimensional beam elements. It has the capability to model large displacements, nonlinear material behavior, local buckling, and various end release conditions for beam elements.

The digital computer program based on the occupant and seat models described above has been written entirely in FORTRAN to ensure a high degree of compatibility with various computer systems. During development, the program has been run on IBM and Digital computer systems. Output data include occupant segment positions, velocities, and accelerations; restraint system and cushion forces; injury criteria; and details of contact between the occupant and the seat in front. Seat output includes nodal displacements, element stresses, and forces at the points of attachment to the aircraft structure.

Dynamic tests of transport seats conducted by the Federal Aviation Administration Civil Aeromedical Institute in 1983 were used in validation of Program SOM-TA. Three production seat designs and various modifications to the production design were tested. The design that was chosen for validation utilized a production seat modified by incorporating energy-absorption capability in the longitudinal direction. This seat produced more interesting results for validation than others because it underwent large deformations while maintaining structural integrity in the dynamic test.

1.0 INTRODUCTION

The design of crashworthy seats and restraint systems for transport aircraft presents a complex engineering problem, the solution of which can be greatly aided by sufficiently rigorous analytical techniques. The crash environment can vary widely from one accident to another, so a great number of conditions must be evaluated to establish those critical to occupant survival. A crashworthy seat should include the capacity to absorb energy through controlled deformation, thus reducing the accompanying loads (reference 1).

In the initial design phases, it is desirable to evaluate, in some detail, existing seats and restraint systems in their surroundings, thus establishing existing weaknesses. It is then desirable to make modifications and to evaluate the effect of these modifications on improving the performance of the system. These evaluations must be conducted for a great many of the possible crash environments, thus constituting a relatively large matrix. Testing is costly and is often time consuming since design modifications must be developed and fabricated prior to testing. Therefore, an analytical technique, such as this effort, is cost effective.

A number of one-, two-, and three-dimensional mathematical models of the human body have been developed for crash survivability analysis. These models vary in complexity and possess from one to forty degrees-of-freedom. The simplest models have been developed primarily for prediction of injury to a single component or subsystem of the body, such as vertebral injury due to the vertical force that might be experienced in a crash or the firing of an ejection seat. Simulation of the three-dimensional response of the entire body requires many more degrees-of-freedom, but permits more general use. Most of the three-dimensional models have been developed for use in evaluation of automobile interior designs with respect to injuries caused by secondary impacts, such as the three-dimensional models described in references 2 through 5. Seats have been represented in a very simple manner because in automobiles the role of the seat design in determining occupant survival is minimal. Therefore, a simulation model intended specifically for the aircraft application is desired.

The development of a three-dimensional mathematical model of a transport aircraft seat, including passengers, and restraint system is described in this report. This model forms the basis for a simulation computer program that has been written specifically for use in crashworthy design and analysis of transport aircraft seats and restraint systems, Program SOM-TA. The program, which combines a finite element model of the seat structure with lumped-parameter models of the aircraft passengers, has been organized so as to minimize the volume and complexity of input data and to focus on seat and restraint system design parameters.

Program SOM-TA seat and occupant models are based on those presently used in Program SOM-LA (Seat/Occupant Model - Light Aircraft), (reference 6). The program was modified to allow simulation of one, two, or three passengers of the same or different sizes. The capacity of the seat model has been increased to accommodate the more complex transport seat structures. The seat model has also been modified to simulate floor-warping conditions.

In this report, the details of the occupant and seat models are presented, along with the results of model validation. Operation of the computer program is described in Volume II, Program SOM-TA User Manual.

2.0 OCCUPANT MODEL

The SOM-TA mathematical model includes a lumped-parameter representation of the aircraft occupant(s) and a finite element characterization of the seat. Interface between the seat and its occupant is provided by seat cushions and a restraint system, which consists of a lap belt and, if desired, a single-strap or double-strap shoulder harness. The response of the occupant(s) and seat can be predicted for any given set of aircraft impact conditions, including the initial velocity, attitude and the input acceleration.

As mentioned previously, both a three-dimensional occupant model consisting of rigid links and a two-dimensional model with deformable spinal elements are included. This chapter provides a discussion of the development of both occupant models, including details of the approach used to formulate the equations of motion and the techniques used for their solution. Section 2.1 presents the three-dimensional model and section 2.2, the two-dimensional model. Subsequent sections cover aspects of the equations which apply to both models, specifically the body joint model, the treatment of external forces, and body dimensions and properties.

2.1 THREE-DIMENSIONAL OCCUPANT MODEL

The three-dimensional mathematical model of the aircraft occupant is made up of twelve rigid segments, as shown in figure 1. This number is thought to represent the minimum segments that will permit accurate, meaningful simulation a of three-dimensional response. A greater number of segments might possibly improve the accuracy of simulation but would, in turn, also increase program execution cost. Arm and leg segments are included to enable prediction of injuries to these extremities. Although leg and arm injuries, in themselves, may not be as serious as head or chest injuries, they may prevent egress from a stricken aircraft and increase the potential hazard to the occupants of a postcrash fire.

Each of the body joints, with the exception of the elbow, knee, and head-neck joints, possesses three rotational degrees of freedom. Because of the hinge-type motion of a forearm or lower leg relative to an upper arm or thigh, the position of each of these segments is described by one additional angular

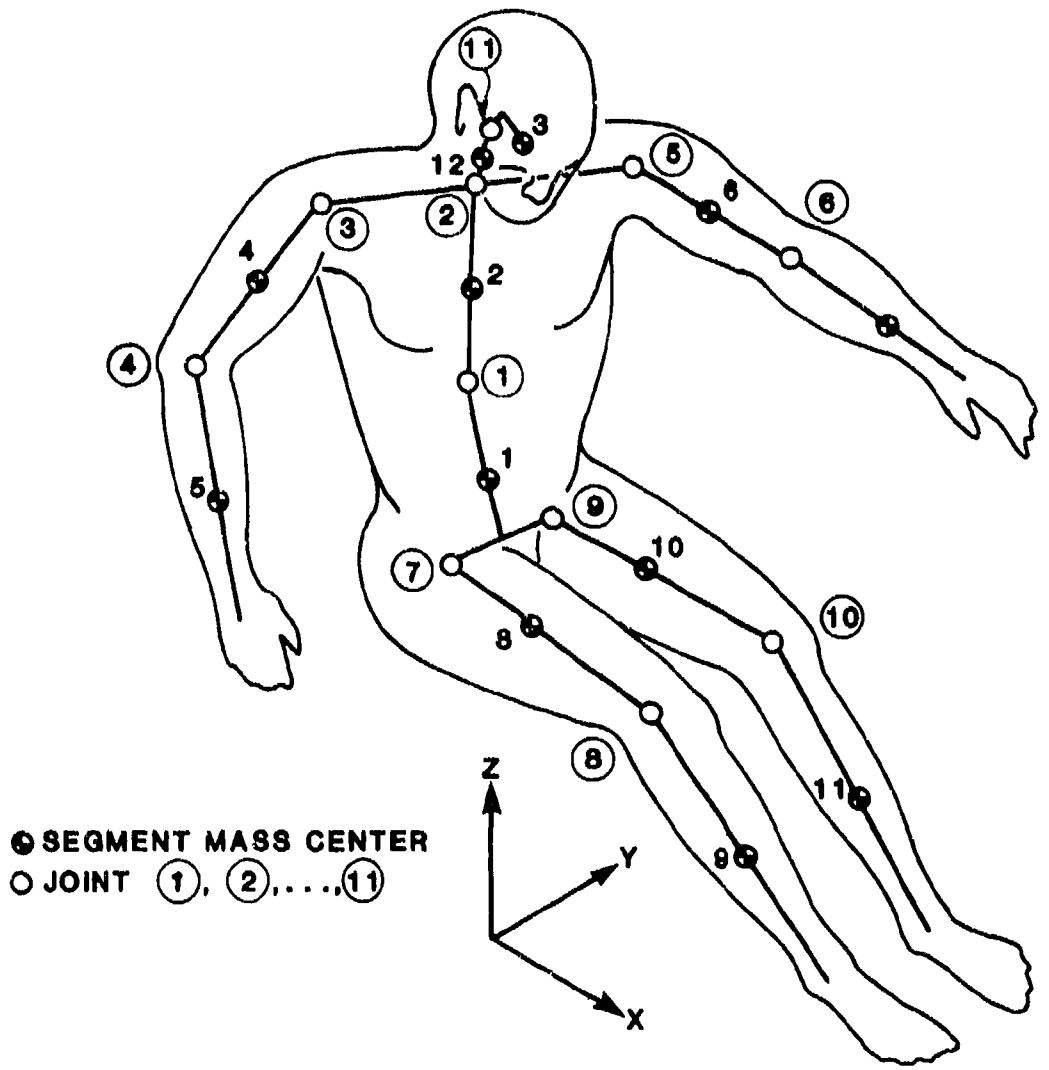

Figure 1. Twelve-segment (three-dimensional) occupant model.

coordinate, as also is the position of the head relative to the neck. Therefore, the occupant system possesses a total of 29 degrees-of-freedom.

2.1.1 Coordinate Systems

Fixed at the center of mass of each of the 12 segments is a right-handed Cartesian coordinate system. For segment n (n = 1, 2,..., 12) the local coordinate system is denoted by axes (x_n, y_n, z_n). Positive directions are defined such that when the body is seated as shown in figure 2, with the torso and head

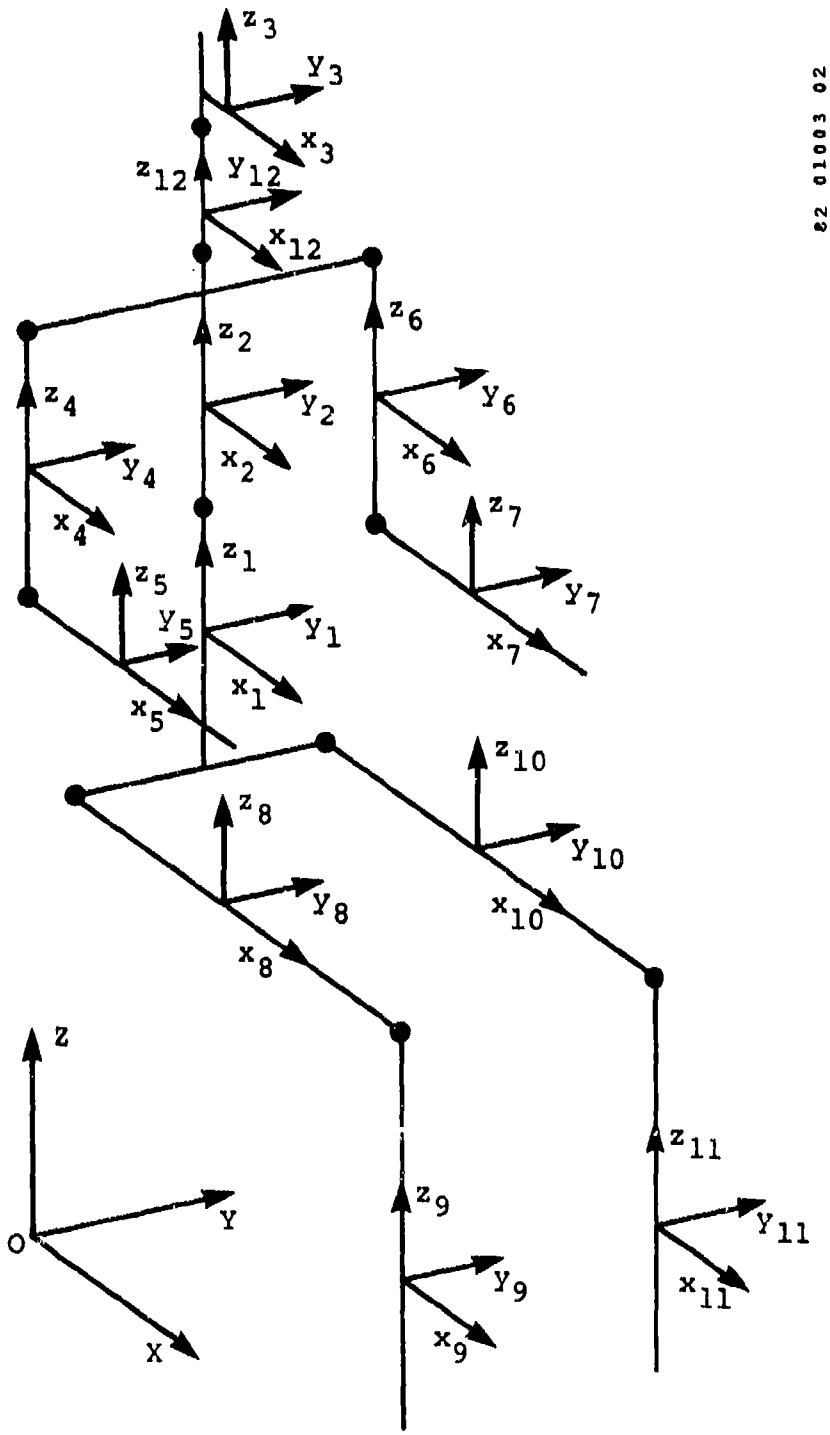

Figure 2. Segment-fixed local coordinate systems.

upright, the upper arms parallel to the torso, and the elbows and knees bent at right angles, positive x_n is directed forward, y_n to the left, and z_n upward.

In order to describe a general position of the body, it is necessary to relate the orientation of each segment (x_n, y_n, z_n) to the inertial system (X, Y, Z). The angular relationship between the local, segment-fixed coordinates and the inertial system can be expressed by the transformation

$$\begin{Bmatrix} X_n \\ Y_n \\ Z_n \end{Bmatrix} = \begin{bmatrix} T^n \end{bmatrix} \begin{Bmatrix} x_n \\ y_n \\ z_n \end{Bmatrix} \qquad (1)$$

Because three angular coordinates can be used to define the rotation of a given segment, it is convenient to utilize a set of coordinates that will suffice as generalized coordinates in the formulation of the equations of motion. A system of Eulerian angles provides a convenient set of three independent angular coordinates. Assuming that the local (x_n, y_n, z_n) system is initially coincident with the inertial (X, Y, Z) system, the Euler angles are a series of three rotations, which, when performed in the proper sequence, permit the system to attain any orientation and uniquely define that position. The particular set of Euler angles selected for use here is illustrated in figure 3 and defined as follows:

1. A positive rotation ψ about the Z-axis, resulting in the primed (x', y', z') system.

2. A positive rotation θ about the y'-axis resulting in the double-primed (x", y", z") system.

3. A positive rotation ϕ about the x"-axis resulting in the final (x, y, z) system.

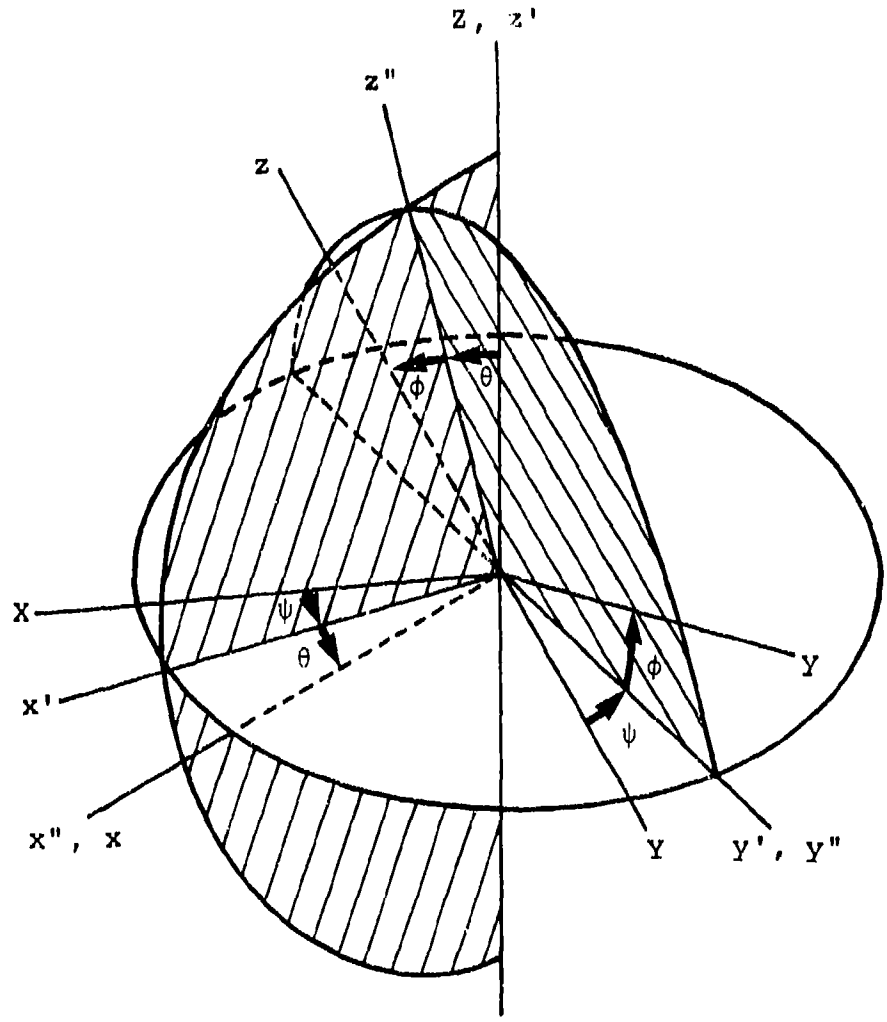

Figure 3. The Euler angles.

In order to determine the elements of the transformation matrix $[T^n]$, it is necessary to consider the matrix equations that indicate the three individual rotations previously described above. Referring again to these definitions of ψ, θ, and ϕ, the following equations are obtained:

$$\begin{Bmatrix} X \\ Y \\ Z \end{Bmatrix} = \begin{bmatrix} \cos\psi & -\sin\psi & 0 \\ \sin\psi & \cos\psi & 0 \\ 0 & 0 & 1 \end{bmatrix} \begin{Bmatrix} x' \\ y' \\ z' \end{Bmatrix} \tag{2}$$

$$\begin{Bmatrix} x' \\ y' \\ z' \end{Bmatrix} = \begin{bmatrix} \cos\theta & 0 & \sin\theta \\ 0 & 1 & 0 \\ -\sin\theta & 0 & \cos\theta \end{bmatrix} \begin{Bmatrix} x'' \\ y'' \\ z'' \end{Bmatrix} \tag{3}$$

$$\begin{Bmatrix} x'' \\ y'' \\ z'' \end{Bmatrix} = \begin{bmatrix} 1 & 0 & 0 \\ 0 & \cos\phi & -\sin\phi \\ 0 & \sin\phi & \cos\phi \end{bmatrix} \begin{Bmatrix} x \\ y \\ z \end{Bmatrix} \tag{4}$$

Writing equations (2) through (4) in abbreviated form

$$\{R\} = [\psi]\ \{r'\}$$

$$\{r'\} = [\theta]\ \{r''\}$$

$$\{r''\} = [\phi]\ \{r\}$$

or

$$\{R\} = [\psi]\ [\theta]\ [\phi]\ \{r\} \tag{5}$$

where $\{R\}$ represents the components of a vector in the inertial system and $\{r\}$ represents the same vector in the final (x, y, z) system. Performing the matrix multiplications indicated in equation (5), the elements of the transformation matrix in equation (1) are obtained:

$$T_{11}^{n} = \cos\psi_n \cos\theta_n$$

$$T_{12}^{n} = \cos\psi_n \sin\theta_n \sin\phi_n - \sin\psi_n \cos\phi_n$$

$$T_{13}^{n} = \cos\psi_n \sin\theta_n \cos\phi_n + \sin\psi_n \sin\phi_n$$

$$T_{21}^{n} = \sin\psi_n \cos\theta_n$$

$$T_{22}^{n} = \sin\psi_n \sin\theta_n \sin\phi_n + \cos\psi_n \cos\phi_n$$

$$T_{23}^{n} = \sin\psi_n \sin\theta_n \cos\phi_n - \cos\psi_n \sin\phi_n$$

$$T_{31}^{n} = -\sin\theta_n$$

$$T_{32}^{n} = \cos\theta_n \sin\phi_n$$

$$T_{33}^{n} = \cos\theta_n \cos\phi_n$$

for n = 1, 2, 3, 4, 6, 8, 10 (6)

The constraint of hinge-type rotation, at the elbows and knees, requires the use of one additional angular coordinate to define the position of each of the forearm and lower leg segments. Referring to figure 4, the angular position of the forearm segments (ℓ = 5, 7) is given by

$$\begin{Bmatrix} X_\ell \\ Y_\ell \\ Z_\ell \end{Bmatrix} = \begin{bmatrix} \\ T^n \\ \\ \end{bmatrix} \begin{bmatrix} \sin\alpha_\ell & 0 & \cos\alpha_\ell \\ 0 & 1 & 0 \\ -\cos\alpha_\ell & 0 & \sin\alpha_\ell \end{bmatrix} \begin{Bmatrix} x_\ell \\ y_\ell \\ z_\ell \end{Bmatrix} \quad (7)$$

and the lower leg segments (m = 9, 11) by

$$\begin{Bmatrix} X_m \\ Y_m \\ Z_m \end{Bmatrix} = \begin{bmatrix} \\ T^n \\ \\ \end{bmatrix} \begin{bmatrix} \sin\alpha_m & 0 & -\cos\alpha_m \\ 0 & 1 & 0 \\ \cos\alpha_m & 0 & \sin\alpha_m \end{bmatrix} \begin{Bmatrix} x_m \\ y_m \\ z_m \end{Bmatrix} \quad (8)$$

From equations (6) and (7), the elements of the transformation matrix for the forearms (segments 5 and 7) are written as:

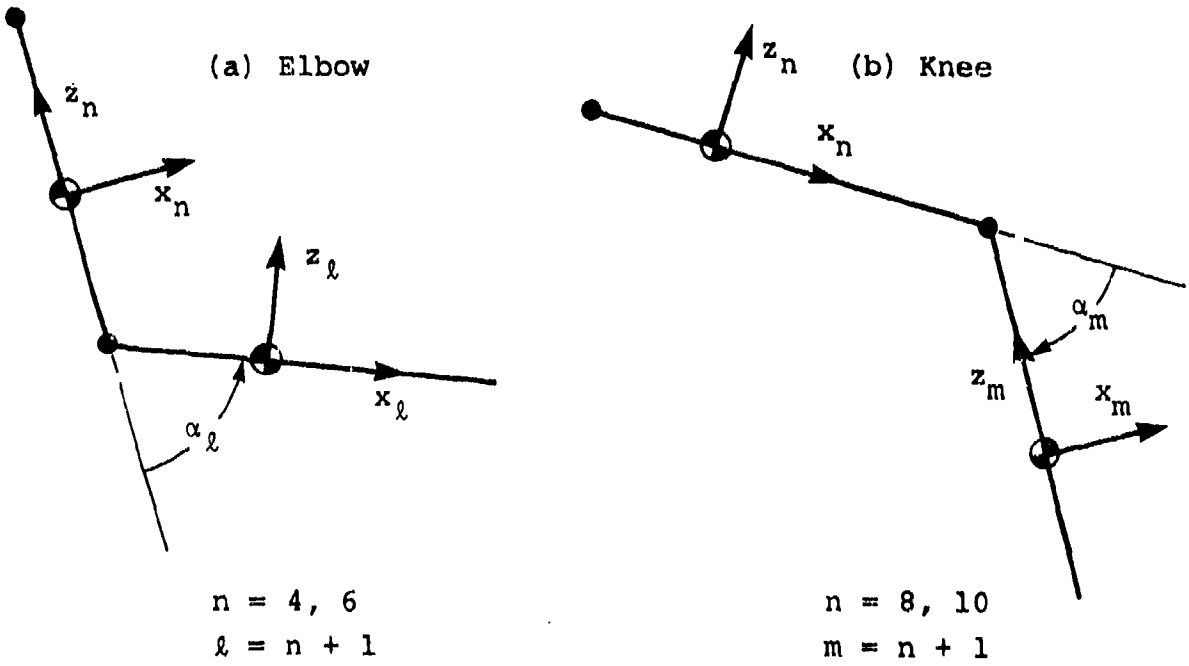

$n = 4, 6$
$\ell = n + 1$

$n = 8, 10$
$m = n + 1$

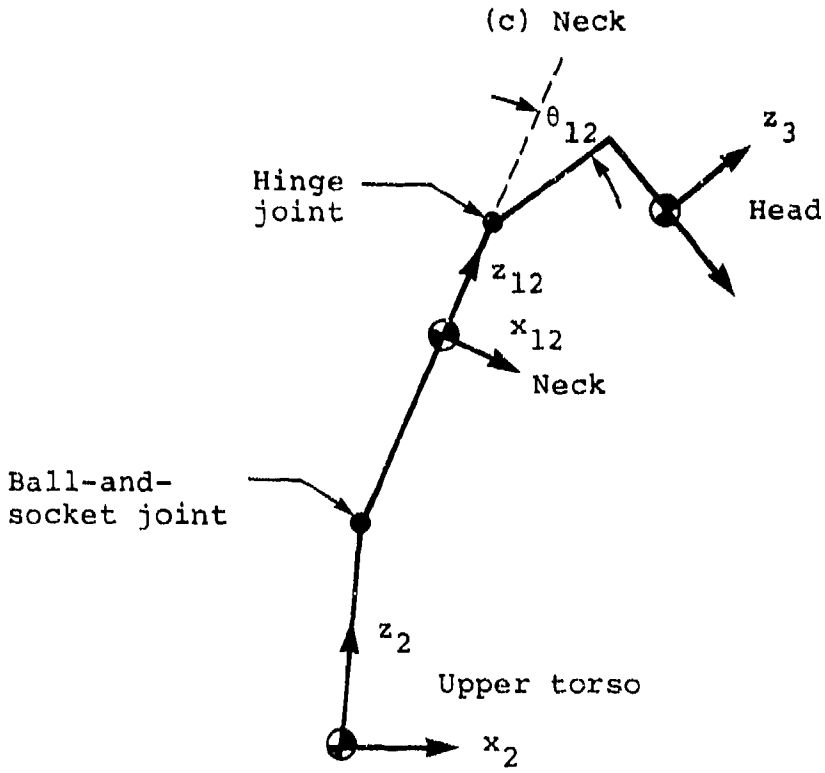

Figure 4. Definition of angular coordinates α for elbows, knees, and neck.

$$T_{11}^{\ell} = \cos\psi_n \cos\theta_n \sin\alpha_\ell - \cos\psi_n \sin\theta_n \cos\phi_n \cos\alpha_\ell$$
$$- \sin\psi_n \sin\phi_n \cos\alpha_\ell$$

$$T_{12}^{\ell} = \cos\psi_n \sin\theta_n \sin\phi_n - \sin\psi_n \cos\phi_n$$

$$T_{13}^{\ell} = \cos\psi_n \cos\theta_n \cos\alpha_\ell + \cos\psi_n \sin\theta_n \cos\phi_n \sin\alpha_\ell$$
$$+ \sin\psi_n \sin\phi_n \sin\alpha_\ell$$

$$T_{21}^{\ell} = \sin\psi_n \cos\theta_n \sin\alpha_\ell - \sin\psi_n \sin\theta_n \cos\phi_n \cos\alpha_\ell$$
$$+ \cos\psi_n \sin\phi_n \cos\alpha_\ell$$

$$T_{22}^{\ell} = \sin\psi_n \sin\theta_n \sin\phi_n + \cos\psi_n \cos\phi_n$$

$$T_{23}^{\ell} = \sin\psi_n \cos\theta_n \cos\alpha_\ell + \sin\psi_n \sin\theta_n \cos\phi_n \sin\alpha_\ell$$
$$- \cos\psi_n \sin\phi_n \sin\alpha_\ell$$

$$T_{31}^{\ell} = - \sin\theta_n \sin\alpha_\ell - \cos\theta_n \cos\phi_n \cos\alpha_\ell$$

$$T_{32}^{\ell} = \cos\theta_n \sin\phi_n$$

$$T_{33}^{\ell} = - \sin\theta_n \cos\alpha_\ell + \cos\theta_n \cos\phi_n \sin\alpha_\ell \qquad (9)$$

From equations (6) and (8), the elements of the transformation matrix elements for the legs (segments 9 and 11) are obtained:

$$T_{11}^{m} = \cos\psi_n \cos\theta_n \sin\alpha_m + \cos\psi_n \sin\theta_n \cos\phi_n \cos\alpha_m$$
$$+ \sin\psi_n \sin\phi_n \cos\alpha_m$$

$$T_{12}^{m} = \cos\psi_n \sin\theta_n \sin\phi_n - \sin\psi_n \cos\phi_n$$

$$T_{13}^{m} = -\cos\psi_n \cos\theta_n \cos\alpha_m + \cos\psi_n \sin\theta_n \cos\phi_n \sin\alpha_m + \sin\psi_n \sin\phi_n \sin\alpha_m$$

$$T_{21}^{m} = \sin\psi_n \cos\theta_n \sin\alpha_m + \sin\psi_n \sin\theta_n \cos\phi_n \cos\alpha_m - \cos\psi_n \sin\phi_n \cos\alpha_m$$

$$T_{22}^{m} = \sin\psi_n \sin\theta_n \sin\phi_n + \cos\psi_n \cos\phi_n$$

$$T_{23}^{m} = -\sin\psi_n \cos\theta_n \cos\alpha_m + \sin\psi_n \sin\theta_n \cos\phi_n \sin\alpha_m - \cos\psi_n \sin\phi_n \sin\alpha_m$$

$$T_{31}^{m} = -\sin\theta_n \sin\alpha_m + \cos\theta_n \cos\phi_n \cos\alpha_m$$

$$T_{32}^{m} = \cos\theta_n \sin\phi_n$$

$$T_{33}^{m} = \sin\theta_n \cos\alpha_m + \cos\theta_n \cos\phi_n \sin\alpha_m \qquad (10)$$

Segment 12, the neck, was added later. The hinge-type joint between the neck and the head is treated similarly to the knee joints, adding the generalized coordinate θ_{12}, as illustrated in figure 4.

Having developed the relationships expressed in the equations (1) through (10), the position of the occupant can be described by the following set of generalized coordinates:

$q_1 = X_1$	$q_{11} = \theta_3$	$q_{21} = \psi_8$
$q_2 = Y_1$	$q_{12} = \phi_3$	$q_{22} = \theta_8$
$q_3 = Z_1$	$q_{13} = \psi_4$	$q_{23} = \phi_8$
$q_4 = \psi_1$	$q_{14} = \theta_4$	$q_{24} = \alpha_9$

$$q_5 = \theta_1 \qquad q_{15} = \phi_4 \qquad q_{25} = \psi_{10}$$

$$q_6 = \phi_1 \qquad q_{16} = \alpha_5 \qquad q_{26} = \theta_{10}$$

$$q_7 = \psi_2 \qquad q_{17} = \psi_6 \qquad q_{27} = \phi_{10}$$

$$q_8 = \theta_2 \qquad q_{18} = \theta_6 \qquad q_{28} = \alpha_{11}$$

$$q_9 = \phi_2 \qquad q_{19} = \phi_6 \qquad q_{29} = \theta_{12}$$

$$q_{10} = \psi_3 \qquad q_{20} = \alpha_7 \qquad (11)$$

The above coordinates include the Cartesian coordinates of the mass center of segment 1 (X_1, Y_1, Z_1), selected as a reference point on the body, seven sets of Eulerian angles, and the five additional angular coordinates for the elbows, knees, and neck. Positions of the segment mass centers are presented in appendix A.

2.1.2 Lagrange's Equations

The response of the occupant system is described by Lagrange's equations of motion, which are written for the 29 generalized coordinates. The equations are developed according to

$$\frac{d}{dt}\left(\frac{\partial L}{\partial \dot{q}_j}\right) - \frac{\partial L}{\partial q_j} = Q_j \qquad (j = 1, 2, \ldots, 29) \qquad (12)$$

where L is the Lagrangian function

$$L = T - V \qquad (13)$$

t represents time, Q_j are the generalized forces not derivable from a potential function. (Forces that are derivable from a potential function are obtained from L, and T and V are the system kinetic and potential energies, respectively.)

Because the system being treated does not involve any velocity-dependent potentials, equation (12) can be written as

$$\frac{d}{dt}\left(\frac{\partial T}{\partial \dot{q}_j}\right) - \frac{\partial T}{\partial q_j} + \frac{\partial V}{\partial q_j} = Q_j \qquad (j = 1, 2, \ldots, 29) \tag{14}$$

The system kinetic energy contains both translational and rotational parts:

$$T = \frac{1}{2} \sum_{n=1}^{12} M_n \left[(\dot{X}_n)^2 + (\dot{Y}_n)^2 + (\dot{Z}_n)^2\right]$$

$$+ \frac{1}{2} \sum_{n=1}^{12} \left(I_{x_n}\, \omega_{x_n}^{\ 2} + I_{y_n}\, \omega_{y_n}^{\ 2} + I_{z_n}\, \omega_{z_n}^{\ 2}\right) \tag{15}$$

where M_n is the mass of segment n and I_{x_n}, I_{y_n}, and I_{z_n} are mass moments of inertia of segment n with respect to the local coordinate axes (x_n, y_n, z_n), assumed to be principal moments of inertia.

The absolute velocities of the 12 mass segments required for the translational kinetic energy must, of course, be written as functions of the generalized coordinates and generalized velocities in order to use equation (14). The angular velocity components $(\omega_{x_n}, \omega_{y_n}, \omega_{z_n})$ seen in equation (15) are parallel to the local (x_n, y_n, z_n) coordinate systems. These angular velocity components cannot be used directly in Lagrange's equations because they do not correspond to the time derivatives of any set of coordinates that specify the position of the segment. They must be written as functions of the generalized coordinates, using the generalized angular velocities $(\dot{\underline{\psi}}_n, \dot{\underline{\theta}}_n, \dot{\underline{\phi}}_n)$, which are parallel to the axes Z, y_n', and x_n'', respectively.

An arbitrary angular velocity of segment n, $\underline{\omega}_n$, can be expressed as a function of the generalized angular velocities according to

$$\underline{\omega}_n = \dot{\underline{\psi}}_n + \dot{\underline{\theta}}_n + \dot{\underline{\phi}}_n \tag{16}$$

Referring to figure 3, $\dot{\underline{\psi}}_n$, $\dot{\underline{\theta}}_n$, and $\dot{\underline{\phi}}_n$ do not, in general, form a mutually perpendicular vector triad. ($\underline{\psi}$ and $\underline{\phi}$ are both perpendicular to $\underline{\theta}$ but are not necessarily perpendicular to each other.) However, they can be considered as a nonorthogonal set of components of $\underline{\omega}$ since their vector sum is equal to $\underline{\omega}$.

Summing the orthogonal projections of $\dot{\underline{\psi}}_n$, $\dot{\underline{\theta}}_n$, and $\dot{\underline{\phi}}_n$ on the (x_n, y_n, z_n) axes yields the angular velocity components required for the kinetic energy expression:

$$\omega_{x_n} = \dot{\phi}_n - \dot{\psi}_n \sin \theta_n$$

$$\omega_{y_n} = \dot{\psi}_n \cos \theta_n \sin \phi_n + \dot{\theta}_n \cos \phi_n \qquad (17)$$

$$\omega_{z_n} = \dot{\psi}_n \cos \theta_n \cos \phi_n - \dot{\theta}_n \sin \phi_n$$

The system potential energy is simply gravitational potential, which is written as

$$V = \sum_{n=1}^{12} M_n g \, (Z_n - Z_{n_o}) \qquad (18)$$

where g is the acceleration due to gravity and Z_{n_o} is an arbitrary datum.

2.1.3 Matrix Equations

For the purposes of computation, the equations of motion are rewritten in the following form:

$$[A(q)] \{\ddot{q}\} = \{B(\dot{q},q)\} + \{P(q)\} + \{R(\dot{q},q)\} + \{Q(\dot{q},q)\} \qquad (19)$$

where the elements of the inertia matrix [A] and the vector {B} are derived from the kinetic energy derivatives of Lagrange's equations. In other words,

$$\frac{d}{dt}\left(\frac{\partial T}{\partial \dot{q}_j}\right) - \frac{\partial T}{\partial q_j} = \sum_{k=1}^{29} A_{jk} \ddot{q}_k \qquad (20)$$

$$- B_j \; (\dot{q}_1, \dot{q}_2, \ldots, \dot{q}_{29}, q_1, q_2, \ldots, q_{29})$$

$$(j = 1, 2, \ldots, 29)$$

The force vector {P} is derived from the system potential energy according to

$$P_j \ (q_1, q_2, \ldots, q_{29}) = - \frac{\partial V}{\partial q_j} \quad (j = 1, 2, \ldots, 29) \qquad (21)$$

Both {R} and {Q} are vectors of generalized forces derived from the right-hand side of Lagrange's equations. The vector {R} describes the resistance of the body joints to rotation, discussed in detail in section 2.3; {Q} is the vector of generalized external forces, discussed in detail in section 2.4.

2.2 TWO-DIMENSIONAL OCCUPANT MODEL

In order to achieve economical program solutions for cases where occupant response is expected to be symmetrical with respect to the X-Z plane, a two-dimensional occupant model option was included in Program SOM-TA. This two-dimensional model was configured like the three-dimensional model shown in figure 1, with the exception of all joints being hinge-type joints. Because of the potential for vertebral injury in aircraft accidents that involve a significant vertical component of impact velocity, some measure of vertebral loading was considered desirable in the occupant model. The two-dimensional occupant model was configured to include beam elements in both the torso and neck, as shown in figure 5, replacing joints that exist in the three-dimensional model. The two-dimensional model has 11 degrees-of-freedom, as illustrated in figure 6. Simulation of purely vertical ($+G_z$) impact with the three-dimensional occupant model produced less bending of the torso than observed in tests with either dummies or human cadavers. Therefore, in order to produce the moments on the vertebral column that are induced by $+G_z$ acceleration in both human and dummy occupants, the mass centers of the torso segments, segments 1 and 2, are offset from the vertebral column by the dimensions e_1 and e_2, respectively. The dimension e_3, by which the center of mass of the head segment is placed forward of the neck, is used in both three-dimensional and two-dimensional models.

Development of the equations of motion for the two-dimensional occupant follows a procedure similar to that described in section 2.1 for the three-dimensional model. However, the procedure is simplified because the transformation between

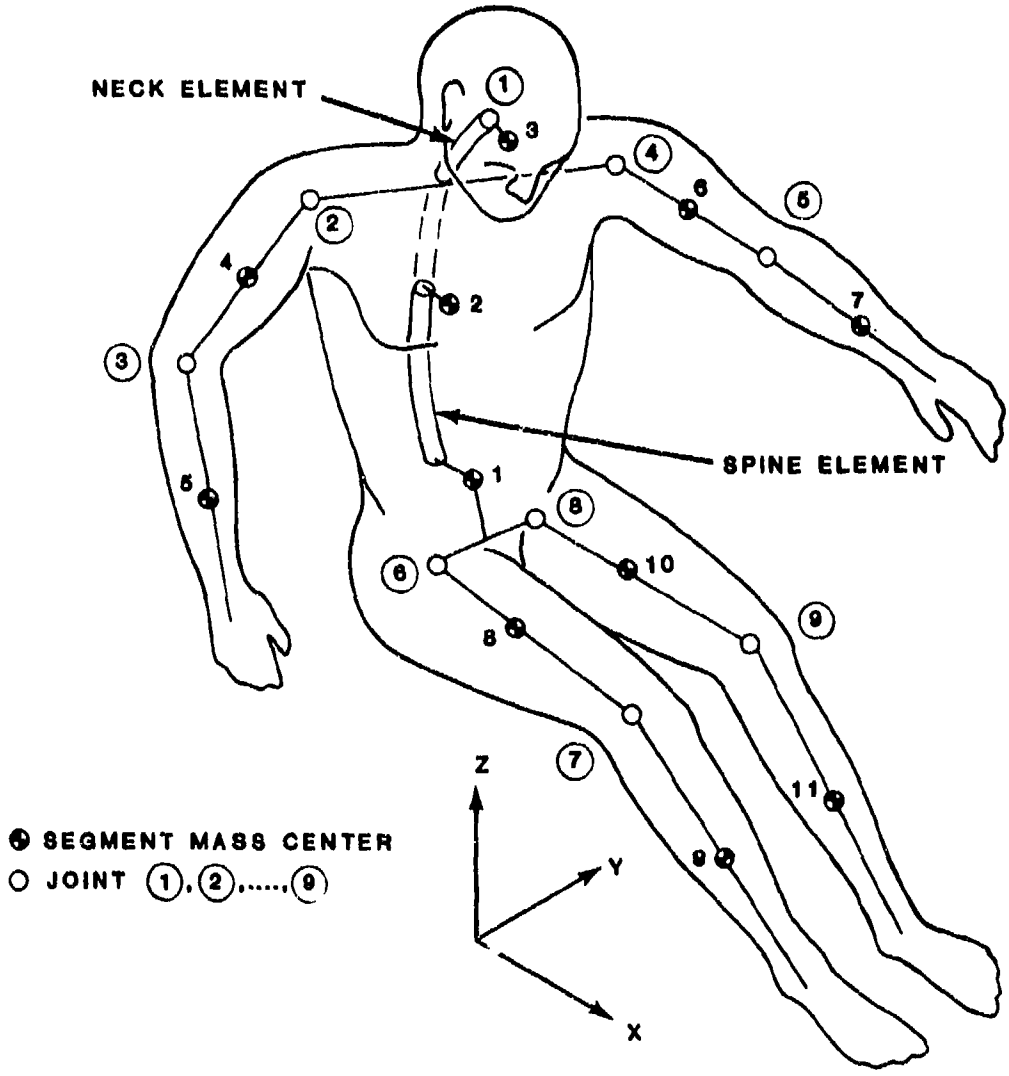

Figure 5. Eleven-segment (two-dimensional) occupant model.

a local, segment-fixed coordinate system and the inertial system is dependent only on the angle θ. Transformations, therefore, take the form of equation (3). The position of the center of mass of segment 2, with respect to that for segment 1 and the position of the center of mass of segment 3, relative to segment 2, depend on the length and curvature of the beam elements in the spine and neck, respectively.

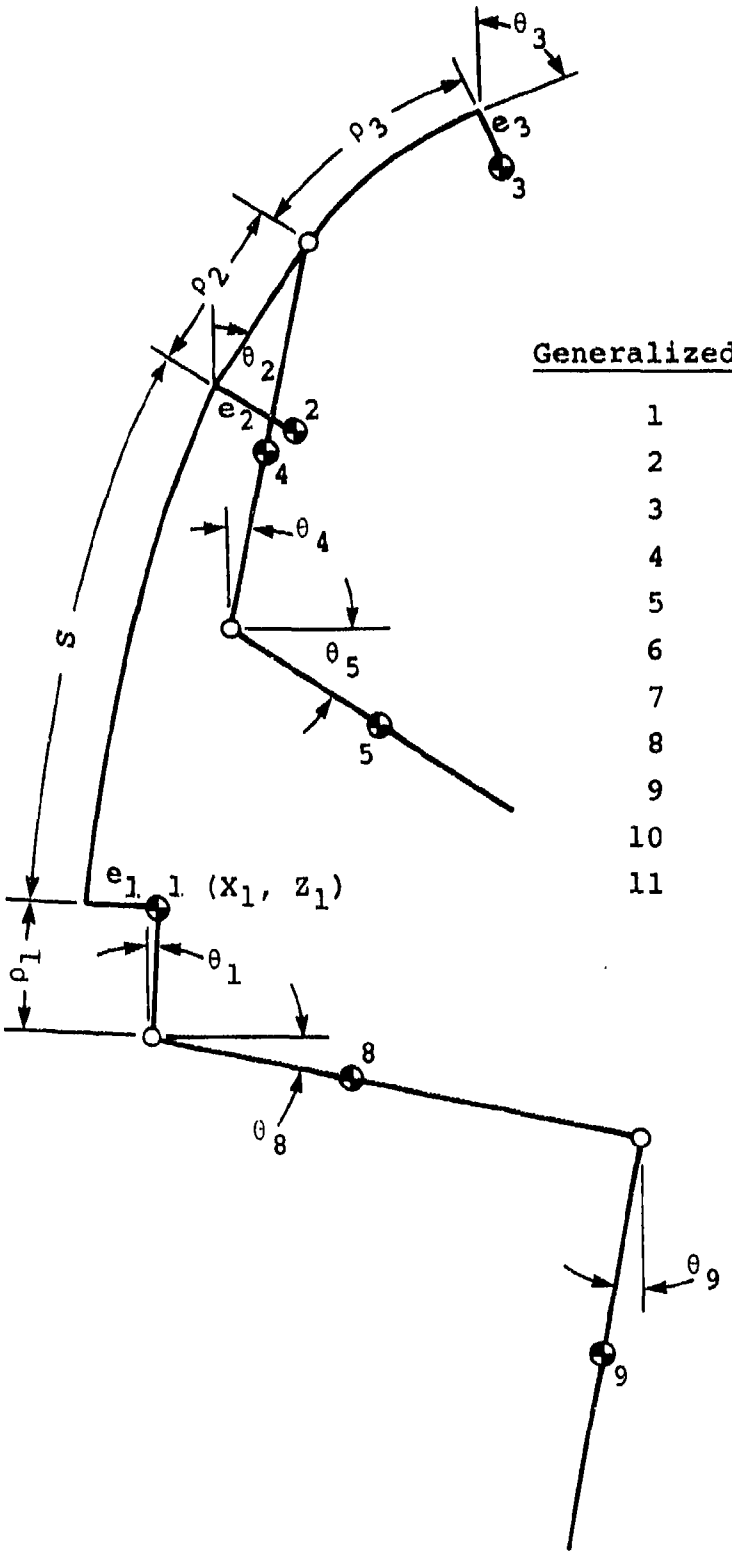

Generalized coordinates

1	X_1
2	Z_1
3	θ_1
4	S
5	θ_2
6	ρ_3
7	θ_3
8	θ_4
9	θ_5
10	θ_8
11	θ_9

Figure 6. Generalized coordinates for two-dimensional occupant model.

A detailed representation of the kinematics and mechanics of the spinal column would be complicated. The presence of the intervertebral disks leads to high flexibility in bending and high stiffness in compression. In addition, the column is tapered and possesses considerable initial curvature. A simplified model is incorporated into SOM-TA by using continuous beam elements for the neck and spine. These beam elements are intended to model the flexural, as well as axial, motion of the spine and neck and are subject to the following assumptions. The deformed beam elements take the shape of circular arc segments, therefore assuming flexure to be primarily due to the applied bending moment. This is equivalent to the assumption in beam theory that the span/depth ratio is large and that the modulus of elasticity and shear modulus are of the same order of magnitude so that shear deformation is negligible.

As illustrated in figure 7, The position of one end relative to the other in terms of arc length and angular coordinates at each end of the arc, is then given by

$$x_2 - x_1 = 2\left(\frac{S}{\theta_2 - \theta_1}\right)\sin\left(\frac{\theta_2 - \theta_1}{2}\right)\sin\left(\frac{\theta_2 + \theta_1}{2}\right)$$

$$z_2 - z_1 = 2\left(\frac{S}{\theta_2 - \theta_1}\right)\sin\left(\frac{\theta_2 - \theta_1}{2}\right)\cos\left(\frac{\theta_2 + \theta_1}{2}\right) \qquad (22)$$

Positions of the mass centers for the eleven body segments of the two-dimensional model are presented in appendix B.

2.3 JOINT RESISTANCE

The form of the joint resistance vector {R} in equation (19) depends on the user's selection of occupant type - either dummy or human. Although both joint models contain the same types of elements, a nonlinear torsional spring and a viscous torsional damper, the relative contributions of each of these elements determine the type of occupant.

The 11 body joints for the three-dimensional model, illustrated in figure 1, are defined as follows:

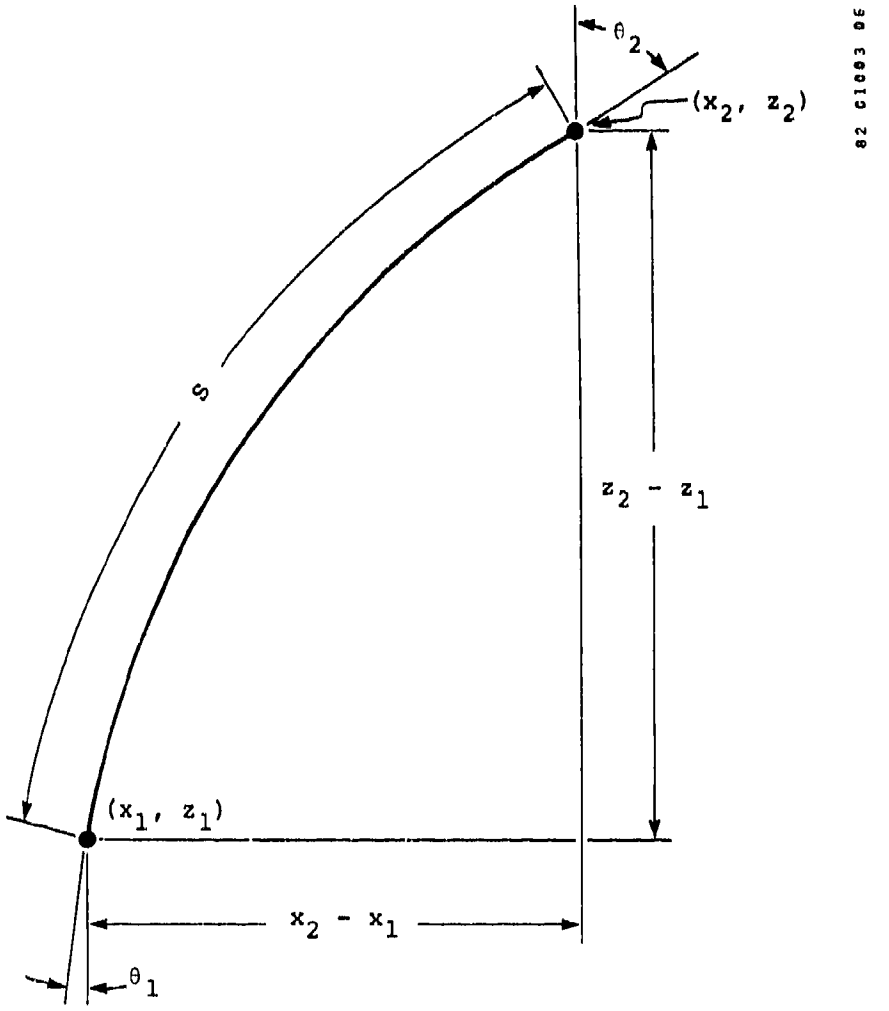

Figure 7. Position of segment 2 relative to segment 1.

Joint 1 - Back, between 12th thoracic and 1st lumbar vertebrae

Joint 2 - Torso-neck, between 7th cervical and 1st thoracic vertebrae

Joint 3 - Right shoulder

Joint 4 - Right elbow

Joint 5 - Left shoulder

Joint 6 - Left elbow

Joint 7 - Right hip

Joint 8 - Right knee

Joint 9 - Left hip

Joint 10 - Left knee

Joint 11 - Head-neck, at occipital condyles

The angular displacement of joint i from its reference position (figure 2) is given by β_i. If (i_m, j_m, k_m) and (i_n, j_n, k_n) are triads of unit vectors in the local coordinate systems of two adjacent segments connected at joint i, as shown in figure 8, the joint angle is given by

$$\beta_i = \cos^{-1} (k_m \cdot k_n) \tag{23}$$

where $(k_m \cdot k_n)$ is the scalar product. Considering the geometry of the occupant model in the reference position, the β_i for the 11 joints are given by

$$\begin{aligned}
\beta_1 &= \cos^{-1} (k_1 \cdot k_2) \\
\beta_2 &= \cos^{-1} (k_2 \cdot k_{12}) \\
\beta_3 &= \cos^{-1} (k_2 \cdot k_4) \\
\beta_4 &= \alpha_5 \\
\beta_5 &= \cos^{-1} (k_2 \cdot k_6) \\
\beta_6 &= \alpha_7 \\
\beta_7 &= \cos^{-1} (i_1 \cdot i_8) \\
\beta_8 &= \alpha_9 \\
\beta_9 &= \cos^{-1} (i_1 \cdot i_{10}) \\
\beta_{10} &= \alpha_{11} \\
\beta_{11} &= \cos^{-1} (k_3 \cdot k_{12})
\end{aligned} \tag{24}$$

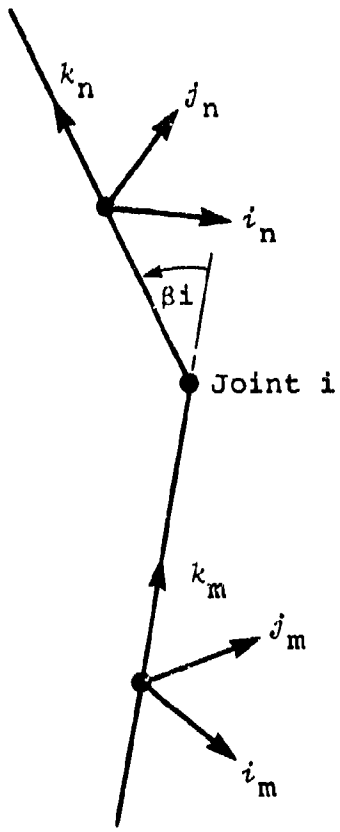

Figure 8. Joint angle β_i between segments m and n.

If at each joint i, a moment M_i and a torsional damper with coefficient J_i act to resist motion of the joint, then the virtual work done on the system as each joint i undergoes a virtual displacement $\delta\beta_i$ is

$$\delta W = - \sum_{i=1}^{11} (M_i \, \delta\beta_i + J_i \dot{\beta}_i \, \delta\beta_i) \qquad (25)$$

Since the β_i are functions of the generalized coordinates q_j, the virtual displacements $\delta\beta_i$ can be expressed in terms of corresponding virtual displacements of the q_j. In general, such an expression would take the form

$$\delta\beta_i = \sum_{j=1}^{29} \frac{\partial\beta_i}{\partial q_j} \delta q_j \qquad (i=1, 2, \ldots, 11) \qquad (26)$$

where the partial derivatives $\partial\beta_i/\partial q_j$ are functions of the generalized coordinates. Substituting into equation (25) gives

$$\delta W = - \sum_{i=1}^{11} \sum_{j=1}^{29} (M_i + J_i \ddot{\beta}_i) \frac{\partial \beta_i}{\partial q_j} \delta q_j \qquad (27)$$

Changing the order of summation, equation (27) can be written in the general form

$$\delta W = \sum_{j=1}^{29} R_j \delta q_j \qquad (28)$$

where R_j are the generalized forces acting on the system. As seen in equation (19), the generalized forces are treated as two distinct types: joint resistance forces and external forces. Since the joint resistance terms are being treated here, the generalized joint forces referred to as R_j will be considered alone. Equation (28) becomes, more specifically

$$\delta W = \sum_{j=1}^{29} R_j \delta q_j \qquad (29)$$

and, from equation (27), R_j can be written

$$R_j = - \sum_{i=1}^{11} (M_i + J_i \ddot{\beta}_i) \frac{\partial \beta_i}{\partial q_j} \qquad (j=1, 2, \ldots, 29) \qquad (30)$$

As mentioned earlier in this section, the type of occupant is determined by the relative contributions of M_1 and J_1 to the R_j terms. For the dummy joint, the resisting torque M_i is constant throughout the normal range of joint motion and increases rapidly along a third-order curve to a higher value at the limiting displacement β_{S_i}, as shown in figure 9. The normal values M_{D_i} are set equal to those resulting from the joint-tightening procedure of SAE Recommended Practice, Anthropomorphic Test Device for Dynamic Testing - SAE J963. That is, the body joints will just support a 1-G load in the reference (seated)

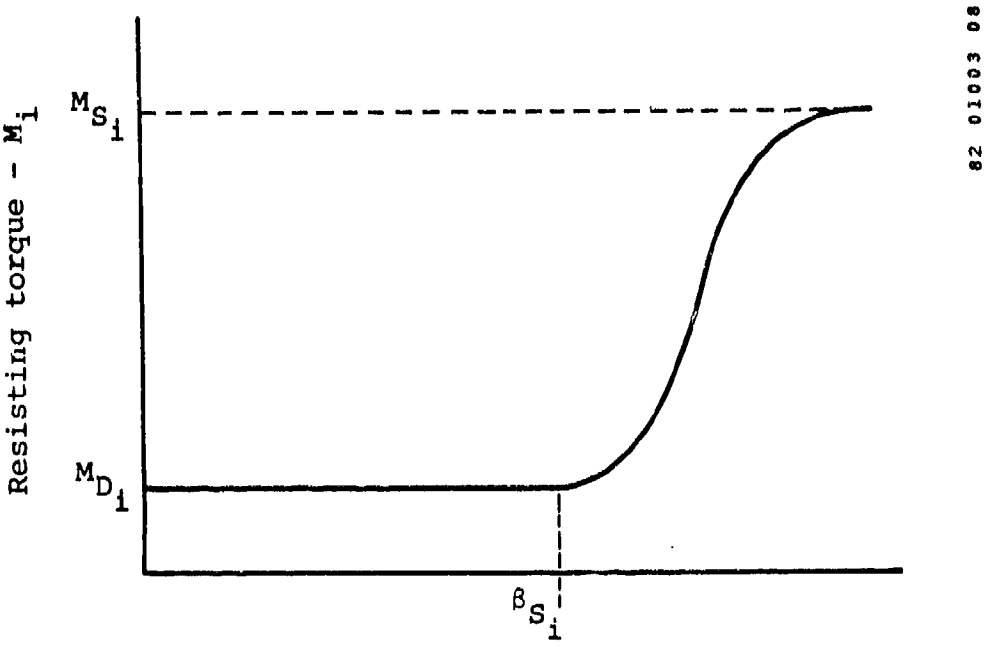

Figure 9. Dummy joint resisting torque.

position, with the exception of the torso joints, which will support a 2-G load. In addition to M_i, a small viscous damping term with constant J_i is included for energy dissipation.

The resistance of each human joint consists of up to three terms. The primary resisting force during normal joint rotation is a viscous damping term with constant coefficient J_i. In a manner similar to the case of the dummy, a resisting torque is applied at the limit of the joint range of motion, as shown in figure 10(a). An additional term used to simulate muscle tone is the moment M', which drops to zero after a small angular displacement from the initial position, provided that the crash deceleration is sufficient to overcome it (figure 10(b)).

For the two-dimensional model, the equations presented in this section are correct except that summations are performed for 8 joints and 11 degrees of freedom, rather than the 11 and 29 presented here, respectively.

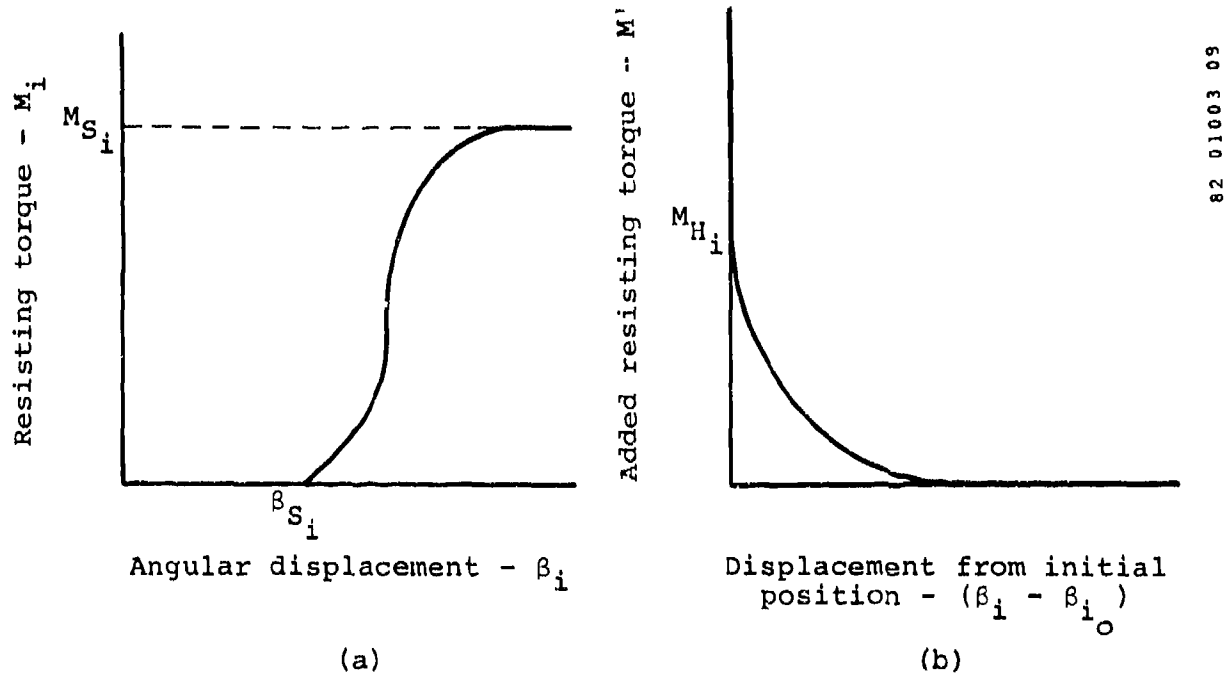

Figure 10. Human joint resisting torques: (a) displacement-limiting moment and (b) muscular resistance.

2.4 EXTERNAL FORCES

The vector of gereralized external forces $\{Q\}$ is developed in a manner similar to that discussed in the previous section for the joint resistance vector. Equations presented in this section include summations whose upper limits are correct for the three-dimensional model, with 12 segments and 29 degrees-of-freedom. The approach for the two-dimensional model is the same, except for the use of 11 segments and 11 degrees-of-freedom.

The resultant external force $\underline{F}_i$ acting on segment i is given by

$$\underline{F}_i = F_{X_i}\, i + F_{Y_i}\, j + F_{Z_i}\, k \qquad (31)$$

where F_{X_i}, F_{Y_i}, and F_{Z_i} are components in the inertial (X, Y, Z) system. The absolute position of the point P_i on segment i, where the resultant force acts, can be represented by

$$\underline{r}_{P_i} = X_{P_i} i + Y_{P_i} j + Z_{P_i} k \tag{32}$$

As the resultant force applied to each segment i undergoes a virtual displacement δr_{P_i}, having components (δX_{P_i}, δY_{P_i}, δZ_{P_i}), the virtual work on the system done by the $\underline{F}_i$ is

$$\delta W = \sum_{i=1}^{12} (F_{X_i} \delta X_{P_i} + F_{Y_i} \delta Y_{P_i} + F_{Z_i} \delta Z_{P_i}) \tag{33}$$

Writing the virtual displacement components in terms of the generalized coordinates q_j:

$$\begin{aligned} \delta X_{P_i} &= \sum_{j=1}^{29} \frac{\partial X_{P_i}}{\partial q_j} \delta q_j \\ \delta Y_{P_i} &= \sum_{j=1}^{29} \frac{\partial Y_{P_i}}{\partial q_j} \delta q_j \\ \delta Z_{P_i} &= \sum_{j=1}^{29} \frac{\partial Z_{P_i}}{\partial q_j} \delta q_j \end{aligned} \tag{34}$$

results in

$$\delta W = \sum_{j=1}^{29} \sum_{i=1}^{12} (F_{X_i} \frac{\partial X_{P_i}}{\partial q_j} + F_{Y_i} \frac{\partial Y_{P_i}}{\partial q_j} + F_{Z_i} \frac{\partial Z_{P_i}}{\partial q_j}) \delta q_j \tag{35}$$

Using equation (28)

$$\delta W = \sum_{j=1}^{29} Q_j \delta q_j$$

yields the components of the generalized external force vector:

$$Q_j = \sum_{i=1}^{12} \left(F_{X_i} \frac{\partial X_{P_i}}{\partial q_j} + F_{Y_i} \frac{\partial Y_{P_i}}{\partial q_j} + F_{Z_i} \frac{\partial Z_{P_i}}{\partial q_j}\right) \qquad (36)$$

The external forces acting on the body segments can be characterized as either contact forces or restraint forces. These forces are discussed in further detail in the sections following.

2.4.1 Contact Forces

The contact forces applied to the occupant in all cases are those forces exerted by the cushions and floor, illustrated in figure 11. The forces of the seat back pass through the mass centers of the upper torso and head segments, and the normal forces applied to the legs by the seat bottom cushion pass through the mass centers of the thigh segments. The contact surface for the lower torso is not located at the mass center of that segment but is an ellipsoid whose major axis passes through both hip joints. The force of the back cushion and the normal component of the seat bottom cushion force both pass through the center of this ellipsoid, i.e., through a point midway between the hips. The normal components of the floor and footrest forces are applied to the body at the lower ends of the leg segments. If contact between the occupants and the seat in front of them is to be simulated, eight surfaces on each seat back are defined by user input. If contact occurs between an occupant and a seat back, forces are computed in the same manner as for cushions.

Each of the forces mentioned above acts normal to the surface applying the force, or, in other words, its direction is determined by the plane of the surface, whether cushion or floor. As shown in figure 11, friction forces are also applied by the seat bottom cushion and the floor. The friction force is computed as the product of the coefficient multiplied by the normal force. It is applied in a direction opposite to the tangential component of relative velocity between the occupant segment and the appropriate cushion or floor surface. In order to avoid abrupt changes in direction of the friction force, the force is reduced sinusoidally when the magnitude of the tangential velocity drops below a predetermined limit. (A limiting value of 1 ft/sec has produced satisfactory results in SOM-TA and is thus used by the program.)

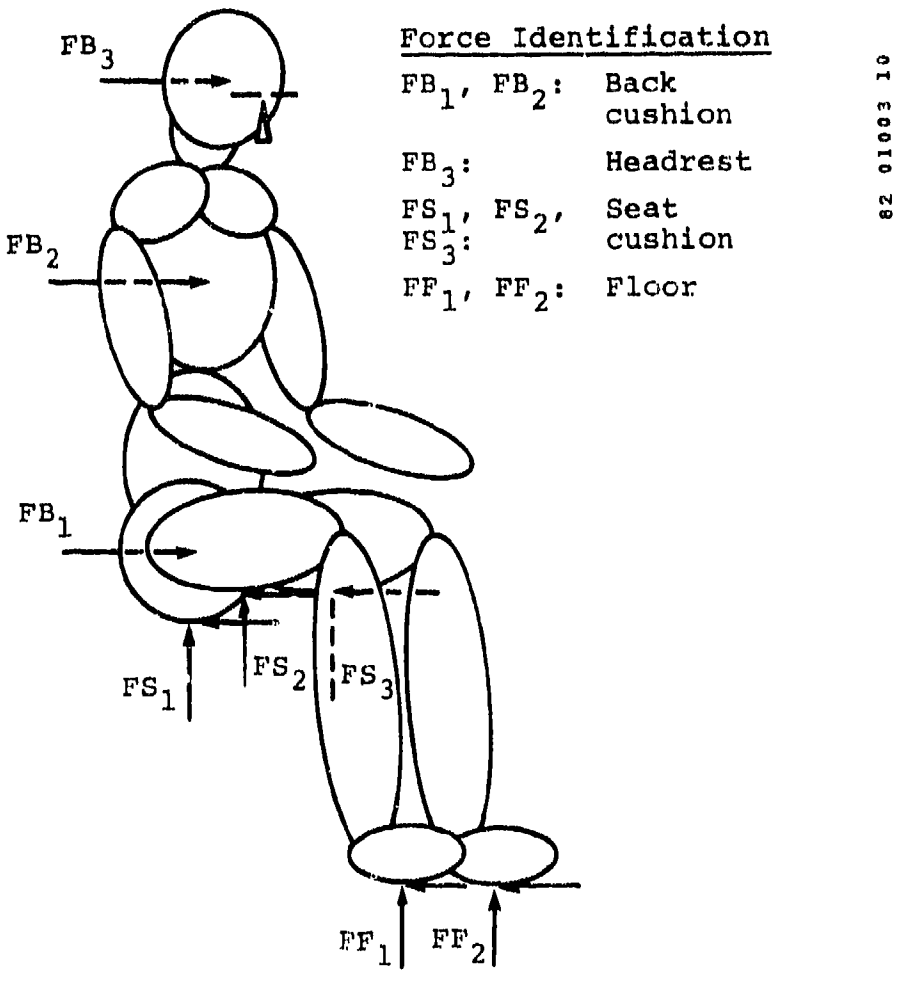

Figure 11. External forces of cushions and floor.

All contact forces are calculated by first determining the penetration of a contact surface on the occupant into a surface with known force-deflection characteristics. Using the seat cushion force as an example, the pertinent dimensions of the seat and the parameters required to determine the penetration of the abdomino-pelvic segment (segment 1) into the cushion are illustrated in figure 12. X_p and Z_p are coordinates of the center of the contact surface of segment 1, and R_1 is the radius of the contact surface in the (x_1 - z_1) plane. (Although this contact surface is an ellipsoid, cross-sections parallel to the (x_1 - z_1) plane are circular. The dimensions of the contact

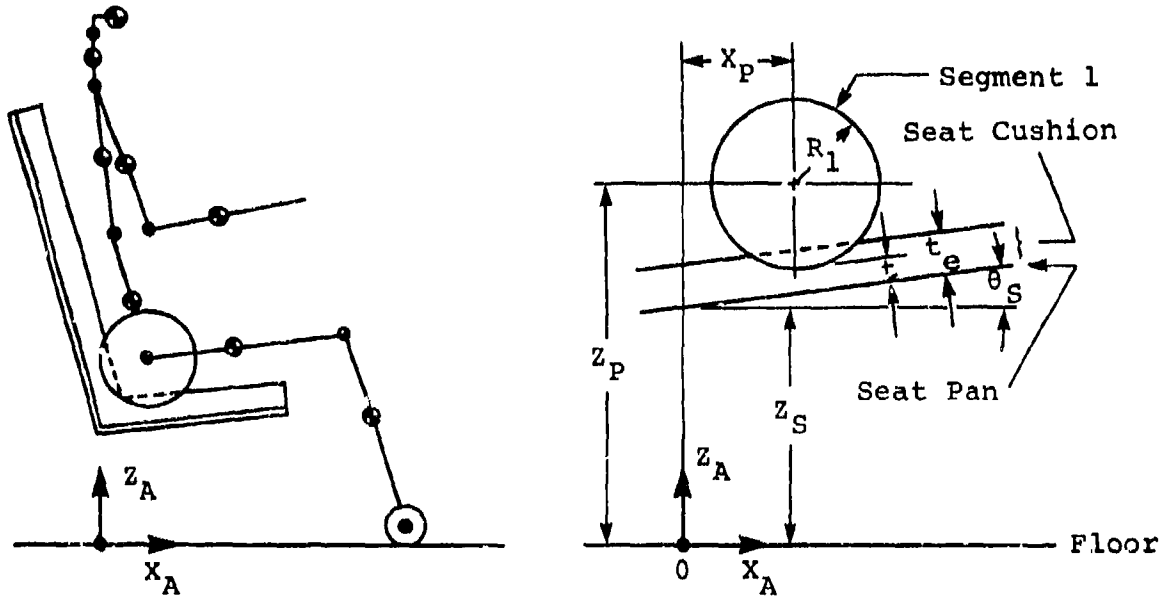

Figure 12. Seat cushion deflection.

surfaces will be discussed in section 2.5.) The position of the seat pan is defined by its height Z_S above the origin of the aircraft coordinate system and the angle θ_S that it makes with the aircraft (X_A - Y_A) plane. The unloaded thickness of the seat cushion is t_e, and the loaded thickness under segment 1 is t. Summing the dimensions in the Z_A direction gives

$$Z_P = Z_S + (R_1 + t)/\cos\theta_S + X_P \tan\theta_S \tag{37}$$

Solving equation (37) for the cushion thickness,

$$t = (Z_P - Z_S)\cos\theta_S - R_1 - X_P \sin\theta_S \tag{38}$$

The deflection of the seat cushion is then

$$\delta_c = t_e - t \tag{39}$$

and the force, which is assumed to act normal to the plane of the seat pan and pass through the center of curvature of the contact surface, is calculated from deflection according to

$$F_c = A(e^{b\delta_c} - 1) \tag{40}$$

To each normal force, a damping term is applied which is proportional to the deflection rate. The damping coefficient is based on the Rayleigh formulation in which the coefficient is proportional to both mass and stiffness according to

$$C = 2\beta m + \alpha K \tag{41}$$

For a multidegree-of-freedom system there will be a discrete damping coefficient associated with each characteristic mode. In a continuous system there will be an infinite number of coefficients, although several modes will generally dominate the dynamic solution. It was assumed for the formulation in SOM-TA that the damping ratio, ζ, was constant for all deformation modes of interest. This assumption greatly simplifies the solution of equation (41) because the damping coefficient is not dependent on the system mass. Equation (41) can then be simplified to

$$C = 2K\alpha \tag{42}$$

where the stiffness K is the gradient of the cushion force-deflection curve, and α is a constant for the system.

The procedure used in SOM-TA to calculate the current value of the damping coefficient is based on the curent value of K, and the constant, α, which is determined from input data. The slope of the exponential load/deflection curve at deflection δ_c is

$$K = Abe^{b\delta_c} \tag{43}$$

The user supplies a damping coefficient, C_o, for the zero-deflection condition which the program uses to calculate α by applying equations (43) and (42), thereby resulting in

$$\alpha = \frac{C_o}{2K_o} \tag{44}$$

The constant, α, and the current gradient of the cushion load-deflection curve, K, are used at each time step to determine the instantaneous cushion damping coefficient from equation (42).

2.4.2 Restraint System Forces

The method used in calculating the forces exerted on the body by the restraint system differs considerably from that described in the preceding section for the contact forces. The primary reason for this difference is that the restraint forces do not act at any fixed points on the occupant, but, rather, the points of application vary with the restraint system geometry.

Although other configurations can be selected by the user, a restraint system consisting of a lap belt and diagonal shoulder strap will be used as an example. The restraint loads are transmitted to the occupant model through ellipsoidal surfaces fixed to the upper and lower torso segments. These surfaces are shown in figure 13. The locations of the anchor points A_1, A_2, and A_3 are determined by user input along with the webbing properties. The buckle B for a single shoulder belt is located according to an input parameter which specifies the distance from the appropriate point, in this case A_1, along the path of the lap belt. For a double-strap shoulder harness, the buckle is placed on the abdominal contact surface between its intersections with the thigh surfaces.

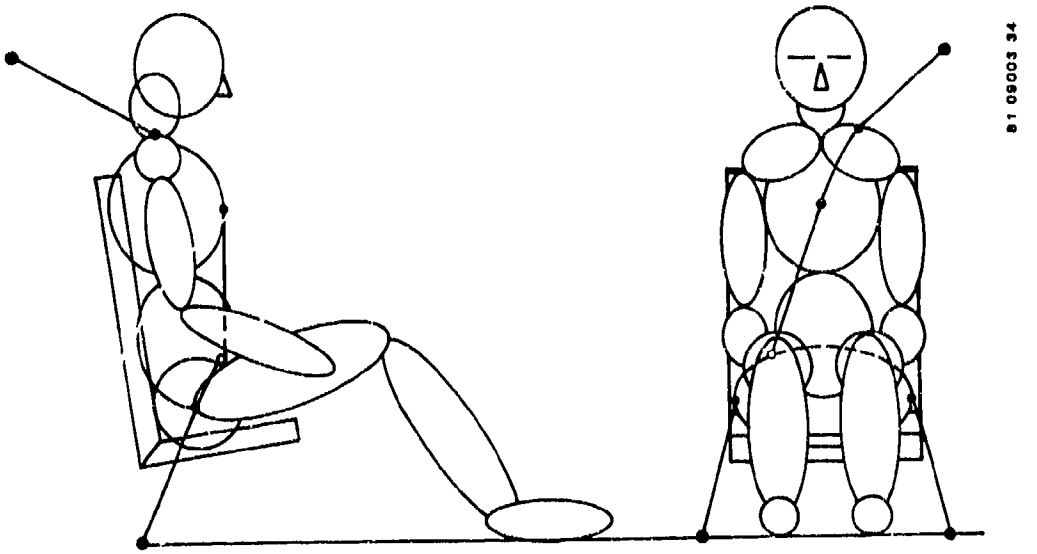

Figure 13. Restraint system configuration variables.

The ellipsoidal surfaces are described by

$$x_1^2/a_1^2 + y_1^2/b_1^2 + z_1^2/c_1^2 = 1 \qquad (45)$$

for the lower torso, where

$$a_1 = R_1$$

$$b_1 = L_H$$

$$c_1 = R_1$$

and

$$x_2^2/a_2^2 + y_2^2/b_2^2 + z_2^2/c_2^2 = 1 \qquad (46)$$

for the upper torso, where

$$a_2 = R_2$$

$$b_2 = L_2/2$$

$$c_2 = L_2/2$$

and these body dimensions are defined in section 2.5.

The restraint forces are determined in the same manner for both the upper and lower torso. First, the belt loads are calculated from the displacements of the torso segments, and the resultant force on each segment is then applied at the point along the arc of contact between the belt and the ellipsoidal surface where the force is normal to the surface.

Explaining this procedure in further detail for the restraint system configuration shown in figure 13, for any position of the occupant, the coordinates of the left shoulder, the hips, and the buckle connection B are calculated in the aircraft reference frame. The length of each side of the lap belt is equal to the sum of the free length in a straight line from an anchor point (A_1 or A_2) to the outermost point on the hip contact surface (C_1 or C_2) added to the length of an arc from that point on the hip to the buckle (B). The shoulder belt length is computed as the sum of the distance from the anchor point (A_3) to a point of tangency on the top of the shoulder contact surface (D), the distance from the buckle to the extreme anterior (forward) point on the ellipsoidal chest surface (E), and the length of an arc over the chest surface between points D and E. If the length of the belt segment should exceed the equilibrium (zero load) length calculated initially, then there is some tensile force in the belt. The resultant force on each segment is the vector sum of the belt forces. Friction between the shoulder belt and chest along the length of the belt is taken into account by reducing the load in the belt between the chest and buckle by a constant fraction of the load in the free length between the anchor point and the body surface. The resultant force on the lower or upper torso segment may be written generally as

$$\underline{F} = F_x i + F_y j + F_z k \tag{47}$$

where F_x, F_y, and F_z are components in the local, segment-fixed coordinate system.

To find the point on the segment where $\underline{F}$ is normal to the surface, consider first the equation of an ellipsoid:

$$x^2/a^2 + y^2/b^2 + z^2/c^2 = 1 \tag{48}$$

which may also be expressed in functional form as

$$f(x, y, z) = x^2/a^2 + y^2/b^2 + z^2/c^2 - 1 \tag{49}$$

where the ellipsoid can be regarded as the level surface f=0 of the function. At any point (x, y, z) on the surface, the gradient of f is normal to the surface. The gradient is given by

$$\text{grad } f = (2x/a^2)\, i + (2y/b^2)\, j + (2z/c^2)\, k \tag{50}$$

and at the point of application of the resultant force, grad f is collinear with $\underline{F}$. Making use of the proportionality between the components of the two vectors,

$$\begin{aligned} F_x &= Cx/a^2 \\ F_y &= Cy/b^2 \\ F_z &= Cz/c^2 \end{aligned} \tag{51}$$

where C is an arbitrary constant. Solving equation (51) for the coordinates (x, y, z) and substituting into equation (48)

$$\left(\frac{F_x a^2}{C}\right)^2 \frac{1}{a^2} + \left(\frac{F_y b^2}{C}\right)^2 \frac{1}{b^2} + \left(\frac{F_z c^2}{C}\right)^2 \frac{1}{c^2} = 1 \tag{52}$$

$$\left(\frac{F_x a}{C}\right)^2 + \left(\frac{F_y b}{C}\right)^2 + \left(\frac{F_z c}{C}\right)^2 = 1 \tag{53}$$

which leads to

$$\begin{aligned} C^2 &= F_x{}^2 a^2 + F_y{}^2 b^2 + F_z{}^2 c^2 \\ C &= \pm\sqrt{F_x{}^2 a^2 + F_y{}^2 b^2 + F_z{}^2 c^2} \end{aligned} \tag{54}$$

the point of application of $\underline{F}$ is then

$$\begin{aligned} x &= F_x a^2/C \\ y &= F_y b^2/C \\ z &= F_z c^2/C \end{aligned}$$

with

$$C = -\sqrt{F_x^2 a^2 + F_y^2 b^2 + F_z^2 c^2} \tag{55}$$

The negative sign on C can be explained by the fact that each coordinate in the local system is opposite in sign to the corresponding component of the resultant force, or

$$\begin{aligned} x &> 0 \text{ if } F_x < 0 \\ y &> 0 \text{ if } F_y < 0 \\ z &> 0 \text{ if } F_z < 0 \end{aligned} \tag{56}$$

The capability of the belt's point of application of resultant belt loads to move relative to the torso surfaces allows simulation of the "submarining" under the lap belt.

2.5 OCCUPANT DIMENSIONS AND INERTIAL PROPERTIES

Characteristics required by the occupant model for each of the segments are the length, mass, center of mass location, and moments of inertia. Also required are the axial and flexural stiffnesses and damping coefficients for both vertebral elements, as well as compliance characteristics for the chest and abdomen. It is assumed that, for each segment, a line connecting the joints is a principal axis, so that the required moments of inertia are all principal moments. For each torso element, of the two-dimensional model, the center of mass may, in general, be offset from the spine as shown in figure 6. Moments of inertia are then moments with respect to axes located at the mass center. Final data required to describe the occupant are radii of 26 contact surfaces, which are ellipsoids and spheres.

For two "standard" occupants, a 50th-percentile human male and a 50th-percentile anthropomorphic (Part 572) dummy, all the required data are stored within the program. For other nonstandard occupants, the above-described data must be provided as input. The human data are based on the U.S. Air Force drawing board manikin (reference 7), whose dimensions were extracted by the FAA Civil Aeromedical Institute and tabulated with appropriate inertial properties in reference 8. Dummy dimensions and characteristics were obtained from reference 9.

Most of the dimensions and inertial properties used in SOM-TA were taken from references 8 and 9, but because fewer segments are used in the mathematical model, some properties needed to be combined. That is, in the model, the hands are combined with the lower arms, the feet with the lower legs, and the mid torso with the lower torso. The distance from the wrist pivot to the mass center of the hand was added to the lower arm length; a contact sphere centered on the end of this link accounts for the remaining reach of the hand. Similarly, the distance from the ankle pivot to the foot center of mass was added to the lower leg length, and a contact sphere was sized to provide the correct distance between the knee pivot and the floor. Composite mass center locations and moments of inertia were calculated for the lower torso, lower arms, and lower legs.

2.5.1 Body Segment Dimensions

The basic dimensions of the occupant segments that are required in writing the equations of motion are illustrated in figure 14. The lengths of the segments are, in most cases, effective "link lengths" between joint centers, rather than standard anthropometric dimensions based on external measurements. These lengths, for the standard 50th-percentile occupants, are presented in table 1.

For segments other than the torso segment, the distance of the mass center of segment n from the end nearest the body reference point (m_1) is ρ_n. The distance between the mass center and the far end is given by

$$\overline{\rho}_n = L_n - \rho_n \tag{57}$$

Note that the lengths of the torso segments, L_1 and L_2, are not used in the two-dimensional model shown in figure 5 although they are used to generate contact surface ellipsoids for the graphics display. However, the center of mass distances, ρ_1 and ρ_2, and the spinal length, S, are used and

$$L_1 + L_2 = \rho_1 + \rho_2 + S \tag{58}$$

Also, the seated height is equal to

$$R_1 + \rho_1 + S + \rho_2 + N + L_3/2 \tag{59}$$

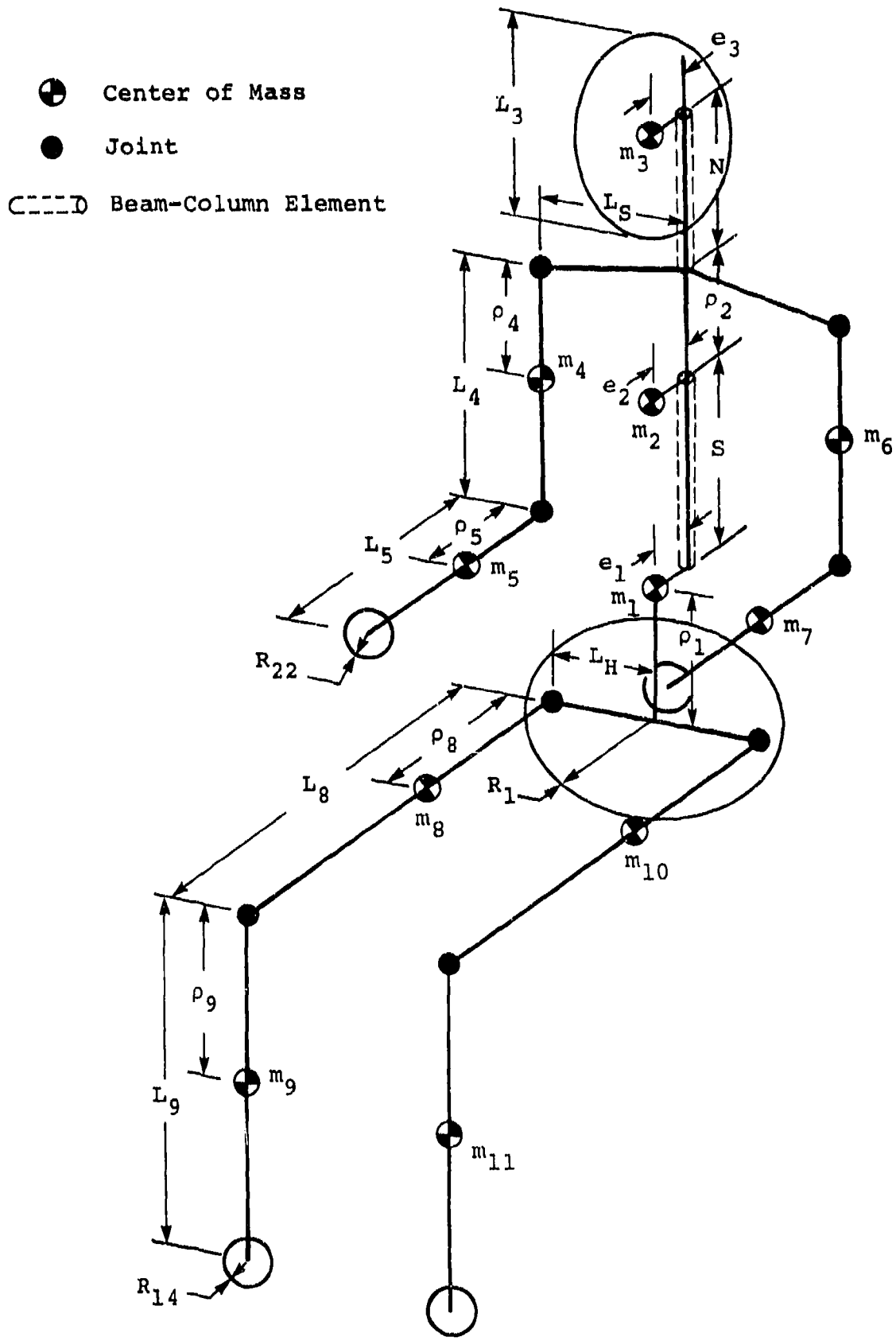

Figure 14. Program SOM-TA body segment dimensions.

TABLE 1. BODY SEGMENT LENGTHS (IN.)

Segment	50th-Percentile Aircrewmember (reference 8)	Part 572 Dummy (reference 9)
Lower Torso, L_1	9.44	10.5
Upper Torso, L_2	13.1	11.5
Neck, N	5.10	4.88(2)
Head, L_3	8.50(1)	8.35(2)
Upper Arm, L_4	11.6	11.3
Lower Arm, L_5	14.8(3)	13.3(3)
Upper Leg, L_8	17.1	16.5
Lower Leg, L_9	18.4(3)	18.0(3)
Spine, S	12.4(3)	10.85(3)
Seated Height	37.0(3)	36.0(3)

(1) Scaled from manikin drawing.
(2) Scaled from Part 572 drawing.
(3) Calculated.

where R_1 is the radius of the pelvic contact ellipsoid in the midsagittal plane, N is the neck length, and L_3 is the head segment length (z-direction, approximately menton to top of head, in anthropometric terms).

2.5.2 Body Segment Weights and Center of Mass Locations

Body segment weights and axial locations of centers of mass for the two standard occupants are presented in table 2. The dimensions e_1 and e_2, by which the torso mass centers are offset from the spine were determined to be 0.20 and 0.70 in., respectively, based on simulation of vertical ($+G_z$) tests. A

TABLE 2. BODY SEGMENT WEIGHTS AND CENTER OF MASS LOCATIONS

Segment	Weight (lb)		Center of Mass Location (in.)	
	50th-Percentile Aircrewmember (reference 8)	Part 572 Dummy (reference 9)	50th-Percentile Aircrewmember (reference 8)	Part 572 Dummy (reference 9)
Lower Torso	31.3	28.6	2.50(1)	4.17(1)
Upper Torso	55.0	42.0	7.60(1)	6.55(1)
Neck	2.34	1.98	1.93	2.44
Head	9.35	10.1	5.57	5.05
Upper Arm	8.78(2)	9.70(2)	6.02	4.72
Lower Arm (including hand)	8.34(2)	9.70(2)	7.07(1)	6.26(1)
Upper Leg	43.4(2)	43.4(2)	8.46	8.35
Lower Leg (including foot)	21.2(2)	19.0(2)	9.06(1)	11.0(1)
TOTAL	179.7	164.5		

(1) Calculated.
(2) Combined weight for two appendages.

value of 1.17 in. for the corresponding dimension for the head, e_3, is based on Part 572 dummy drawings.

2.5.3 Body Segment Moments of Inertia

Body segment moments of inertia are presented in table 3. As indicated, moments of inertia with respect to lateral (y) axes were taken from references 8 and 9 for the standard human and dummy occupants, respectively. The moments of inertia with respect to the segment x- and z-axes were determined using approximations to segment geometry. The torso and head segments were approximated by ellipsoids. Assigning appropriate anthropometric dimensions to the ellipsoid axes, ratios I_x/I_y and I_z/I_y were calculated for unit mass. These ratios, multiplied by the I_y from reference 8 or 9, gave values of I_x and I_z for the torso and head segments. The identical procedure was used for the extremities, except that these segments were approximated by solid circular cylinders.

TABLE 3. BODY SEGMENT MOMENTS OF INERTIA (lb-in.-sec^2)

Segment	I_x	I_y		I_z
		50th-Percentile Aircrewmember (reference 8)	Part 572 Dummy (reference 9)	
Lower Torso	4.03	1.19	0.760	2.323
Upper Torso	2.37	3.29	0.926	1.70
Neck	-	0.019	0.0177	-
Head	0.160	0.199	0.266	0.233
Upper Arm	0.131	0.120	0.135	0.022
Lower Arm (including hand)	0.105	0.254	0.185	0.195
Upper Leg	0.212	1.41	1.22	0.873
Lower Leg (including foot)	1.28	1.17	0.994	0.505

2.5.4 Body Contact Surfaces

Twenty-six surfaces are defined on the body for calculation of external forces exerted on the occupant by the seat cushions, the restraint system, and the rear of the seat in front. These surfaces are ellipsoids, cylinders and spheres, as shown in figure 15. The dimensions of these surfaces, listed in table 4, were obtained from anthropometric data in references 8 and 9 or scaled off the drawings of the manikin and dummy. The surfaces and the dimensions required for their description are illustrated in detail in figure 16.

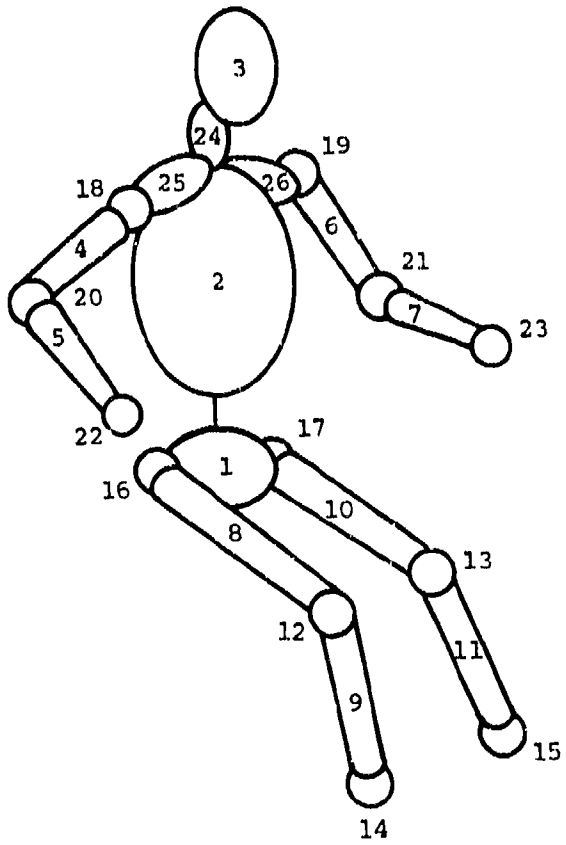

Surface Identification

1. Lower Torso
2. Upper Torso
3. Head
4. Right Upper Arm
5. Right Forearm
6. Left Upper Arm
7. Left Forearm
8. Right Thigh
9. Right Lower Leg
10. Left Thigh
11. Left Lower Leg
12. Right Knee
13. Left Knee
14. Right Foot
15. Left Foot
16. Right Hip
17. Left Hip
18. Right Shoulder Joint
19. Left Shoulder Joint
20. Right Elbow
21. Left Elbow
22. Right Hand
23. Left Hand
24. Neck
25. Right Shoulder
26. Left Shoulder

82 01003 28

Figure 15. Occupant contact surfaces

TABLE 4. BODY CONTACT SURFACE RADII (IN.)

Contact Surface	50th-Percentile Aircrewmember (scaled from manikin)	Part 572 Dummy (scaled from drawing)
Lower Torso	4.00	4.50
Upper Torso	5.00	4.50
Neck(1)	2.00	2.00
Head(2)	3.75	3.44
Upper Arm	2.10	1.95
Lower Arm	1.65	1.85
Upper Leg	3.28	3.10
Lower Leg	2.23	2.30
Hip(3)	3.56	3.56
Shoulder(4)	2.00	2.00
Foot	1.60	1.60

(1) Neck circumference divided by 2π.
(2) Head length (anterior-posterior).
(3) Hip breadth (sitting)/2 - hip link length (L_H).
(4) Shoulder breadth/2 - shoulder link length (L_S).

2.5.5 Joint Rotation

The results of several studies on the limits of human joint motion have been published. Two of these studies, in particular, were examined for applicability to the occupant model. First of all, Dempster's (reference 10) data on link lengths and inertial properties were used, as discussed in preceding sections, so it was considered appropriate to include his joint data here. Glanville and Kreezer (reference 11) presented limits of joint motion for both voluntary and forces rotation; their results appear, along with Dempster's, in table 5. Definitions of the various joint motions are illustrated in figure 17. Also included in table 5 are the rotations required for the Part 572 anthropomorphic dummy.

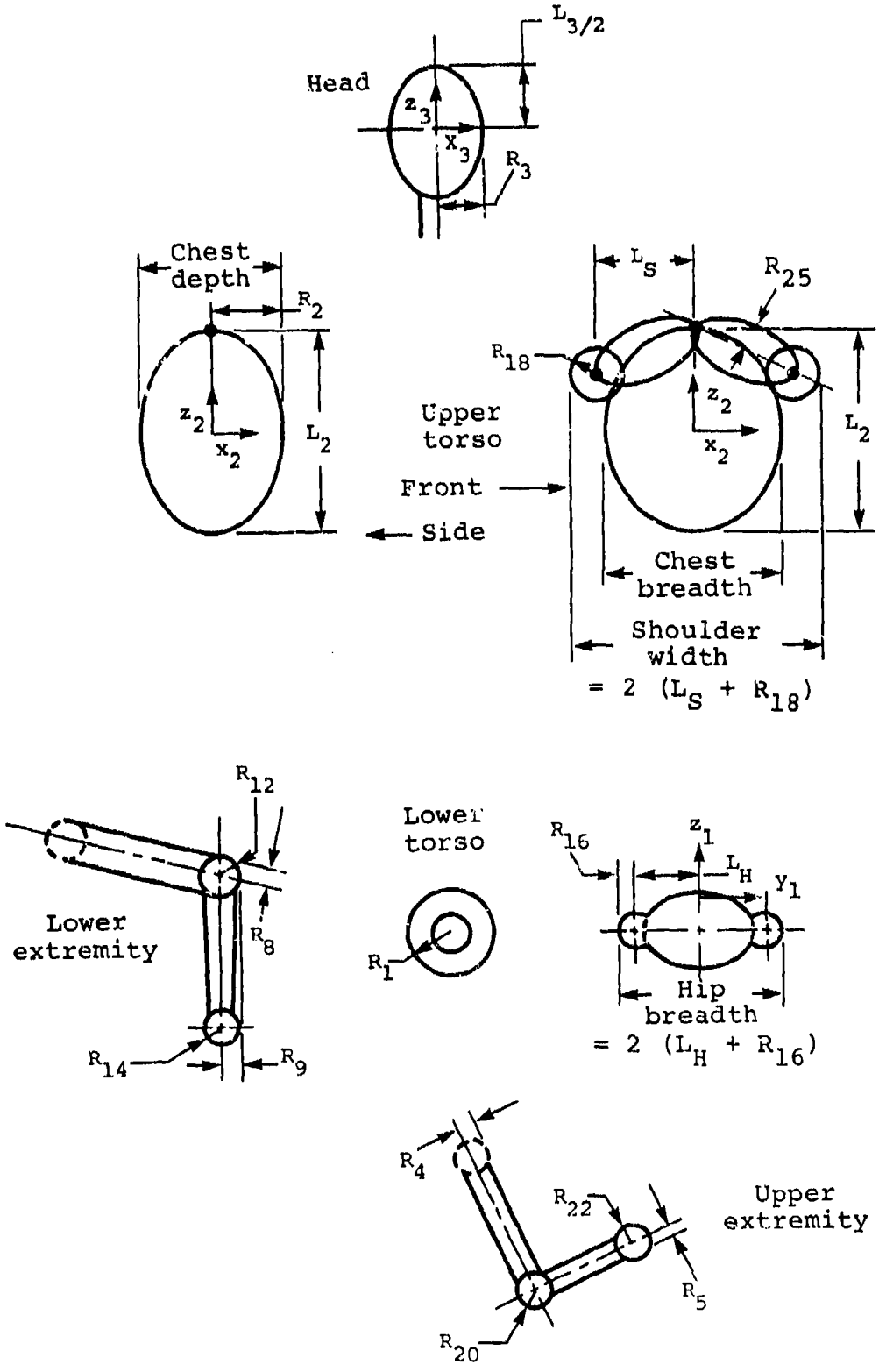

Figure 16. Body contact surface dimensions.

TABLE 5. RANGE OF JOINT ROTATION

Body Component Motion	Symbol	Motion Description	Measured Rotation - Deg: Human: Glanville and Kreezer[11] Voluntary	Human: Glanville and Kreezer[11] Forced	Human: Dempster[10]	Part 572 Dummy
Head - With Respect to Torso	A	Dorsiflexion	61	77	-	60
	B	Ventriflexion	60	76	-	60
	C	Lateral Flexion	41	63	-	40
	D	Rotation	78	63	-	70
Upper Arm - At Shoulder	E	Abduction (Coronal Plane)	130	137	134	135
	F	Flexion	180	185	188	180
	G	Hyperextension	58	69	61	60
Forearm - At Elbow	H	Flexion	141	146	142	135
Thigh - At Hip	I	Flexion	102	112	113	120
	J	Hyperextension	45	54	-	45
	K	Medial Rotation	-	-	39	50
	L	Lateral Rotation	-	-	34	50
	M	Adduction	-	-	31*	10
	N	Abduction	71	79	53*	50
Lower Leg - At Knee	P	Flexion	125	138	125	135
Long Axis of Torso	Q	Flexion	-	-	-	40
	R	Hyperextension	-	-	-	30
	S	Lateral Flexion	-	-	-	35
	T	Rotation	-	-	-	35

*Transverse plane.

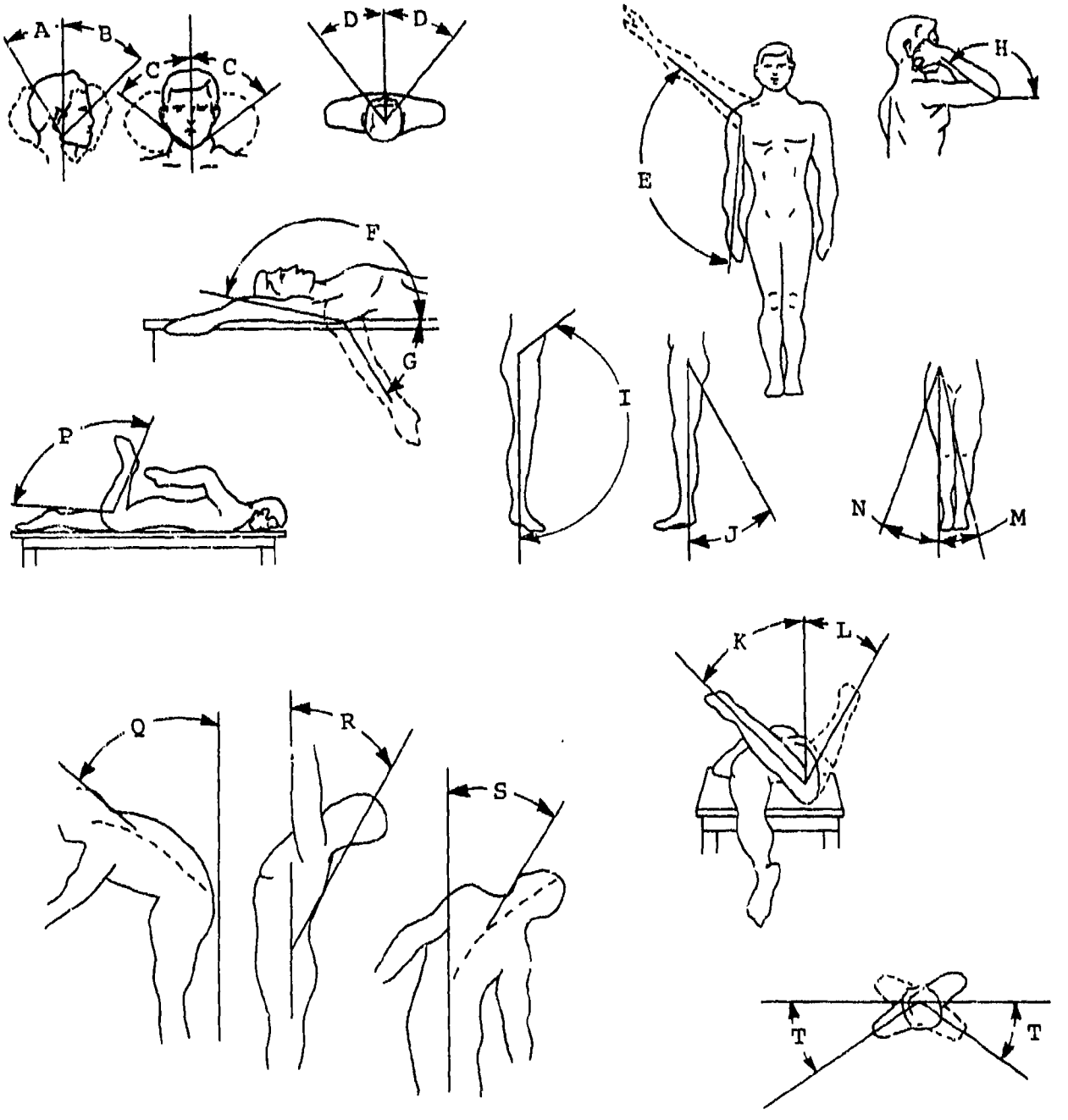

Figure 17. Motion diagrams.

All of the rotations possible in the mathematical model are included in table 5 and figure 17, but some are, naturally, more important than others in determining permissible ranges of motion for the model. For the head, ventriflexion (B) is certainly the most important component of motion for frontal impact. Dorsiflexion (A) may also be important for frontal impact, but the angles reported are sufficiently close to those for ventriflexion to be considered the

same. Laterial flexion (C) is certainly less important since a pure lateral impact of an aircraft would be rare indeed, and rotation (D) will have an insignificant effect on model response. Therefore, the limiting rotation β_{S_i} (see section 2.3) for the neck joint (i = 2) has been taken as the limit for voluntary ventriflexion, or 60 degrees. This angle can be found in table 6, along with the limiting angles for the other body joints. For all of the other angles, flexion is the most significant component for the type of motion that can usually be expected to take place in a crash environment. Therefore, the limiting angles were all taken as the limits for voluntary flexion. Note that, for the hip joint, the reference position of the body used in the mathematical model includes 90-degree flexion. Therefore, this amount has been subtracted from the angle reported in table 5, which is defined relative to the standard anatomical reference position. Since the seated position appears to aid in flexion of the hip joint, the largest angle in the table, the one given by the Part 572 specifications, was used in determining β_{S_7} which is thus given by $\beta_{S_7} = 120° - 90° = 30°$.

TABLE 6. JOINT LIMITING ANGLES

Joint	Location	Angle - β_{S_i} (deg)
1	Back	40
2	Neck	60
3, 5	Shoulder	180
4, 6	Elbow	142
7, 9	Hip	30
8, 10	Knee	125

2.5.6 Body Stiffnesses

The lumbar spine and neck of the two-dimensional model possess exponential stiffness characteristics, in the form of equation (40), for both axial and rotational deformation. Exponential stiffness characteristics for the abdomen and chest are used to soften the input force-deflection values for the lap belt and shoulder belt, respectively.

3.0 SEAT MODEL

The seat structure is modeled using the finite element method of analysis. This method has been selected because it is not reliant on previous testing, and it has the flexibility to deal with a wide range of design concepts. The specific finite element formulation used in the program is based on the WRECKER II program, developed at the ITT Research Institute (reference 12).

Program SOM-TA seat analysis uses three-dimensional beam elements. It has the capability to model large displacements, nonlinear material behavior, local buckling, and various end release conditions for beam elements. The large displacement formulation separates the element displacement field into a rigid body rotation and translation associated with a local coordinate system that moves with the element and small element distortions relative to the current position of the element coordinate system. This formulation can accommodate extremely large rotations and deflections with accuracy depending on the size of the elements relative to the curvature of the structure. Nonlinear material formulation is based on a uniaxial elastic-plastic stress-strain law. Beam end release conditions include axial load, shear, moment, and torque releases. Also, a simple local buckling model for thin-walled tubes subjected to axial compressive and/or bending loads was incorporated into the program. This model simulates the reduction in bending rigidity of the tube as the cross section distorts during local buckling.

3.1 SOLUTION PROCEDURE

The solution procedure is based on formulation of equations of quasi-static equilibrium for the finite element model in an incremental form according to

$$\underline{K}_T \, (\bar{u}_{i+1} - \bar{u}_i) = \bar{F}^E_{i+1} - \bar{F}^I_i \qquad (60)$$

where $\underline{K}_T$ = Tangent stiffness matrix

$\bar{F}^E_{i+1}$ = The vector of external applied loads at $i+1^{th}$ solution time step.

$\bar{F}^I_i$ = The vector of internal forces associated with element deformations at i^{th} solution time step.

$\bar{u}_i$ = Displacements/rotations at i^{th} solution time step.

The external forces, $\bar{F}^E$, including restraint system loads, occupant loads on the seat pan and seat back, and seat support reactions are treated as static loads on the seat structure. The mass of the seat structure is neglected, since in most simulations it will be a small percentage of the total occupant weight, and the seat structure is assumed to be in a quasi-static equilibrium with the applied external forces $\bar{F}^E$.

The tangential stiffness matrix $\underline{K}_T$ depends on the state of stress of the seat structure and varies with time during the simulation. Therefore, it must be recomputed, assembled and inverted at selected time steps during the solution. The major computational effort is the inversion of $\underline{K}_T$, which requires NB^2 multiplications where B is the semibandwidth and N is the number of degrees of freedom.

3.2 BEAM ELEMENT FORMULATION

Large displacement formulation separates the beam element displacement field into rigid body rotation and translation and small element distortion relative to the current position of the element coordinate system. After the rigid body motion is removed, it is possible to use the classical small deformation finite element formulations. Consequently, extremely large rotations and translations can be accommodated with accuracy depending on the size of the elements relative to the deformed curvature of the structure.

The beam element is based on the conventional small-deflection formulation involving cubic displacement fields for transverse displacements and linear displacements for axial and torsional displacements.

From the principle of virtual work, the general form of the beam element tangent stiffness matrix (reference 12) is given by

$$\underline{K}_T = \int_V \underline{D}^T \underline{C}\, \underline{D}\, dV \tag{61}$$

where $\underline{K}_T$ = Element tangent stiffness matrix

$\underline{D}$ = Matrix that relates element strains to nodal displacements

$\underline{C}$ = Constitutive matrix that relates stresses and strains.

For linear elastic beams, the form of the equation given in equation (61) results in the classical 12 x 12 elastic beam stiffness matrix shown in figure 18.

Where

A = area of cross section

E = modulus of elasticity

I = moment of inertia

G = modulus of rigidity

J = torsion constant

L = length of member

M_{x_i}, (M_{y_i}), (M_{z_i}) = moment about x, (y), (z) at node i

F_{x_i}, (F_{y_i}), (F_{z_i}) = force in x, (y), (z) direction at node i

θ_{x_i}, (θ_{y_i}), (θ_{z_i}) = rotation about x, (y), (z) axis at node i

u_{x_i}, (v_{y_i}), (w_{z_i}) = x, (y), (z) component of displacement at node i

For nonlinear materials the constitutive matrix $\underline{C}$ is given by

$$\underline{C} = \frac{\Delta\sigma}{\Delta\varepsilon} \tag{62}$$

where $\Delta\sigma$ = incremental stress

$\Delta\varepsilon$ = incremental strain.

Using the cubic shape functions for the transverse displacements and linear shape functions for axial and torsional displacements in matrix $\underline{D}$ it can be shown that (reference 12)

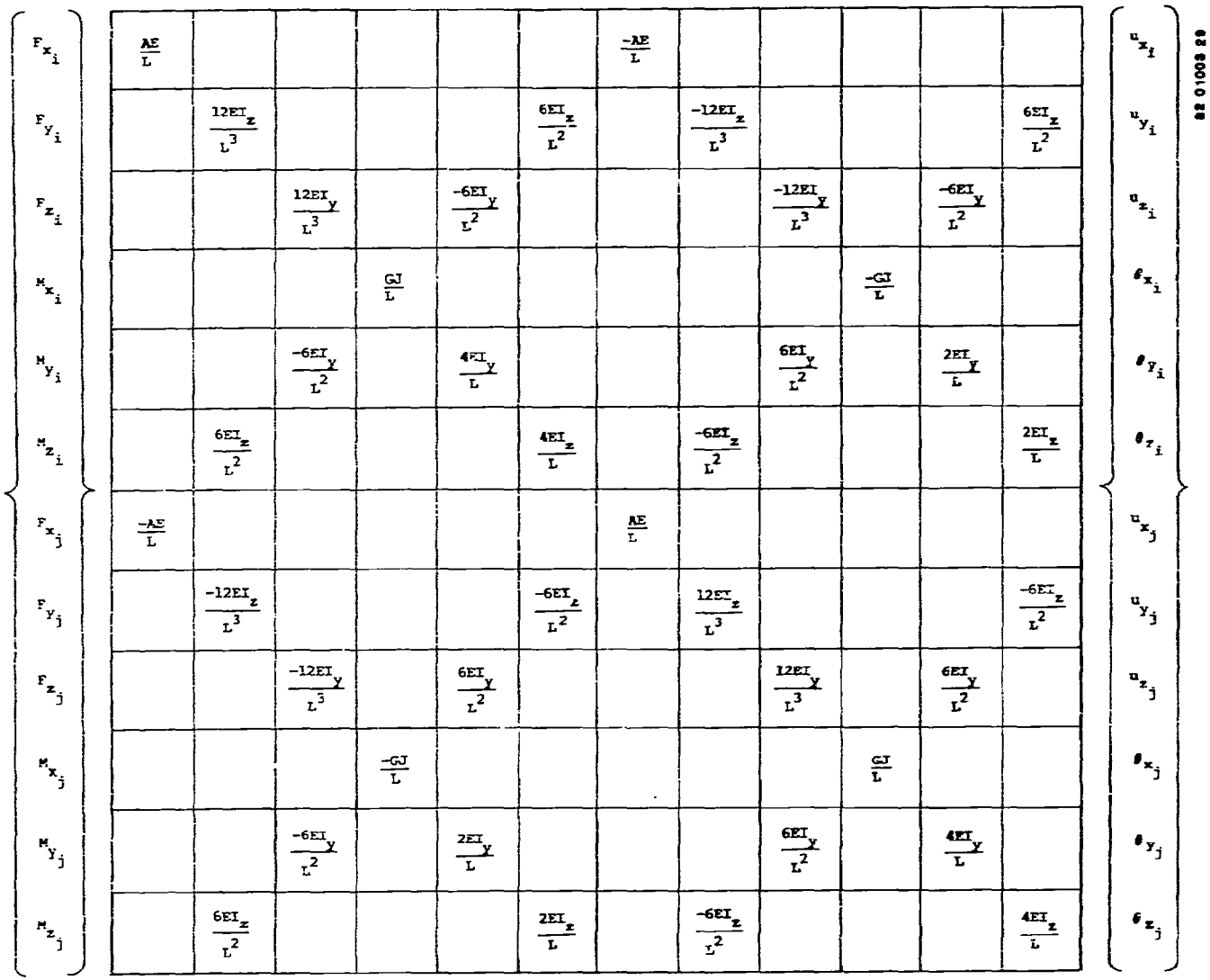

F_{x_i}	$\frac{AE}{L}$						$\frac{-AE}{L}$					u_{x_i}
F_{y_i}		$\frac{12EI_z}{L^3}$				$\frac{6EI_z}{L^2}$		$\frac{-12EI_z}{L^3}$				$\frac{6EI_z}{L^2}$	u_{y_i}
F_{z_i}			$\frac{12EI_y}{L^3}$		$\frac{-6EI_y}{L^2}$				$\frac{-12EI_y}{L^3}$		$\frac{-6EI_y}{L^2}$		u_{z_i}
M_{x_i}				$\frac{GJ}{L}$						$\frac{-GJ}{L}$			θ_{x_i}
M_{y_i}			$\frac{-6EI_y}{L^2}$		$\frac{4EI_y}{L}$				$\frac{6EI_y}{L^2}$		$\frac{2EI_y}{L}$		θ_{y_i}
M_{z_i}		$\frac{6EI_z}{L^2}$				$\frac{4EI_z}{L}$		$\frac{-6EI_z}{L^2}$				$\frac{2EI_z}{L}$	θ_{z_i}
F_{x_j}	$\frac{-AE}{L}$						$\frac{AE}{L}$						u_{x_j}
F_{y_j}		$\frac{-12EI_z}{L^3}$				$\frac{-6EI_z}{L^2}$		$\frac{12EI_z}{L^3}$				$\frac{-6EI_z}{L^2}$	u_{y_j}
F_{z_j}			$\frac{-12EI_y}{L^3}$		$\frac{6EI_y}{L^2}$				$\frac{12EI_y}{L^3}$		$\frac{6EI_y}{L^2}$		u_{z_j}
M_{x_j}				$\frac{-GJ}{L}$						$\frac{GJ}{L}$			θ_{x_j}
M_{y_j}			$\frac{-6EI_y}{L^2}$		$\frac{2EI_y}{L}$				$\frac{6EI_y}{L^2}$		$\frac{4EI_y}{L}$		θ_{y_j}
M_{z_j}		$\frac{6EI_z}{L^2}$				$\frac{2EI_z}{L}$		$\frac{-6EI_z}{L^2}$				$\frac{4EI_z}{L}$	θ_{z_j}

Figure 18. Elastic three-dimensional beam stiffness matrix.

$$\underline{K}_T = \frac{1}{\ell^4} \int_0^{\ell} \begin{bmatrix} \alpha\ell^2 & -\beta_z \ell f_2 & \beta_y \ell f_2 & -\beta_z \ell f_1 & \beta_y \ell f_1 \\ & \delta_z f_2^2 & -\delta_x f_2^2 & \delta_z f_3 & -\delta_x f_3 \\ & & \delta_y f_2^2 & -\delta_x f_3 & \delta_y f_3 \\ & & & \delta_z f_1^2 & -\delta_x f_1^2 \\ & & & & \delta_y f_1^2 \end{bmatrix} d \qquad (63)$$

where ℓ = element length

$$f_1 = 6x - 2\ell$$

$$f_2 = 6x - 4\ell$$

$$f_3 = f_1 f_2$$

$$\alpha = \int_A \frac{\Delta\sigma}{\Delta\epsilon}\, dA$$

$$\beta_y = \int_A y \frac{\Delta\sigma}{\Delta\epsilon}\, dA, \quad \beta_z = \int_A z \frac{\Delta\sigma}{\Delta\epsilon}\, dA$$

$$\delta_x = \int_A yz \frac{\Delta\sigma}{\Delta\epsilon}\, dA, \quad \delta_y = \int_A y^2 \frac{\Delta\sigma}{\Delta\epsilon}\, dA,$$

$$\delta_z = \int_A z^2 \frac{\Delta\sigma}{\Delta\epsilon}\, dA \qquad (64)$$

The integrals defined in equations (**63**) and (**64**) are calculated numerically through the cross section and along the length of the beam element. The integration is piecewise linear through the depth and linear along the length.

Once the element stiffness matrices have been evaluated, it is necessary to assemble each matrix to some global system. To accomplish this, an element coordinate system $(\hat{x}, \hat{y}, \hat{z})$ is attached to each beam element and serves to define the rigid body rotation and translation of the element. The orientation of element axes $(\hat{x}, \hat{y}, \hat{z})$ with respect to the global axes at any time is established by the components of three vectors $\bar{e}_1$, $\bar{e}_2$, $\bar{e}_3$ which remain fixed along the element axes $(\hat{x}, \hat{y}, \hat{z})$, respectively, as the element translates and rotates. If these three unit vectors $\bar{e}_1$, $\bar{e}_2$, $\bar{e}_3$ form the columns of a 3 x 3 matrix $\underline{E}$, then any vector $\bar{v}$ can be transformed from element to global coordinate system by the following time dependent transformation:

$$\bar{v}_G = \underline{E}\, \bar{v}_E \tag{65}$$

For beam elements (figure 19), the x-axis is defined by a line connecting the end points of the beam, and the y-axis, by a line normal to the x-axis and lying in a plane containing both the coordinate reference point and x-axis. The remaining z-axis is determined as a normal to x- and y-axes by the righthand rule.

Also accounted for in the transformation between the local and global systems is the offset of the beam end nodal point from the beam cross-section centroid and shear center (figure 19b). This transformation is particularly important for open beam cross-sections where the centroid and the shear center do not coincide. The appropriate transformation for the beam end, consistent with the beam kinematic assumptions, can be written as:

$$\begin{Bmatrix} u_i \\ v_i \\ w_i \end{Bmatrix} = \begin{bmatrix} 1 & 0 & 0 & 0 & -(z_n - z_{cg}) & +(y_n - y_{cg}) \\ 0 & 1 & 0 & z_n & 0 & 0 \\ 0 & 0 & 1 & -y_n & 0 & 0 \end{bmatrix} \begin{Bmatrix} u_{n_i} \\ v_{n_i} \\ w_{n_i} \\ \beta_{x_i} \\ \beta_{y_i} \\ \beta_{z_i} \end{Bmatrix} \tag{66}$$

where u_i, v_i, w_i = Displacements at the shear center in beam local x, y, and z directions.

u_{n_i}, v_{n_i}, w_{n_i} = Displacements at the node point in beam local x, y, and z directions.

β_{x_i}, β_{y_i}, β_{z_i} = Cross-section rotations about beam local x, y, and z axes.

y_n, z_n = Distance between the shear center and the node point (see figure 19b).

y_{cg}, Z_{cg} = Distance between the shear center and the centroid.

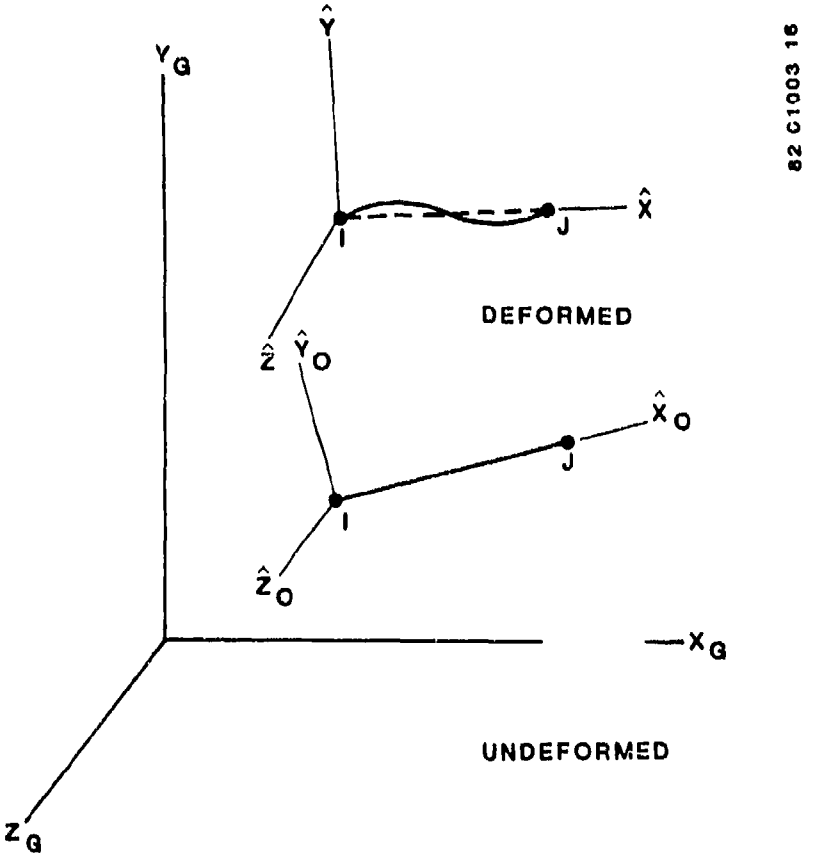

a) Element coordinate system

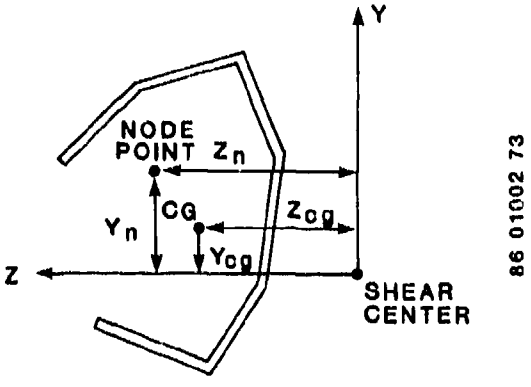

b) Cross-section geometry

Figure 19. Three-dimensional beam element coordinate system and cross-section geometry.

3.3 INTERNAL RELEASES IN BEAM ELEMENTS

The program allows the use of "end releases" in beam elements. The beam end release conditions include axial load, shear, moment, and torque releases at the end nodes. Combinations of these releases are possible, e.g., a ball joint is formed by releasing moments in three different directions.

Depending on the direction of the end release, the original beam element stiffness matrix is modified as follows:

$$\underline{K}_e \, \bar{\Delta}_e = \bar{F}_e \tag{67}$$

where $\underline{K}_e$ = Element stiffness matrix

Δ_e = Element end displacements/rotations

$\underline{F}_e$ = Element end forces/moments

Rewriting equation (67) as

$$\begin{bmatrix} \underline{K}_{FF} & \underline{K}_{FR} \\ \underline{K}_{RF} & \underline{K}_{RR} \end{bmatrix} \quad \begin{Bmatrix} \bar{\Delta}_F \\ \bar{\Delta}_R \end{Bmatrix} = \begin{Bmatrix} \bar{F}_F \\ \bar{0} \end{Bmatrix} \tag{68}$$

where $\bar{\Delta}_F$ = Fixed end displacements

$\bar{\Delta}_R$ = Released end displacements

$\bar{F}_F$ = Fixed end forces/moments

From equation (68)

$$\underline{K}_{FF} \, \bar{\Delta}_F + \underline{K}_{FR} \, \bar{\Delta}_R = \bar{F}_F \tag{69}$$

$$\underline{K}_{RF} \, \bar{\Delta}_F + \underline{K}_{RR} \, \bar{\Delta}_R = 0 \tag{70}$$

Solving for $\bar{\Delta}_R$ from equation (70) and substituting into equation (69)

$$\bar{\Delta}_R = -\underline{K}_{RR}^{-1} \, \underline{K}_{RF} \, \bar{\Delta}_F$$

$$\left[\underline{K}_{FF} - \underline{K}_{FR} \, \underline{K}_{RR}^{-1} \, \underline{K}_{RF} \right] \bar{\Delta}_F = \bar{F}_F$$

The modified beam element stiffness matrix $\underline{K}_e^*$ is then given by:

$$\underline{K}_e^* = \begin{bmatrix} \underline{K}_{FF} - \underline{K}_{FR}\,\underline{K}_{RR}^{-1}\,\underline{K}_{RF} & 0 \\ 0 & 0 \end{bmatrix} \tag{71}$$

3.4 MATERIAL NONLINEARITIES

Nonlinear material formulation for beam elements is based on uniaxial elastic plastic stress-strain law.

The computational algorithm is based on the work of Hartzman and Hutchinson, (reference 14), as specialized for small strain and plane stress conditions. The current stress state at a point on the cross section of the beam is established as follows: let the prior stress state of the point under consideration be σ_x^0 and a small increment in strain from the prior state to the current state by $\Delta\epsilon_x$. First a tentative, current stress state, σ_x is calculated as though the strain increment were completely elastic.

$$\bar{\sigma}_x = \sigma_x^0 + \frac{E\Delta\epsilon_x}{1 - \gamma^2} \tag{72}$$

where E = Modulus of Elasticity

γ = Poisson's ratio

An effective stress $\bar{\sigma}_e = \bar{\sigma}_x$ is used to determine whether plastic flow has taken place during the strain increment. If $\bar{\sigma}_e$ is less than the prior effective stress σ_e^0 at which yielding occurred, elemental loads are decreasing and the tentative stress calculated $\bar{\sigma}_x$ is the correct value of the current stress σ_x. If $\bar{\sigma}_e$ is greater than the prior effective stress σ_e^0, at which yielding occurred, tentative stresses calculated must be modified to account for the plastic behavior. Hartzman and Hutchinson (reference 14) have shown that the true value of the current effective stress will be:

$$\sigma_e = \frac{\sigma_e^{\,o} + \left(\frac{H'}{3G}\right)\bar{\sigma}_e}{1 + \left(\frac{H'}{3G}\right)} \qquad (73)$$

where $$H'_i = \frac{(E)(E_{pi})}{E - E_{pi}} \qquad i = 1,2$$

and E_{pi} = Plastic modulus (figure 20)

G = Shear modulus

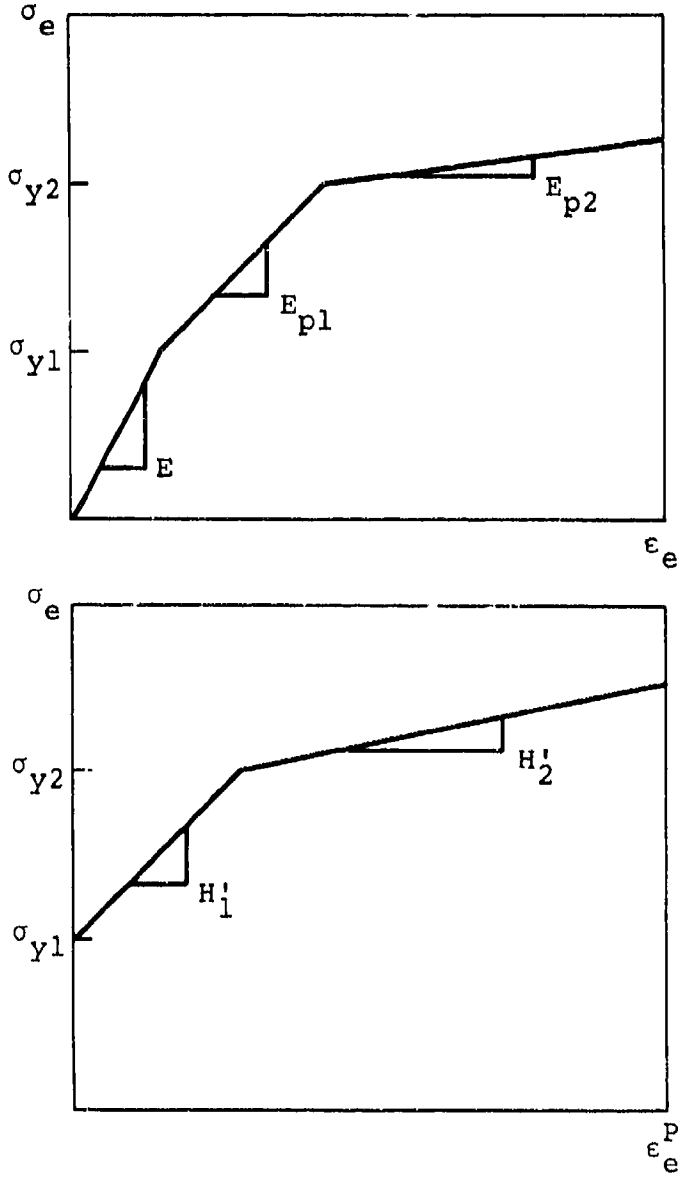

82 01003 18

Figure 20. Trilinear stress-strain relation.

The current state of stress is then given by

$$\sigma_x = \frac{1 + \lambda}{1 + 3\lambda} \bar{\sigma}_x \qquad (74)$$

where $$\lambda = \frac{1}{3} \left(\frac{\bar{\sigma}_e}{\sigma_e} - 1 \right)$$

3.5 LOCAL BUCKLING OF BEAM ELEMENTS

Local buckling is one of the failure modes of thin-walled tubes, typically used in light aircraft seats, when subjected to axial compressive and/or bending loads. Evaluation of the results of dynamic tests of seat-occupant systems have indicated that the local buckling of thin-walled tubes have a significant effect on the response of the seat-occupant system. Therefore, a simple local buckling model for thin-walled tubes was incorporated into the program.

Local buckling is traditionally expressed in terms of a moment-bending curvature diagram as shown in figure 21.

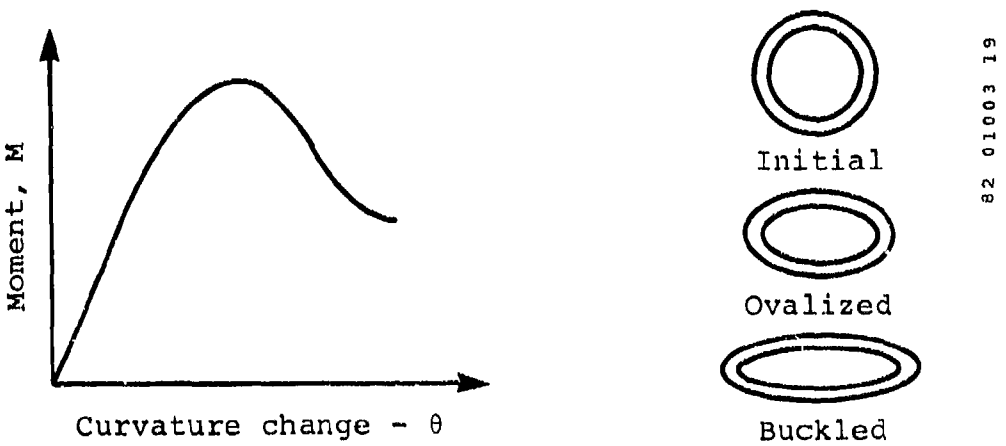

Figure 21. Moment capability versus curvature of a thin-walled circular tube.

The cross section goes through several stages of deformation as the structure bends. Although during this cross-section distortion axial stresses redistribute themselves, it was proposed in reference 15 that the reduced bending rigidity is most strongly related to the loss of lateral moment arm of the axial forces.

For a circular tube under uniform compression the stress, σ_L, at which local buckling starts is given in reference 16 as

$$\sigma_L = K_c E\left(\frac{t}{D}\right) \tag{75}$$

where $0.4 < K_c < 1.2$ (recommended values)

E = modulus of elasticity

t = wall thickness of the tube

D = diameter of the tube.

It was also proposed in reference 16 that for tubes subjected to bending, the local buckling stress, σ_L, as a function of material and geometry, can be taken as that for a circular tube under uniform axial compression, since in bending, a significant portion of the circumference is subjected to a relatively uniform compression field. However, dynamic tests of seat-occupant systems have indicated that the thin-walled circular tubes have suffered local buckling at stress levels much below that predicted by equation (75). This was partly due to the fact that the bending stresses have exceeded the yield point and the tubes have also suffered plastic deformation.

To account for plasticity as well as cross-sectional properties, an empirical relation, equation (76) was used in he program to predict the local-buckling stress

$$\sigma_L = \text{Minimum} \left\{ \begin{array}{c} 0.4\ E\ (t/D) \\ \\ \sigma_y \end{array} \right\} \tag{76}$$

where σ_L = local buckling stress

σ_y = compressive yield stress

t = wall thickness of the tube

D = diameter of the tube.*

The cross sections of beam elements are defined as thin-walled plate segments by specifying their end points and thickness as part of the input data (figure 22). The tangent stiffness matrix for nonlinear beam elements is then computed by evaluating the integrals given in equation (66) over the plate segments defining the beam cross section.

The program computes the stresses at all segment end points across the cross section at each end of the beam elements. These stresses are then compared with the local buckling stress, σ_L, computed from equation (76) for each beam element. If any of the compressive stresses at the segment end points exceed σ_L, the deformation of the cross section is modeled by modifying the radial location of that segment end point using the following expression

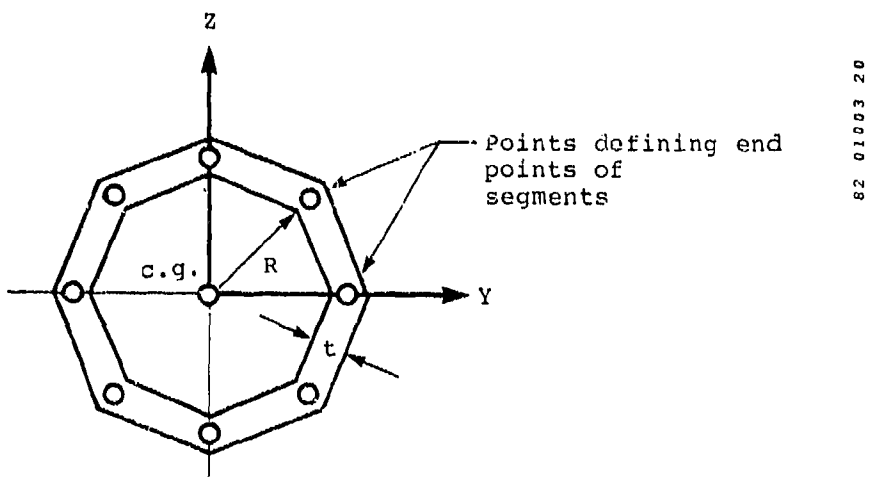

Figure 22. Circular tube cross section defined by eight thin-walled plate segments.

*For rectangular tubes the diameter of a circumscribing circular tube is used.

$$R_{i+1} = \left(\frac{\sigma_L}{\sigma_{i+1}}\right)^K R_i \quad \text{if} \quad |\sigma_{i+1}| > \sigma_L \tag{77}$$

where R_i = radial location of the Gaussian station at time step i

σ_L = local buckling stress

σ_{i+1} = compressive stress at the segment end point at time step i+1

K = local buckling constant (0.50 recommended).

Consequently, reduced bending rigidity of the cross section due to the decrease in the lateral moment arm of axial forces during local buckling can be modeled.

4.0 SIMULATION COMPUTER PROGRAM

The digital computer program based on the occupant and seat models described in sections 2 and 3 is called Seat/Occupant Model - Transport Aircraft (SOM-TA). It has been written entirely in FORTRAN to ensure a high degree of compatibility with various digital computer systems. During development, the program has been run on IBM and Digital computer systems.

The elements of the program can be considered in terms of three general operations:

- Input and initialization
- Solution
- Output

which are summarized below and discussed in detail in the sections following. The general flow of the program is illustrated in figure 23. Input data describing the occupant and crash conditions are read first. Finally, the seat data, either simple dimensions describing a rigid seat model or detailed design data for the finite element seat analysis, are provided. Based on the input data, the values of constants, such as occupant dimensions and properties are calculated, and the initial position of the occupant is determined.

The solution loop is entered for the first time with the aircraft initial velocity and the occupant initial position. At each subsequent entrance to the loop, the current aircraft displacement, velocity, and acceleration components are calculated. The equations of motion for the occupant are set up and solved. If a finite element seat model is being used, the forces applied to the seat, such as the cushion forces, are provided to the seat routines for computation of seat displacements. At time increments equal to a predetermined print interval, the output variables requested by the user are stored for printing after completion of the solution.

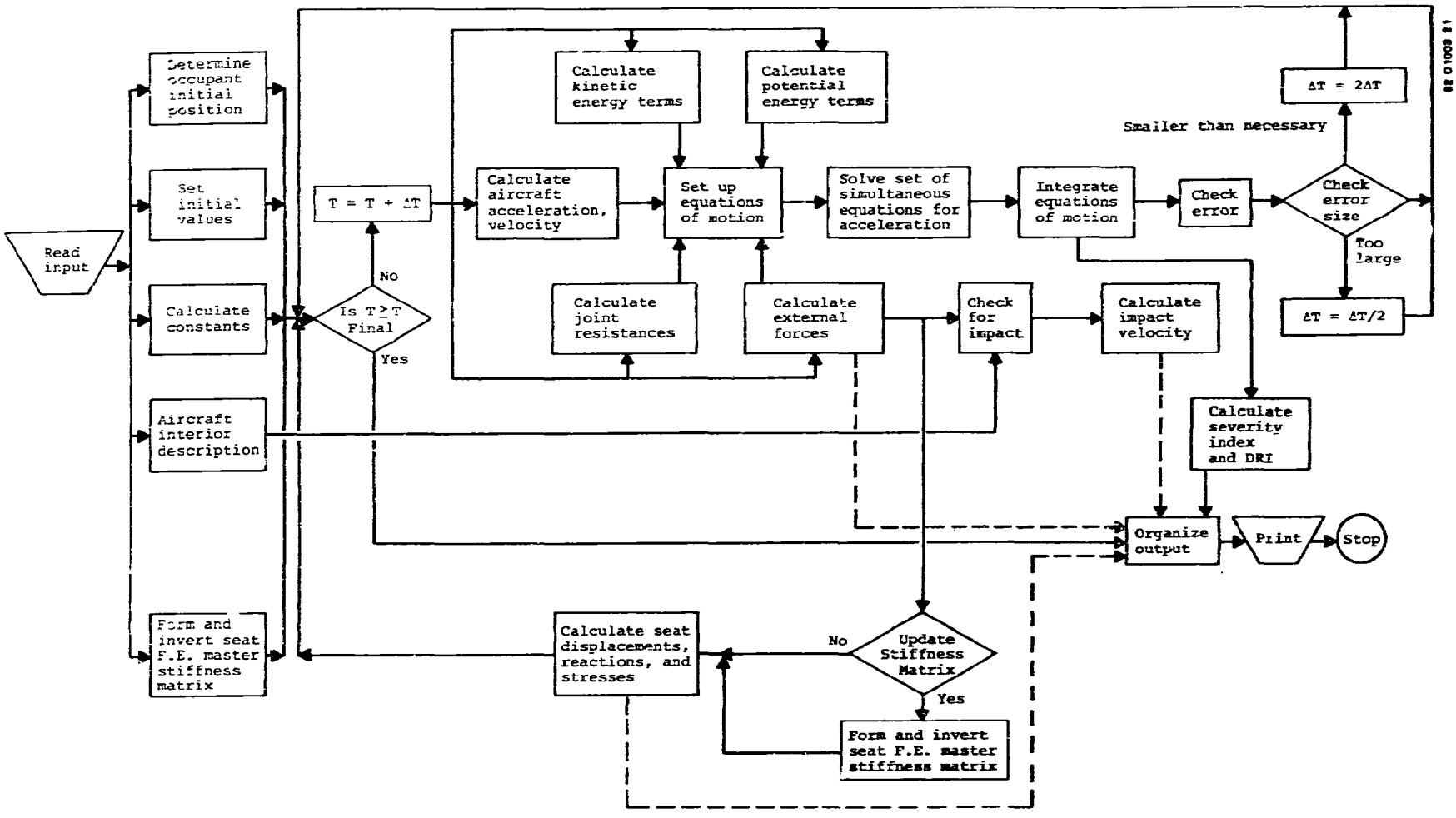

Figure 23. Program flow chart.

4.1 PROGRAM INPUT

Input data are read by the program in the following six blocks:

1. Simulation and output control information
2. Cushion properties
3. Restraint system description
4. Crash conditions
5. Occupant description
6. Seat design information.

4.1.1 Simulation Control Information

The first block of data contains the information required for controlling execution of the program. The selection of system of units (SI or English), two- or three-dimensional occupant, the type of seat (single-, double-, or triple-occupant) along with identification of the positions that are occupied, secondary impact information (if desired), total simulation time, and identification of desired output, are provided here.

4.1.2 Cushion Description

Cushion load-deflection characteristics are described by an exponential function, whose coefficients are provided as input data. The equilibrium (zero load) thickness for both the seat and back cushions are also given. The cushion damping coefficient for zero deflection described in section 2.4.1 is also entered.

4.1.3 Restraint System Description

The restraint system used in the simulation may consist of a lap belt alone or combined with a single- or double-strap shoulder harness. The webbing force-elongation curve is approximated by three linear segments, which are described

by input of points on the curve. The force is computed by linear interpolation in this table, as described in section 4.3.1. The slack in the webbing is also provided by input in units of length.

The anchor points for the lap belt and shoulder harness are located by input of rectangular coordinates in the aircraft reference system. For a double-strap shoulder harness, the buckle, or point of connection to the lap belt, is assumed located on the mid-point of the lap belt. For a single shoulder belt, which may pass over either the left or the right shoulder, an input parameter locates the buckle by the length of webbing between the buckle and the lap belt anchor point. This length may be zero if the buckle attaches directly to a rigid anchor point.

4.1.4 Crash Conditions

The aircraft crash conditions are defined by the initial velocity and attitude and the acceleration as a function of time. Six components of velocity are required: three translational in the aircraft coordinate system (V_{X_A}, V_{Y_A}, V_{Z_A}) and the yaw, pitch, and roll rates ($\dot{\psi}_A$, $\dot{\theta}_A$, $\dot{\phi}_A$). Each of the six acceleration components, which define the acceleration of the aircraft coordinate system, is described by sixteen points in time and acceleration. An example of an approximation to an actual acceleration pulse is illustrated in figure 24. Although many of the higher frequency oscillations observed in the actual pulse probably contribute little to the overall response of the occupant, the use of a large number of points reduces the effect of the investigator's subjectivity in the approximation.

4.1.5 Occupant Description

Because it has been assumed that the principal user of this program is interested primarily in the seat or restraint system, a minimum of information is required to describe the occupants. Data for standard human and dummy occupants, as described in section 2.5, are stored within the program. Additional data must be provided for nonstandard occupants.

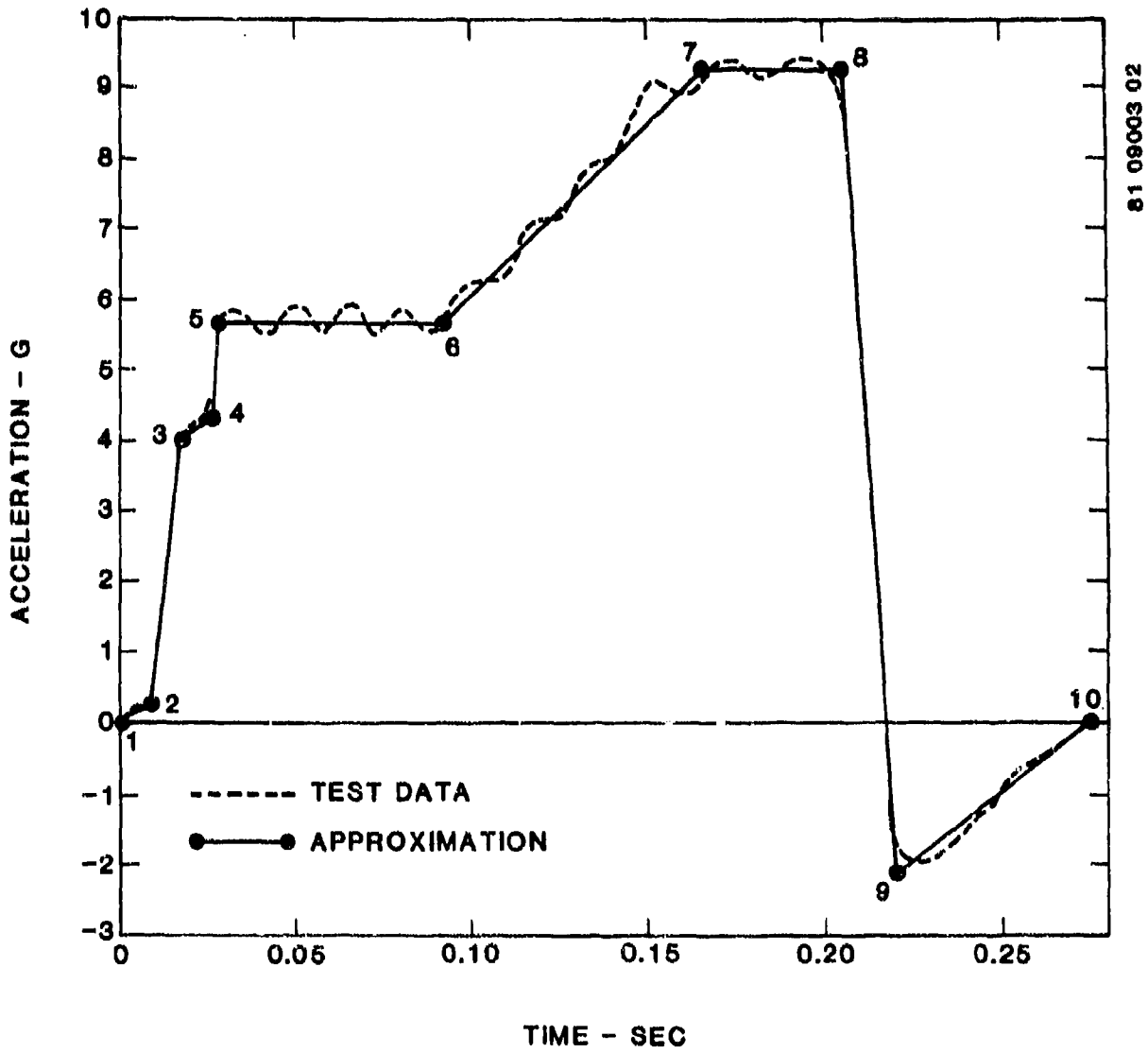

Figure 24. Piecewise approximation to aircraft acceleration component.

4.1.6 Seat Design Information

The input data required to describe the seat consist of nodal coordinates, material properties, cross-section geometries, element locations, and attachment conditions, as described earlier. For possible use in restraint system analyses where detailed seat response may not be important or seat design

unknown, a rigid seat model can be selected. Input data for the rigid seat option consist only of locations of the seat pan and seat back.

4.1.7 Seat Back Contact Surfaces

If contact between the occupants and the back of the seat row in front of them is to be simulated, input data are required to define the dimensions of the surfaces illustrated in figure 25. Additional data are then required to specify the force-deformation characteristics of these surfaces, which represent cushion, tray table, and armrest surfaces.

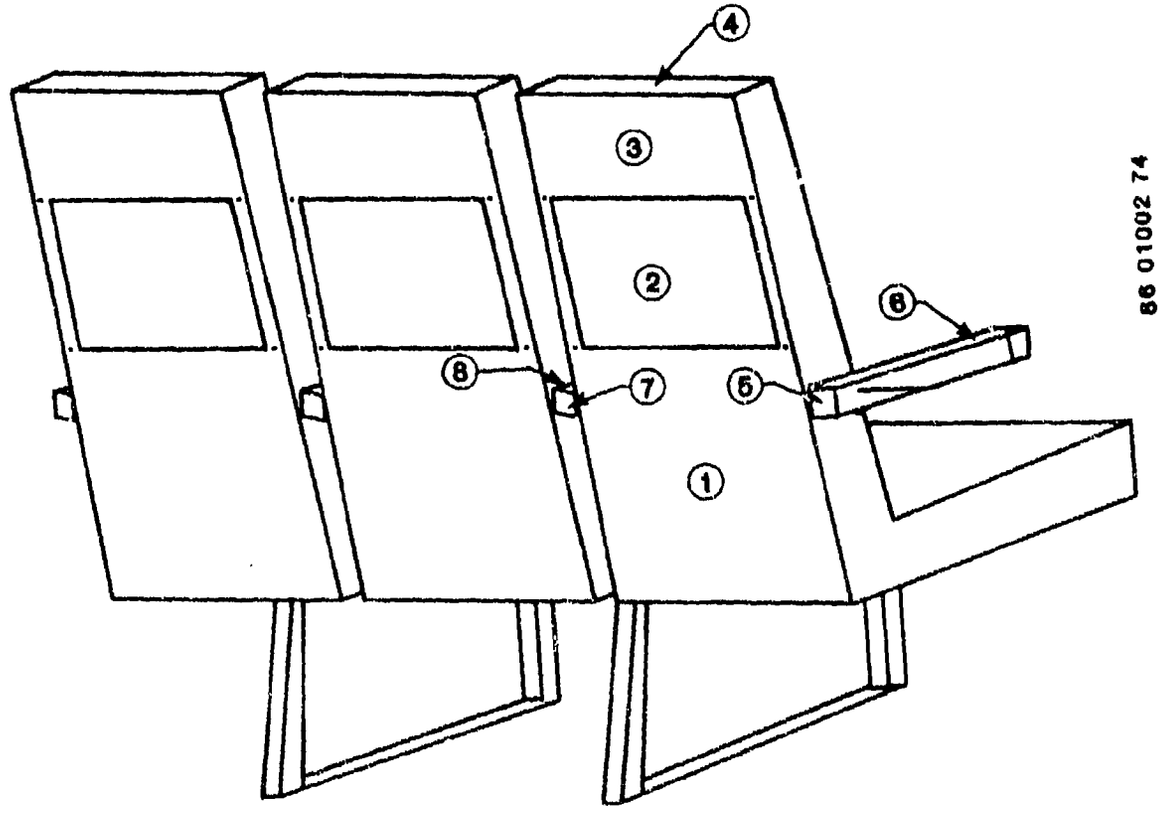

Figure 2.. Seat back contact surfaces.

4.2 OCCUPANT INITIAL POSITION

The initial position of the aircraft occupant is computed from the input parameters shown in figure 25. The occupant is seated at Y-coordinate of the mid-plane (plane of symmetry) for each occupant as specified in the input data. The angular coordinates γ_i ($i = 1, 2, 3, 4$) define the rotation of segments 1-4 relative to the Z_A axis and, because of the symmetry condition, segment 6 is parallel to segment 4. Positive angles are shown in figure 26 although γ_1 and γ_2 are usually negative, considering the torso to be approximately parallel to an aftward-sloping seat back. The angle γ_5 describes the position of the forearms relative to the upper arms, and is the initial value of α_5 and α_7. The distance X_H is the initial X-coordinate of the heels (the inferior ends of segments 9 and 11). The procedure described below consists of seating the occupant in such a position that static equilibrium is achieved among the forces exerted by the seat cushion, floor, and either the restraint system or the back cushion.

The first step in determining the initial position for the three-dimensional occupant involves calculating the Euler angles for the torso, head, and arm segments, since this procedure does not require consideration of the forces due to the cushions and floor. Because the input parameters illustrated in figure 25 define the position of the occupant in the aircraft coordinate system, the orientation of the aircraft must be described in the inertial system. For an aircraft in level flight with zero pitch, roll, and yaw, it is assumed that the aircraft coordinate axes (X_A, Y_A, Z_A) are parallel to the fixed coordinate axes (X, Y, Z) at the initial time ($t = 0$). A general orientation of the aircraft reference frame is obtained by the same sequence of rotations defined in section 2.1.1 for the body segments. Defining the rotations

Ψ_A: Yaw

θ_A: Pitch

Φ_A: Roll

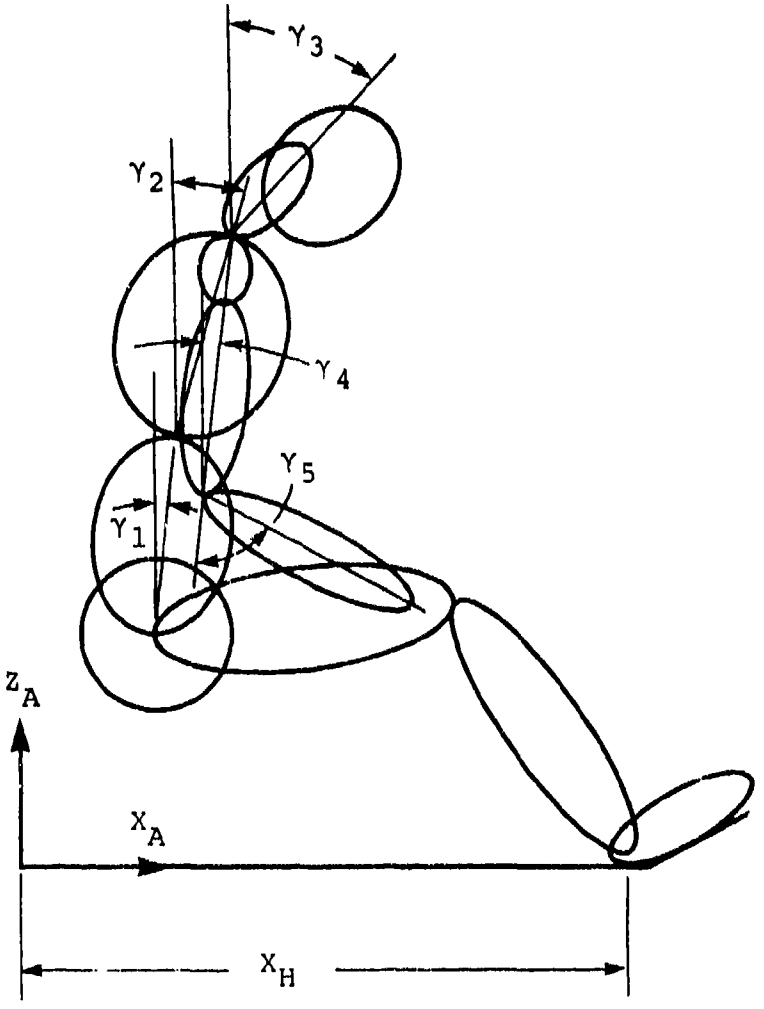

Figure 26. Initial position input parameters.

the orientation of the aircraft relative to the inertial system is described by the coordinate transformation

$$\begin{Bmatrix} X \\ Y \\ Z \end{Bmatrix} = \begin{bmatrix} \quad \\ A \\ \quad \end{bmatrix} \begin{Bmatrix} X_A \\ Y_A \\ Z_A \end{Bmatrix} \tag{78}$$

where the elements of [A] are

$$A_{11} = \cos \psi_A \cos \theta_A$$

$$A_{12} = \cos \psi_A \sin \theta_A \sin \phi_A - \sin \psi_A \cos \phi_A$$

$$A_{13} = \cos \psi_A \sin \theta_A \cos \phi_A + \sin \psi_A \sin \phi_A$$

$$A_{21} = \sin \psi_A \cos \theta_A$$

$$A_{22} = \sin \psi_A \sin \theta_A \sin \phi_A + \cos \psi_A \cos \phi_A$$

$$A_{23} = \sin \psi_A \sin \theta_A \cos \phi_A - \cos \psi_A \sin \phi_A$$

$$A_{31} = -\sin \theta_A$$

$$A_{32} = \cos \theta_A \sin \phi_A$$

$$A_{33} = \cos \theta_A \cos \phi_A \qquad (79)$$

The rotation of body segment n relative to the aircraft, remembering that the symmetry condition requires that y_n is parallel to Y_A, is described by

$$\begin{Bmatrix} X_{A_n} \\ Y_{A_n} \\ Z_{A_n} \end{Bmatrix} = \begin{bmatrix} \cos \gamma_n & 0 & \sin \gamma_n \\ 0 & 1 & 0 \\ -\sin \gamma_n & 0 & \cos \gamma_n \end{bmatrix} \begin{Bmatrix} x_n \\ y_n \\ z_n \end{Bmatrix} \qquad (80)$$

Combining equations (78) and (80) results in the angular relationship between the local coordinate system of segment n and the inertial system expressed by the following transformation, which is a function of the input γ_n and the aircraft pitch, roll, and yaw:

$$\begin{Bmatrix} X_n \\ Y_n \\ Z_n \end{Bmatrix} = \begin{bmatrix} \\ B^n \\ \\ \end{bmatrix} \begin{Bmatrix} x_n \\ y_n \\ z_n \end{Bmatrix} \tag{81}$$

where $[B^n]$ is given by

$$[B^n] = \begin{bmatrix} \\ A \\ \\ \end{bmatrix} \begin{bmatrix} \cos\gamma_n & 0 & \sin\gamma_n \\ 0 & 1 & 0 \\ -\sin\gamma_n & 0 & \cos\gamma_n \end{bmatrix} \tag{82}$$

so that its elements are

$$\begin{aligned}
B^n_{11} &= A_{11}\cos\gamma_n - A_{13}\sin\gamma_n \\
B^n_{12} &= A_{12} \\
B^n_{13} &= A_{11}\sin\gamma_n + A_{13}\cos\gamma_n \\
B^n_{21} &= A_{21}\cos\gamma_n - A_{23}\sin\gamma_n \\
B^n_{22} &= A_{22} \\
B^n_{23} &= A_{21}\sin\gamma_n + A_{23}\cos\gamma_n \\
B^n_{31} &= A_{31}\cos\gamma_n - A_{33}\sin\gamma_n \\
B^n_{32} &= A_{32} \\
B^n_{33} &= A_{31}\sin\gamma_n + A_{33}\cos\gamma_n
\end{aligned} \tag{83}$$

Comparison of equation (81) with equation (1) points out that the transformation matrices $[T^n]$ and $[B^n]$ are equivalent. Because $[T^n]$ is a function of Euler angles for segment n, equating the elements of $[T^n]$ and $[B^n]$ through

$$[T^n] = [B^n] \qquad n = 1, 2, 3, 4, 6, 8, 10 \tag{84}$$

permits calculation of the initial values of the generalized coordinates from input parameters γ_n and ψ_A, θ_A, and ϕ_A. The procedure as used in Program SOM-TA is outlined below.

First θ_n is determined as follows:

$$T^n_{31} = B^n_{31} \text{ or } -\sin\theta_n = B^n_{31}$$

which gives

$$\theta_n = \sin^{-1}(-B^n_{31}) \tag{85}$$

The cosine is then found by

$$\cos\theta_n = \cos[\sin^{-1}(-B^n_{31})]$$

so that ψ_n can be determined:

$$T^n_{11} = B^n_{11} \text{ or } \cos\psi_n \cos\theta_n = B^n_{11}$$

gives

$$\psi_n = \cos^{-1}(B^n_{11}/\cos\theta_n) \tag{86}$$

and, for determination of ϕ_n,

$$T^n_{33} = B^n_{33} \text{ or } \cos\theta_n \cos\phi_n = B^n_{33}$$

gives

$$\phi_n = \cos^{-1}(B^n_{33}/\cos\theta_n) \tag{87}$$

Equations (85) through (87) are used for segments 1, 2, 3, and 4; the symmetry requirement provides the Euler angles for segment 6, which are equal to those

for segment 4. At this point the generalized coordinates q_4 through q_{20} have been determined. The next step involves seating the occupant and calculating X_1, Y_1, and Z_1 (q_1, q_2, and q_3) from static equilibrium.*

Because the problem of seating the occupant is statically indeterminate, certain simplifying assumptions are made. The first assumption, which is approximately correct for typical seating positions, is that 15 percent of the occupant's weight is supported by the floor. In other words, 85 percent is supported by the seat cushion and, depending on the aircraft attitude, the restraint system or the back cushion.

A first approximation to the initial position is made for the assumption of level flight ($\theta_A = \psi_A = \phi_A = 0$). The cushion forces act on the body as shown in figure 27, where it is assumed that 15 percent of the occupant weight is supported by the floor, as discussed in the preceding paragraph. Summing forces gives

$$F_{X_A}: \quad F_B \cos\theta_B - F_S \sin\theta_S = 0$$

$$F_{Z_A}: \quad F_B \sin\theta_B + F_S \cos\theta_S = W' \tag{88}$$

which can be solved for the cushion forces:

$$F_S = W' \cos\theta_B / \cos(\theta_B - \theta_S)$$

$$F_B = W' \sin\theta_S / \cos(\theta_B - \theta_S) \tag{89}$$

Dimensional considerations permit the coordinates of point P to be written as functions of the thicknesses t_S and t_B of the compressed seat and back cushions, respectively.

*Note that the computation of Euler angles is required only for the three-dimensional occupant model. For the two-dimensional model, the corresponding generalized coordinates are obtained directly from input data.

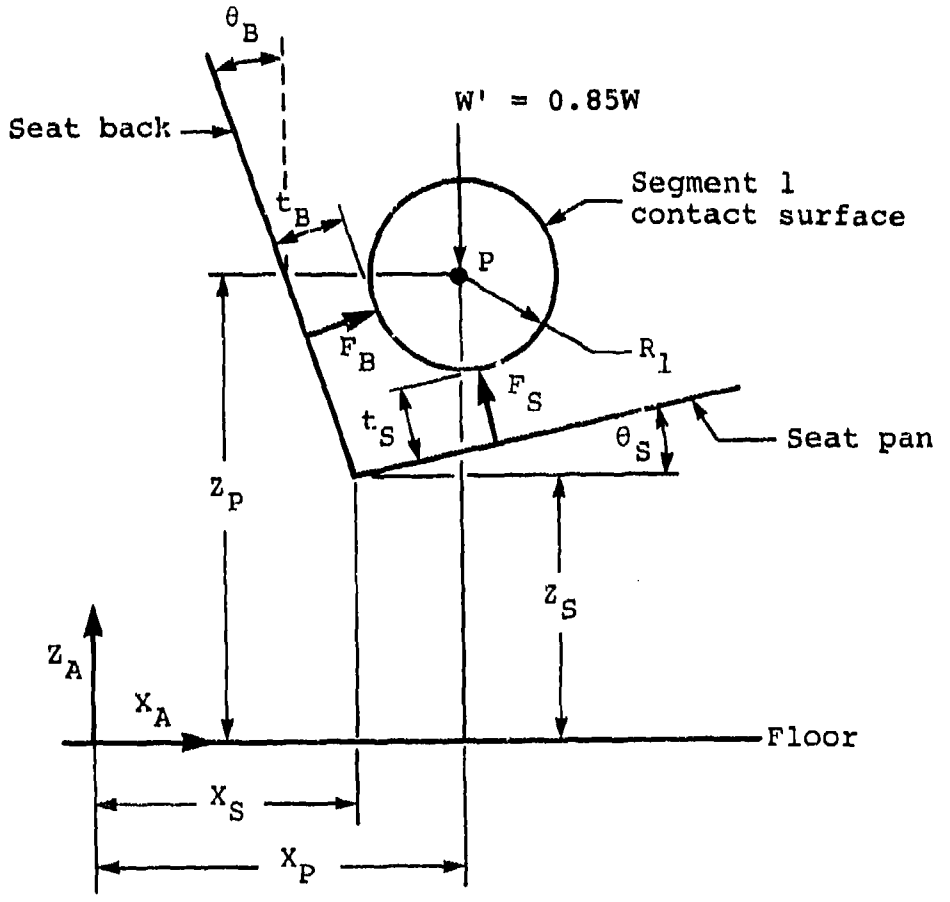

Figure 27. Forces acting on occupant torso (level flight).

$$Z_P = Z_S + (R_1 + t_S)/\cos\theta_S + (X_P - X_S)\tan\theta_S \tag{90}$$

$$X_P = X_S + (R_1 + t_B)/\cos\theta_B - (Z_P - Z_S)\tan\theta_B$$

which can be solved for X_p and Z_p to give

$$X_P = X_S - f_1 \sin\theta_B + f_2 \cos\theta_S \tag{91}$$

$$Z_P = Z_S + f_1 \cos\theta_B + f_2 \sin\theta_S$$

where

$$f_1 = (R_1 + t_S)/\cos(\theta_B - \theta_S)$$

$$f_2 = (R_1 + t_B)/\cos(\theta_B - \theta_S)$$

Since the force-deformation characteristics of the cushions are known from input data, the compressed thicknesses t_S and t_B can be calculated from equation (89). These values, when used in equation (91), give the coordinates of point P for the first approximation of level flight. The equilibrium (zero-load) lengths of the lap belt and shoulder belt(s) are calculated for the body in this position.

Next, the aircraft is rotated to the attitude specified by the input conditions of pitch, roll, and yaw. Nose-up pitch will tend to load the back cushion, and the analysis will be the same as that described above for level flight, except that the W' vector in figure 27 will have a component in the X_A direction.

Nose-down pitch, on the other hand, will tend to load the restraint system. An iterative procedure is used to determine the correct position for this case. Referring to figure 28, summing forces gives a set of transcendental equations

$$F_{X_A}: \quad W' \sin\theta_A - F_S \sin\theta_S - F_L \cos\theta_L = 0$$

$$F_{Z_A}: \quad -W' \cos\theta_A + F_S \cos\theta_S - F_L \sin\theta_L = 0 \tag{92}$$

where θ_L is the angle between the floor and the projection of the lap belt on the X_A - Z_A plane. An initial estimate to θ_L is made using the body position calculated by equation (91) for the level flight assumption. The angle is defined according to

$$\theta_L = \sin^{-1}\left[(Z_P - Z_L)/\sqrt{(X_P - X_L)^2 + (Z_P - Z_L)^2}\right] \tag{93}$$

The forces in the seat cushion F_S and the lap belt F_L are determined using this value of θ_L in equation (92). From the input force-deformation characteristics for the seat cushion and lap belt, the deformations δ_S and δ_L are calculated. These deformations are used to determine new values of X_P and Z_P; this procedure amounts to permitting the body to further compress the seat cushion and slide forward into the lap belt. Following through the procedure,

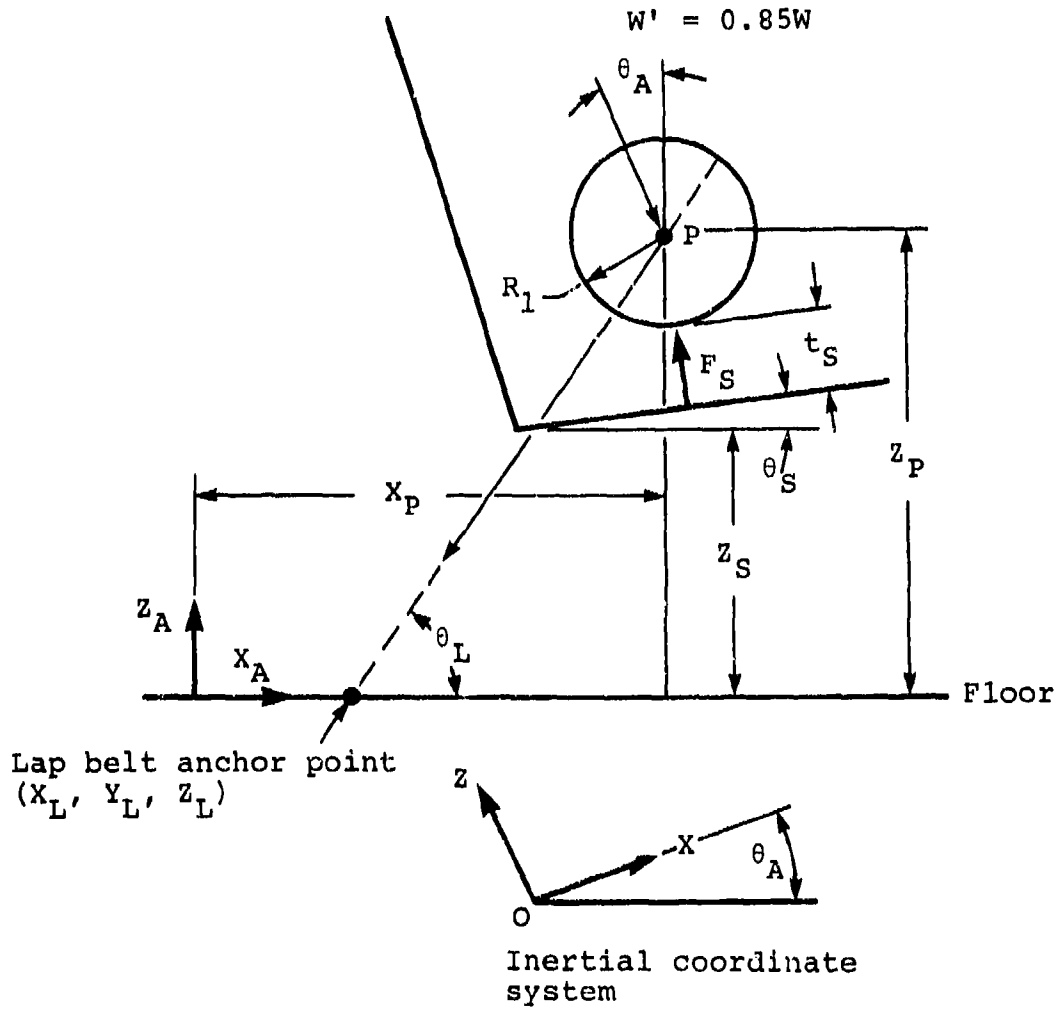

Figure 28. Forces acting on occupant torso (nose-down attitude).

the new length for one side of the lap belt is

$$L_L = L_{Le} + \delta_L \tag{94}$$

where L_{Le} is the equilibrium length. The new value of X_p is given by

$$X_p = X_L + [(L_L - L_H)^2 - (Y_p - Y_L)^2]^{1/2} \cos\theta_L \tag{95}$$

where L_H is one-half the hip breadth and Y_p is the Y-coordinate of the right hip in the aircraft system. The new value of Z_p is computed for the new cushion thickness t_S using equation (90), which is repeated here for continuity:

$$Z_p = Z_S + (R_1 + t_S)/\cos\theta_S + (X_p - X_S)\tan\theta_S$$

The new occupant position, determined by equations (95) and (90) is used in equation (93) to recalculate the lap belt angle θ_L, and the procedure is repeated until two consecutive values of X_p differ by less than 5 percent. The coordinates of the mass center of segment 1 (X_1, Y_1, Z_1) are then calculated from X_p, Y_p, and Z_p.

At this point the generalized coordinates for the upper body have been determined. The final task will be to determine the coordinates for the legs. Referring to figure 29, the angles γ_8 and θ_k can be found from simple geometric relationships among the dimensions shown. The Euler angles ψ_8, θ_8, and ϕ_8 are obtained from γ_8 by using equations (85) through (87), and the corresponding coordinates for segment 10, by symmetry. The knee angles are given by

$$\alpha_m = \pi - \theta_k \qquad m = 9, 11 \tag{96}$$

to complete the initialization of the generalized coordinates.

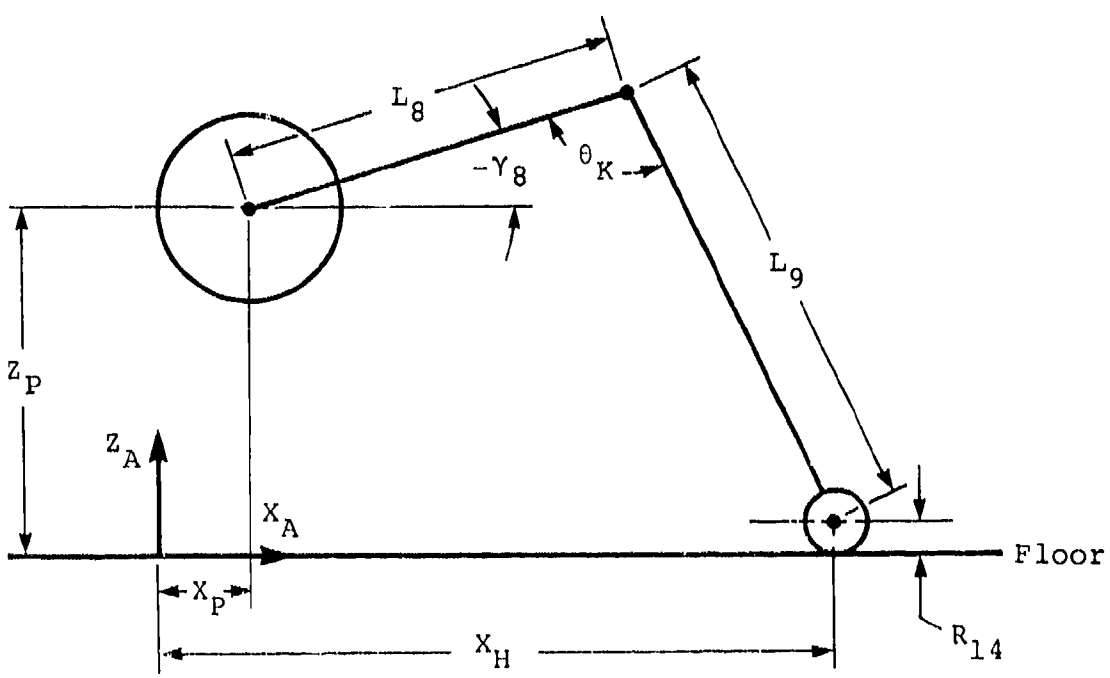

Figure 29. Leg position.

4.3 PROGRAM SOLUTION PROCEDURE

The first operation in each solution step includes the calculation of new values for the aircraft acceleration components and their subsequent integration to obtain aircraft velocity and displacement components. Then the matrix form of the equations of motion, using equation (19)

$$[A(q)]\ \{\ddot{q}\} = \{B(\dot{q},q)\} + \{P(q)\} + \{R(\dot{q},q)\} + \{Q(\dot{q},q)\}$$

are set up for solution and solved, as discussed below.

4.3.1 Setup of Equations of Motion

The elements of [A], {B}, {P}, and {R} are calculated using the current values of the generalized coordinates and velocities. The elements of {Q}, which is the vector of generalized external forces, are calculated, as discussed in section 2.3. The external forces depend on displacements of the aircraft, which determine the motion of the seat, floor, and restraint system anchor points relative to the body. From these displacements new deflections of the cushions, floor, and restraint system are calculated.

4.3.2 Solution of Equations of Motion

The system of equations is solved for the generalized accelerations by first combining the vectors on the right-hand side:

$$[A]\ \{\ddot{q}\} = \{B'\} \qquad (97)$$

where $\{B'\} = \{B\} + \{P\} + \{R\} + \{Q\}$

and solving for $\{\ddot{q}\}$ using Crout decomposition followed by Forsythe-Moler elimination.

The resulting set of N second-order differential equations have the general form

$$\ddot{q}_j = f_j\,(t, \dot{q}_1, \dot{q}_2, \ldots, \dot{q}_N, q_1, q_2, \ldots, q_N)$$

$$q_j\,(t=0) = q_{j0}\quad \dot{q}_j\,(t=0) = \dot{q}_{j0}\qquad j = 1, 2, \ldots, N \tag{98}$$

where N, the number of degrees of freedom, is 12 for the two-dimensional model and 29 for the three-dimensional model.

These equations can be rewritten as 2N first-order equations having the general form

$$\dot{y}_j = f_j\,(t, y_1, y_2, \ldots, y_N, q_1, q_2, \ldots, q_N)$$

$$\dot{q}_j = y_j \tag{99}$$

$$y_j\,(t=0) = \dot{q}_{j0}\qquad q_j\,(t=0) = q_{j0}$$

Numerical integration of this set of equations is accomplished, using the Adams-Moulton predictor-corrector method with a variable step size. This method uses the difference equations

$$y^{(p)}_{j,n+1} = y_{j,n} + \frac{h}{24}\,(55f_{j,n} - 59f_{j,n-1} + 37f_{j,n-2} - 9f_{j,n-3}) \tag{100}$$

as the predictor and

$$y^{(c)}_{j,n+1} = y_{j,n} + \frac{h}{24}\,(9f^{(p)}_{j,n+1} + 19f_{j,n} - 5f_{j,n-1} + f_{j,n-2}) \tag{101}$$

as the corrector. Starting values are provided by the classical fourth-order Runge-Kutta method. Input data includes upper and lower error bounds for the solution. Error bounds for each variable are calculated and compared at each step with the difference between the predicted value $y^{(p)}_j$ and the corrected value $y^{(c)}_j$. If this difference exceeds the upper bound for any j, the step size is halved. If this difference is less than the minimum error bound for all j and for three successive steps, the step size is doubled. Halving the step size is accomplished by interpolation of past data, whereas doubling is effected by alternate selection of past data. The solution can be run with a fixed step size by making the upper and lower error bounds prohibitively large

and small, respectively, or by using equal values for the maximum and minimum step size which are also included among input data.

4.4 PROGRAM OUTPUT

Output data consist of ten blocks of information that are selected for printing by user input. The data include time histories of the variables, which are simply sorted during the solution at predetermined print intervals as follows:

1. Occupant segment positions in the aircraft coordinate system (X, Y, Z, pitch, and roll).
2. Occupant segment velocities in the aircraft coordinate system (X, Y, and Z).
3. Occupant segment accelerations in the segment-fixed coordinate systems (x, y, z, and resultants).
4. Restraint system loads.
5. Cushion loads.
6. Aircraft displacement, velocity, and acceleration.
7. Injury criteria.
8. Details of contact between the occupant and the seat in front.
9. Seat structure nodal forces.
10. Seat structure element stresses.

Printer plots are provided for occupant segment accelerations, restraint system loads, and cushion loads. The option of two different filters is also provided for the occupant segment accelerations and cushion loads.

Two of the above blocks of output data will be discussed in further detail.

4.4.1 Impact Prediction

For prediction of impact between the occupant and the seat in front, 26 surfaces are defined on the body. These surfaces were illustrated in figure 15, and their dimensions discussed in section 2.5.

The distance between each of these occupant contact surfaces and the surfaces of the seat in front is calculated during execution of the program. When contact occurs between an occupant surface and a contact surface, the time and relative velocity of impact are computed and stored for printing. The impact conditions determined in this way can be used in evaluation of injury potential for a given cockpit configuration.

4.4.2 Injury Criteria

The injury criteria used in the program were selected as the most suitable for aircraft crash analysis. SOM-TA output can be used to determine the potential for injury to four regions of the body: head, vertebral column, thorax, and legs. Each of these is discussed in the remainder of this chapter.

4.4.2.1 Head Injury. An accepted criterion for head injury is the Severity Index (SI) developed by C. W. Gadd (references 17 and 18), which is calculated for the head and chest according to

$$SI = \int_{t_o}^{t_f} a^n \, dt \qquad (102)$$

where a = acceleration in G as a function of time

n = weighting factor, 2.5 for head impacts

t = time in seconds.

Although Gadd used uniaxial acceleration in his validation of the Severity Index, Federal Motor Vehicle Safety Standard 208 requires the use of resultant acceleration. A tolerable SI value of 1000 is accepted for frontal impact of the head, and a value of 1500, for distributed, or noncontact accelerations (reference 19).

Also, the Head Injury Criterion (HIC) contained in Federal Motor Vehicle Safety Standard 208 is calculated according to

$$HIC = \max \left(\frac{1}{t_2 - t_1} \int_{t_1}^{t_2} a\,dt \right)^{2.5} (t_2 - t_1) \qquad (103)$$

where a is the resultant head acceleration in G and t_1 and t_2 are any two points in time (sec) during the crash event. A tolerable value of 1000 is accepted for the HIC.

4.4.2.2 Thoracic Injury. Although chest deflection is commonly accepted as the preferred tolerance criterion, it is not presently predicted by SOM-TA.

FMVSS 208 currently specifies as acceptable an acceleration pulse which ". . . shall not exceed 60 G except for intervals whose cumulative duration is not more than 3 msec," where the acceleration is the resultant measured at the center of gravity. This acceleration is printed by SOM-TA. Previously, FMVSS 208 had applied a Severity Index to the chest acceleration pulse. This index was calculated in exactly the same manner as the head Severity Index discussed previously, and the limit of 1000 was the same as that for the head. SOM-TA also prints this SI for the thorax.

4.4.2.3 Vertebral Injury. For determination of the potential of vertebral injury, the SOM-TA two-dimensional occupant model has beam elements in the lumbar spine and neck. Axial forces and bending moments are output for these segments. Tolerable force levels for the lumbar spine have not yet been established. However, based on cadaver tests, references 20 and 21 have published tolerable bending moments for the neck such as 1700 in.-lb in flexion (forward bending) and 500 in.-lb ft-lb in extension (rearward bending), respectively.

The dynamic response index (DRI) is also computed by SOM-TA as a measure of the probability of spinal injury due to a vertical acceleration parallel to the spine (reference 22).

In this model, the response of the body to acceleration parallel to the spine is modeled by a single lumped-mass, damped-spring system as shown in figure 30,

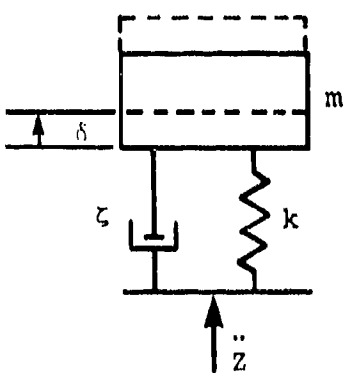

m = mass (lb-sec^2/in.)
δ = deflection (in.)
ζ = damping ratio
k = stiffness (lb/in.)
$\ddot{Z}$ = acceleration input (in./sec^2)

82 01003 27

$$*DRI = \frac{\omega_n^2 \, \delta_{max}}{g}$$

ω_n = natural frequency of the analog = $\sqrt{k/m}$ (rad/sec)

*Dynamic Response Index

g = 386 in./sec^2

Figure 30. Model used for prediction of spinal injury (from reference 22).

or, in other words, the total body mass that acts on the vertebral column to cause deformation is represented by the single mass. In general, the motion of the system shown in figure 29 obeys the relationship

$$\frac{d^2\delta}{dt} + 2\delta\omega_n \frac{d\delta}{dt} + \omega_n{}^2\delta = \ddot{Z} \qquad (104)$$

The solution, the deflection δ, is representative of the deformation of the spine, and the last term of the left-hand side of equation (104), divided by the gravitational acceleration, is the DRI. The properties used in the model were derived from tests involving human subjects and cadavers. For example, the spring stiffness k was determined from tests of human cadaver vertebral segments; damping ratios were determined from measurements of mechanical impedance of human subjects during vibration and impact. The acceleration input, $\ddot{Z}$, is the component of seat pan acceleration parallel to the vertebral column.

Equation (99) is solved for δ simultaneously with the occupant equations of motion, using the constants ζ = 0.224 and ω_n = 52.9 rad/sec. The DRI is then calculated at each step by

$$DRI = \omega_n{}^2\delta/g \qquad (105)$$

4.4.2.4 Leg Injury

FMVSS 208 specifies a limit of 2,250 lb for the axial compressive load in each femur. This tolerance level is based primarily on the work of Patrick, Kroell, and Mertz (references 23 and 24), who tested embalmed human cadavers in full-scale sled experiments. Other experiments that used a stationary seated cadaver struck by a moving rigid impactor produced higher fracture loads, but injury patterns were not representative of field accidents. Viano and Khalil (reference 25) demonstrated that the poor correspondence between the latter tests and actual accidents could be be attributed to the pulse duration (on the order of 10 msec), significantly shorter than that which occurs in real-world accidents.

If simulation of contact between the occupants and the seat back is requested, SOM-TA prints (and plots) the time variation of the axial load in each femur. The time and impact velocity for each such contact is also printed, along with identification of seat back surface.

5.0 MODEL VALIDATION

Dynamic tests of transport seats conducted by the FAA Civil Aeromedical Institute (CAMI) in 1983 for Simula were used in validation of Program SOM-TA. Three production seat designs and various modifications to the production designs were tested. The design that was chosen for validation utilized a production seat modified by incorporating energy-absorption capability in the longitudinal direction. This seat produced more interesting results for validation than others because it underwent large deformations while maintaining structural integrity in the dynamic test.

5.1 Description of Seat Structure

Figure 31 shows the basic production seat. The seat pan assembly is built around aluminum front and rear tubes which are connected by four aluminum supports. The front of each support rests on the top of the front tube and is attached by two bolts running through the support and the tube. The rear of each support has a semicircular cut-out that slips over the rear tube and attaches with one bolt. Three of the supports have cantilevered rear extensions which provide a pivot and anchor point for the arm rests and seat backs. The seat cushions rest on perforated aluminum sheets which are riveted to the front tube in front, and wrapped around a small aluminum tube which slips in between the cantilevered extensions in the rear.

The leg assembly consists of front and rear legs of formed stainless steel sheet, which are connected diagonally by a square aluminum tube. The front legs cradle and bolt to the front tube, while the rear legs are held to the rear tube by steel straps which are wrapped around the tube and bolted to the legs. Each rear leg is connected to the diagonal tube by a steel fitting which is riveted to the leg and the tube, and is also bolted to the steel strap. The seat pan and leg assembly are shown in figure 32.

The rear legs are attached to the floor track by a fitting consisting of two studs and a lever-operated plunger. The plunger moves in and out of the track and is in front of the fitting. The fitting is attached to the leg by a single bolt and is shown in figure 33.

Figure 31. Production transport aircraft seat.

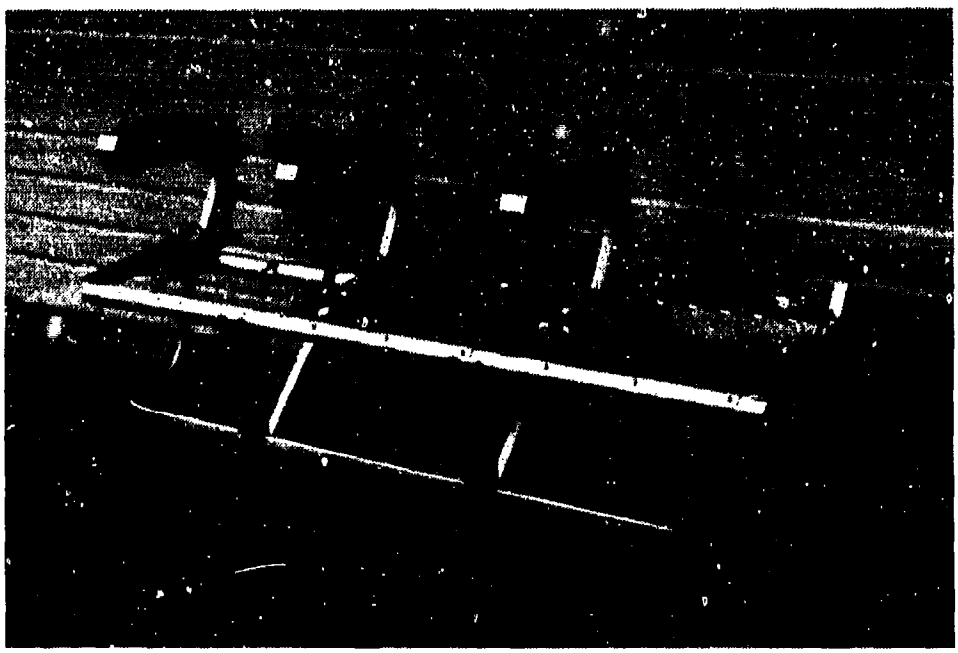

Figure 32. Seat pan and leg assembly of the production transport aircraft seat.

Figure 33. Rear track fitting of a production aircraft seat.

The front legs are attached to the track by a single stud which is incorporated in an antirattle mechanism shown in figure 34. The stud is bolted to the yoke, which is attached to both the front leg and diagonal tube by a single bolt. An aluminum strap connects the front stud and rear fitting in order to transfer the loads from the tubular diagonal brace to the plunger.

The seat structure includes attachment fittings for standard lap belts. These fittings are bolted to the forged aluminum supports. Both the back and bottom cushions are fabricated of plastic foam. The back cushion is contoured for comfort while the bottom cushion is flat on top but curved on the bottom to conform to the performated aluminum seat pan. Each seat has a food tray mounted on its back, and the seat back has an adjustable reclining mechanims. The two middle armrests can pivot up flush with the seat backs.

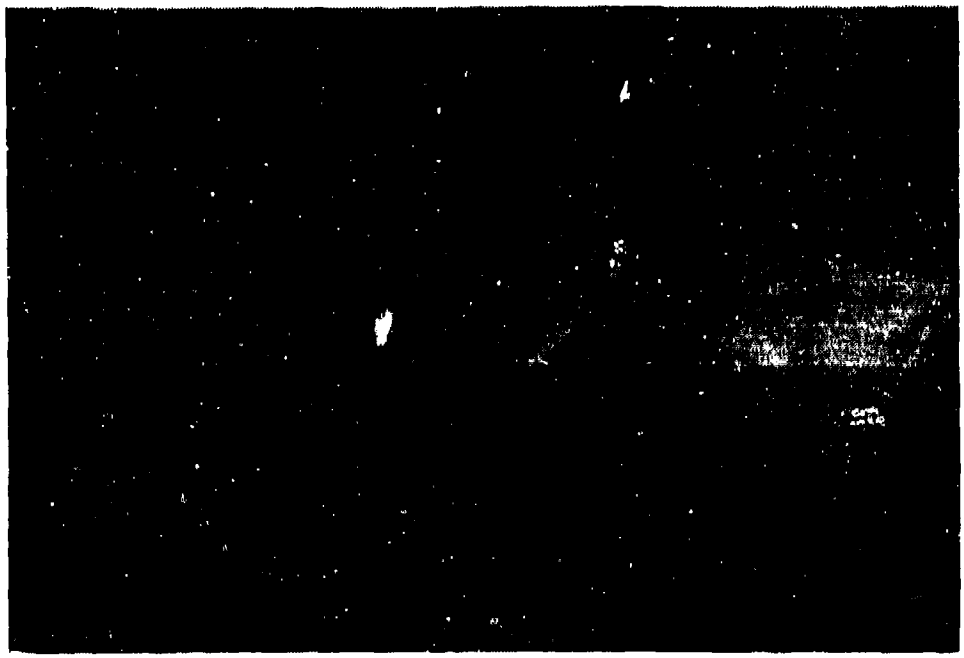

Figure 34. Front track fitting of a production aircraft seat.

The production seat design was modified at Simula to provide longitudinal energy-absorbing capability by replacing the diagonal brace with a compressive inversion tube energy absorber. A sketch of the seat kinematics using the compressive energy absorber is shown in figure 35. In order for the seat to undergo the approximate curvilinear translation the sketch depicts, the front and rear legs needed to be released to act as a linkage.

The energy absorbers used are shown in figure 36. Both employ the load attenuation method of inverting an aluminum tube. Due to the asymmetry of the seat, the window-side energy absorber is required to stroke at twice the load of the aisle-side energy absorber, and thus uses two inversion tubes. The window-side and aisle-side energy absorbers begin to stroke at 2800 lb and 1400 lb, respectively.

The track fittings were also modified to provide release about pitch and roll axes. Both front and rear track fittings had three studs and were locked in both positions. The modified track fitting is shown in figure 37.

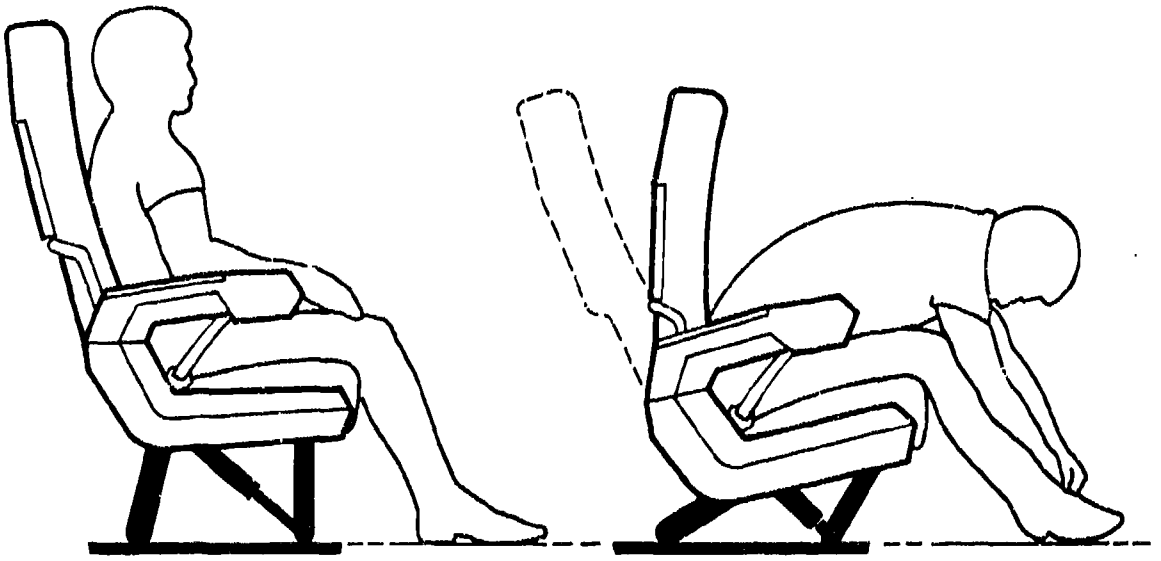

84 01004 36

Figure 35. Modified transport aircraft seat before and after stroking.

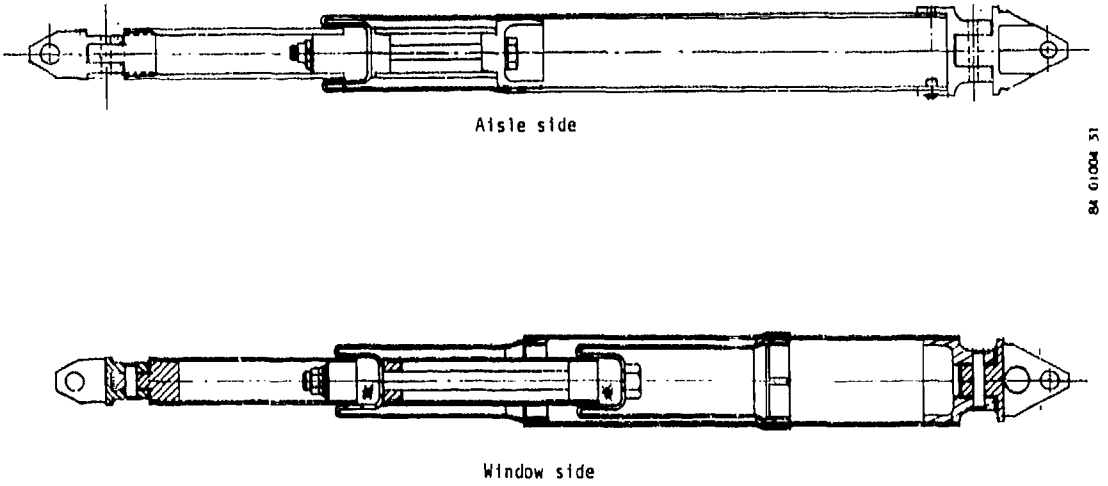

84 01004 51

Figure 36. Modified transport aircraft seat energy absorbers.

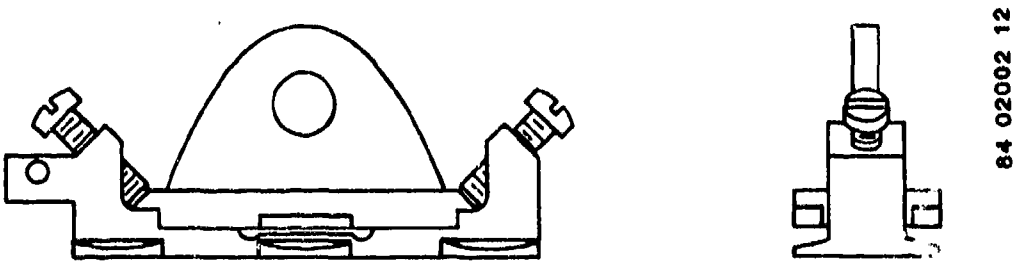

Figure 37. Modified transport aircraft track fittings.

5.2 Dynamic Test Conditions

The seat design was tested at CAMI in the forward-facing configuration with a 9-G, 50 ft/sec. sled deceleration (figure 38). Three 50th-percentile anthropomorphic dummies were used to simulate the seat occupants (figure 39). Six-axis load cells were placed under the seat legs to measure the seat reactions exerted on the floor. Lap belt forces were also measured on both sides of the lap belt for each occupant. Accelerometers were placed at dummy pelvis, chest, and head locations.

Prior to dynamic testing, the test fixture was adjusted to simulate floor warping conditions. The aisle side of the seat was pitched down 10 degrees (figure 40) and the window side of the seat was rolled outwards 10 degrees (figure 41).

5.3 SOM-TA Simulation Results

The finite element model of the seat structure illustrated in figure 42 consists of 26 nodes and 33 beam elements. The complete input data listing is presented in figure 43.

The compressive energy absorbers were modeled with beams 21 and 24 between nodes 9-12 and 18-21, respectively. The ends of the energy absorbers were modeled as pin-socket joints by using the appropriate beam end release codes.

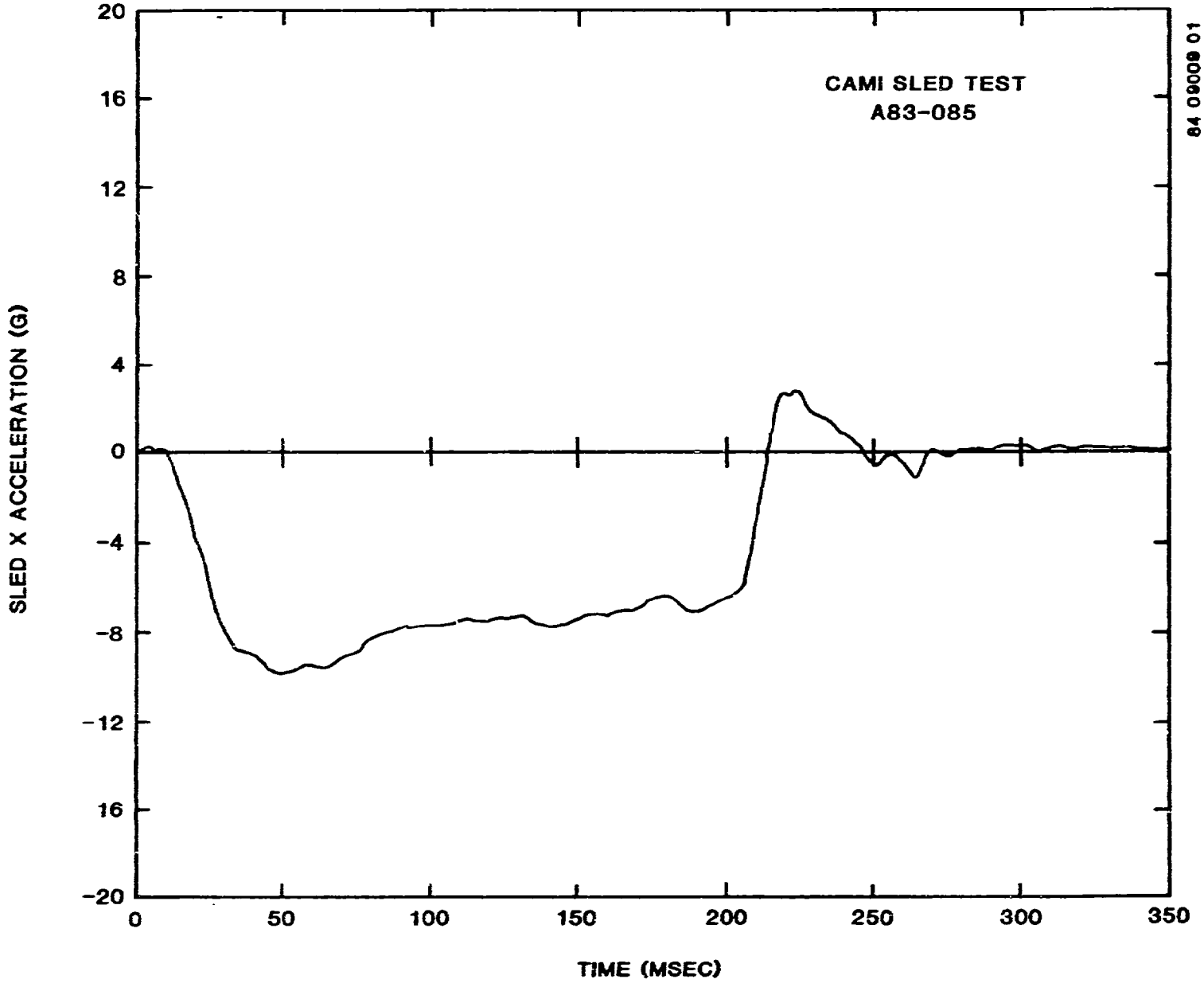

Figure 38. Sled deceleration, CAMI-modified transport aircraft seat Test A83-085.

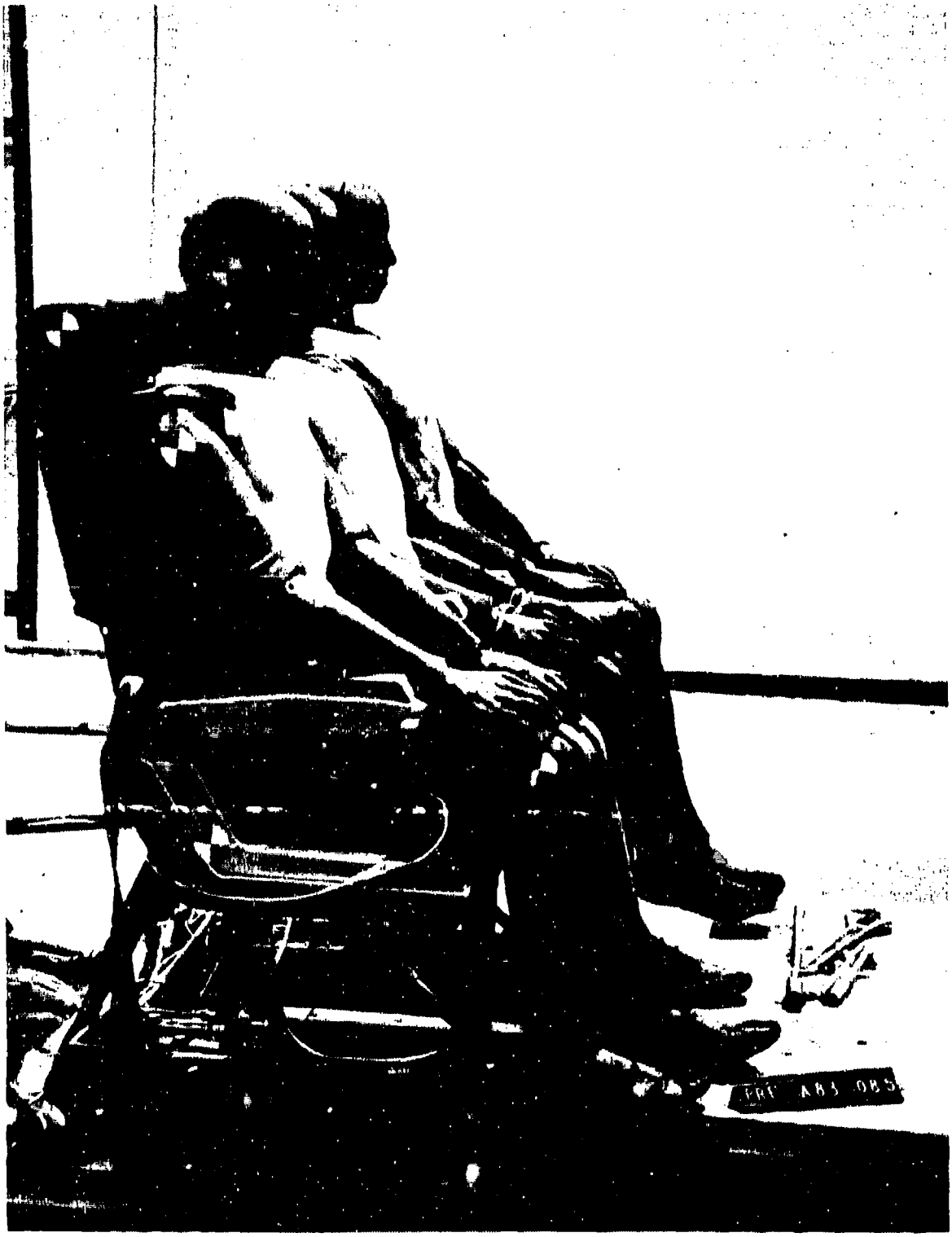

Figure 39. Modified transport aircraft seat and dummies prior to CAMI Test A83-085 (before floor warping).

Figure 40. Modified transport aircraft seat and dummies prior to CAMI Test A83-085, aisle-side view (after floor warping).

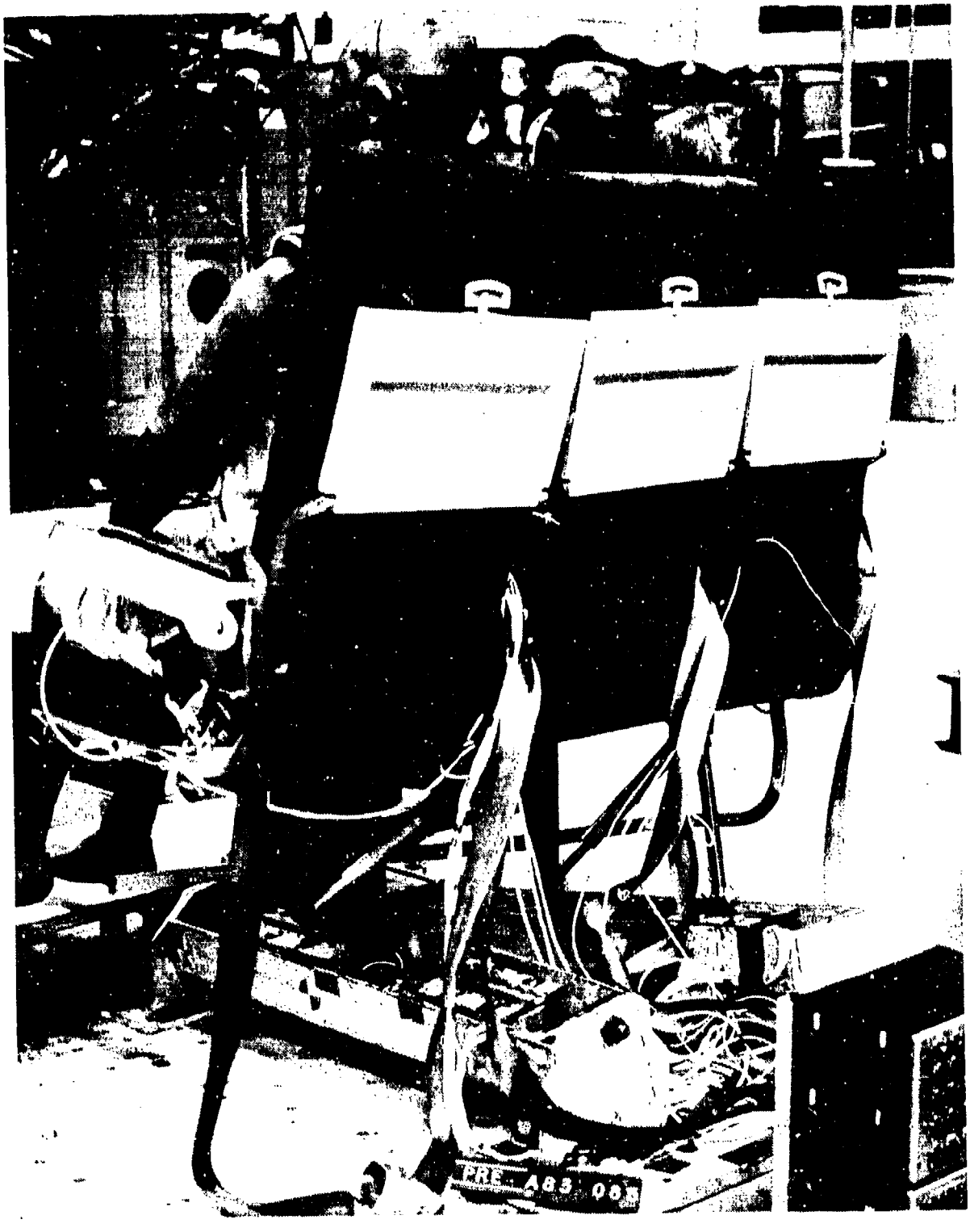

Figure 41. Modified transport aircraft seat and dummies prior to CAMI Test A83-085, window-side view (after floor warping).

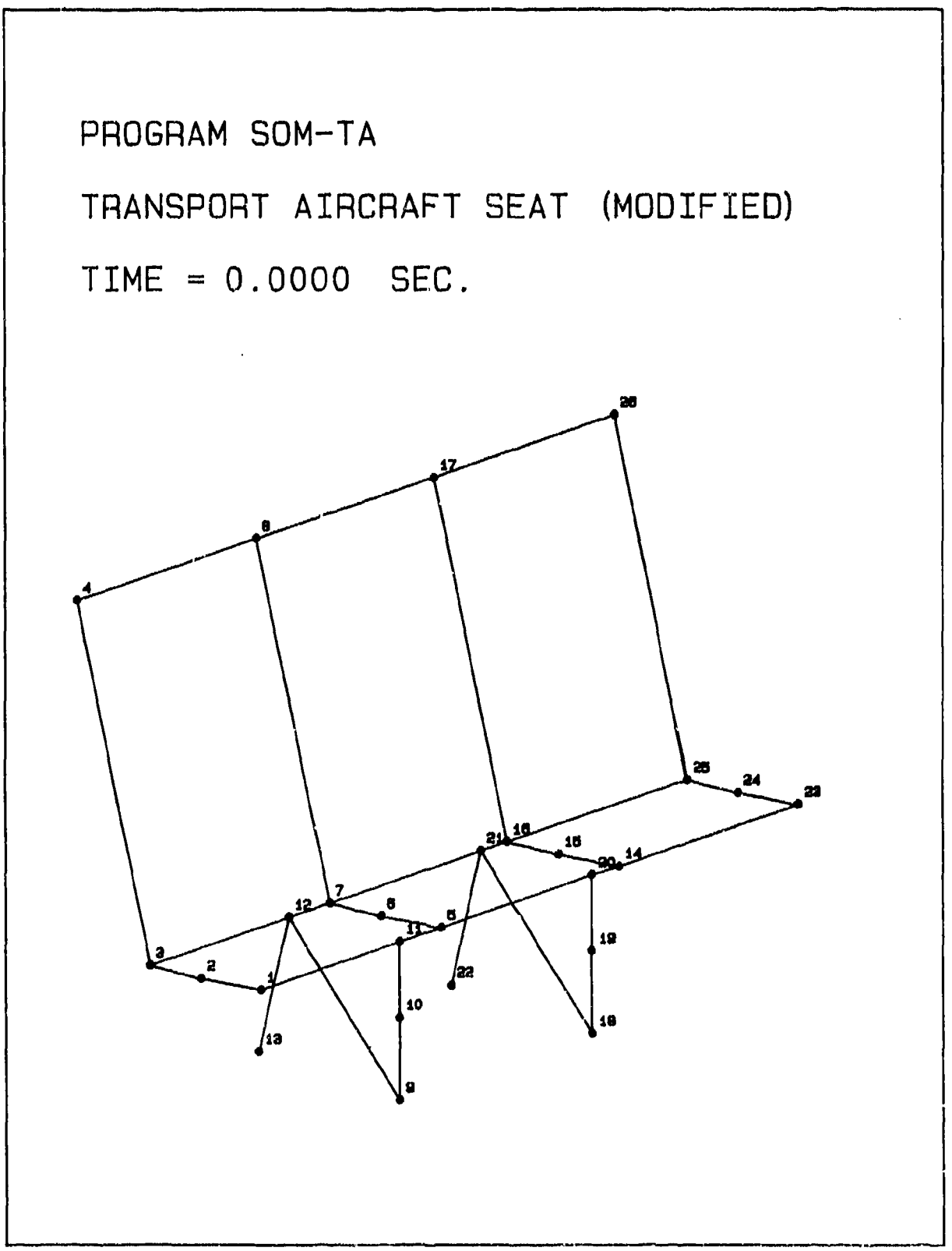

Figure 42. Program SOM-TA finite element model of the modified transport aircraft seat (before floor warping).

```
MODIFIED UOF SEAT (SOMTA VALIDATION)
  1   1   2   3   3   1   1   1   2
  0   0   2   0   1   1   2   1   1   1   8   8.0005 .005
     .000      .040      .080      .120      .160      .200      .240      .300
       0.        0.        0.        0.        0.        0.        0.        0.
      20.       20.       20.       20.       20.       20.       20.       20.
     -45.      -45.      -45.      -45.      -45.      -45.      -45.      -45.
1    26
1    33
     300.      .0001     .0001      0.1      0.001      0.       .300      .0001
     760.      0.50      2.40       1.5
     760.      0.50      2.40       1.5
  0   0   1   0   1
     760.      0.50      2.40       3.0
     550.     1300.     2250.     0.0403    0.1048    0.1613      0.        0.
     5.5      -29.      13.75      5.5      -11.4      13.75
     5.5      -8.7      13.75      5.5       8.7       13.75
     5.5       11.4     13.75      5.5       29.       13.75
      0.        .3       -9.3      -8.6      -9.5      -6.5      -6.5       -8
      -7       -7.8      -5.5      -5.3      -6.9       1.8       -.8        0
      0.       .00625    .0335     .0583     .0667     .092      .10833     .1333
     .1413     .153      .178      .1917     .201      .2208     .264       .3
     49.       0.        0.
      0.       0.        0.
  1           0.18      0.25
    -16.      -16.       7.       -16.       60.       32.       -20.
    -16.      -16.       7.       -16.       60.       32.        0.
    -16.      -16.       7.       -16.       60.       32.       20.
     3.2      11.63     5.33       16.      12.66      19.2       39.      19.2
```

Figure 43. Input data listing for simulation of CAMI Test A83-085.

```
 36   33    3    4    6    0    8 0.3
 16   10
  14130 STEEL
7.324-04      30.E6     70000.      10.E6       .1    90000.       .3
                        80000.     1.25E6
  22024-T3 AL
.2588E-4      10.E6     44600.      4.9E5       .1    62000.       .3
                        58000.      0.1E6
  3E/A DATA
.2568E-4      10.E6     41600.      1.0E6       .1    90000.       .3
                        46800.      0.1E6
 4    0        .490      .0184      .0265      .1086
      0.0       0.0        0.0        0.0

     .513       .23       .165
     .513      -.23       .165
     -.22      -.455      .165
     -.22       .455      .165
 4    0       .6059      .0676      .0873      .0366
      0.0       0.0        0.0        0.0
     .513       .405      .165
     .513      -.405      .165
     -.445     -.455      .165
     -.445      .455      .165
 3    0       .3354      .0127       .122       .122
      0.0       0.0        0.0        0.0
     .8425        0       .065
     .596      -.596       .065
        0      -.8425      .065
     -.596     -.596       .065
    -.8425        0       .065
     -.596      .596       .065
        0       .8425      .065
     .596       .596       .065
 4    0         .105      .0128      .0085      .0085
      0.0       0.0        0.0        0.0
     .375       .375       .035
     .375      -.375       .035
     -.375     -.375       .035
     -.375      .375       .035
 4    0         .054      .0292      .0233      .0233
      0.0       0.0        0.0        0.0
     .745       .745      .0090
     .745      -.745      .0090
     -.745     -.745      .0090
     -.745      .745      .0090
 4    0        .1695      .1101       .055      .0439
      0.0       0.0        0.0        0.0
      .91      -.785       .025
     -.91      -.785       .025
     -.91       .785       .025
      .91       .785       .025
```

Figure 43 (contd). Input data listing for simulation of CAMI Test A83-085.

```
4    0      .2093      .1967      .085       .2067
   0.0        0.0        0.0       0.0
 1.308      -.785       .025
-1.308      -.785       .025
-1.308       .785       .025
 1.308       .785       .025
4    0      .2682      .015       .020       .020
   0.0        0.0        0.0       0.0
  .745       .745       .0045
  .745      -.745       .0045
 -.745      -.745       .0045
 -.745       .745       .0045
1           15.21      - 29.      12.75
2            8.71      -29.0      12.00
3             3.2      - 29.      11.63
4           -4.65      - 29.       39.0
5           15.21       -9.6      12.75
6            8.71       -9.6      12.00
7             3.2       -9.6      11.63
8           -4.65       -9.6       39.0
9           15.21     -14.06         0.
10          15.21     -14.06       6.63
11          15.21     -14.06      12.75
12            3.2     -14.06      11.63
13              0     -14.06         0.
14          15.21        9.6      12.75
15           8.71        9.6      12.00
16            3.2        9.6      11.63
17          -4.65        9.6       39.0
18          15.21       6.72         0.
19          15.21       6.72       6.63
20          15.21       6.72      12.75
21            3.2       6.72      11.63
22              0       6.72         0.
23          15.21        29.      12.75
24           8.71        29.        12.
25            3.2       29.0      11.63
26          -4.65        29.       39.0
1    1    2                    1    1    5    2    2
2    2    3                    1    2    6    2    2
3    5    6                    1    1   11    2    2
4    6    7                    1    2   15    2    2
5   14   15                    1    1   20    2    2
6   15   16                    1    2   24    2    2
7   23   24                    1    1   20    2    2
8   24   25                    1    2   15    2    2
9    3   12                    1    3    1    2    2
10   7   12                    1    3    5    2    2
11   7   21                    1    3   11    2    2
12  16   21                    1    3   14    2    2
13  16   25                    1    3   20    2    2
14   1   11                    1    3    3    2    2
```

Figure 43 (contd). Input data listing for simulation of CAMI Test A83-085.

```
 15    5   11                          1   3   7   2   2
 16    5   20                          1   3  12   2   2
 17   14   20                          1   3  16   2   2
 18   14   23                          1   3  21   2   2
 19   12   13                          1   4  16   2   2  000  010  000  010
 20   21   22                          1   4  25   2   2  000  010  000  010
 21    9   12                          0   8  18   2   3  000  111  000  011
 22    9   13                          1   6  18   2   1  000  010
 23   10   11                          1   7  19   2   1  000  000  000  010
 24   18   21                          0   5   9   2   3  000  111  000  011
 25   18   19                          1   6   9   2   1  000  010
 26   19   20                          1   7  10   2   1  000  000  000  010
 27    3    4                          1   3   7   2   2
 28    7    8                          1   3  12   2   2
 29   16   17                          1   3  21   2   2
 30   25   26                          1   3  21   2   2
 31    4    6                          1   3   3   2   2
 32    8   17                          1   3   7   2   2
 33   17   26                          1   3  16   2   2
  3    7    1    5    7   16          5  14  16  25  14  23
  3    7    4    8    7   16          8  17  16  25  17  26
  3    7    7   16   16   25
9112010
  -2.680
13111010
18111010
22111010
```

Figure 43 (contd). Input data listing for simulation of CAMI Test A83-085.

The nonlinear force-deflection characteristics of the energy absorbers were modeled using a fictitious material property data for the corresponding axial stress and tangent modulus. All other beam elements made of 4130 steel and 2024-T3 aluminum were modeled as elastic beams.

The floor warping condition of 10 degrees pitch on the aisle side was simulated by enforcing a downward displacement of 2.68 in. at node 9. Track fitting design already provided release for floor warping about the roll axis.

The three 50th-percentile dummies were modeled using standard (two-dimensional) occupants, with occupant segment data parameters available in the program. The data set in figure 43 requests all occupant output data for the center occupant.

As evidenced by the post-test view in figure 44, the seat did not experience any failures in the dynamic test. The floor deformation prior to the test did not affect the performance of the seat, due to the releases provided by the track fittings.

The predicted occupant and seat positions from SOM-TA simulations are shown in figures 45 and 46, respectively. The occupant chest contacts the knees at about 200 msec. Program SOM-TA does model the interaction between the chest and the knees using an exponential force-deflection relationship and a viscous damper.

Program SOM-TA predictions for the center occupant head, chest, and pelvis accelerations, lap belt forces, and left-seat leg reactions are compared with the measured test data in figure 47 through figure 53. Occupant accelerations have peaks around 200 msec, an indication of the contact between the occupants' chest and knees.

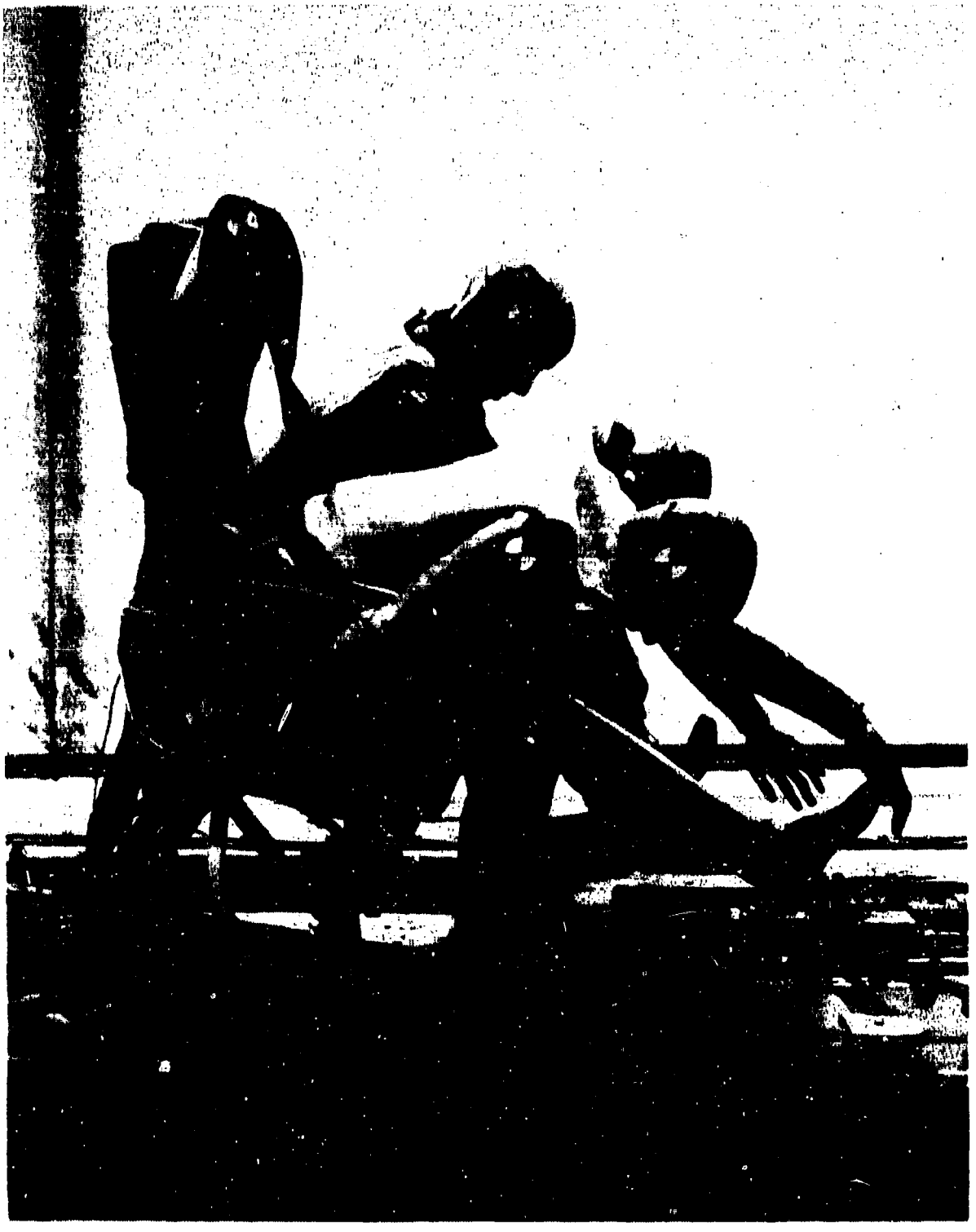

Figure 44. Modified transport aircraft seat and dummies after CAMI Test A83-085.

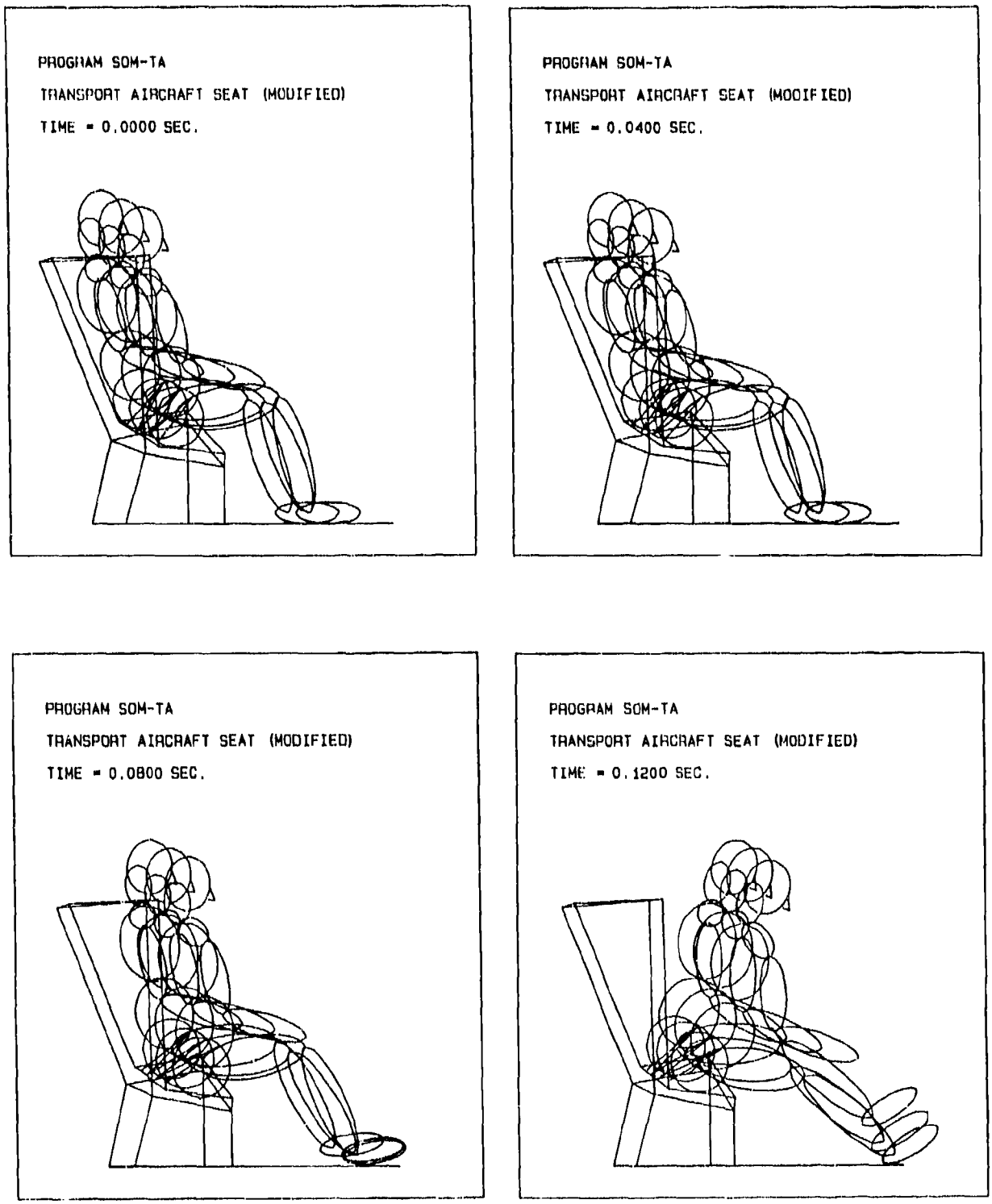

Figure 45. Program SOM-TA-predicted occupant positions for modified transport aircraft seat (CAMI Test A83-085).

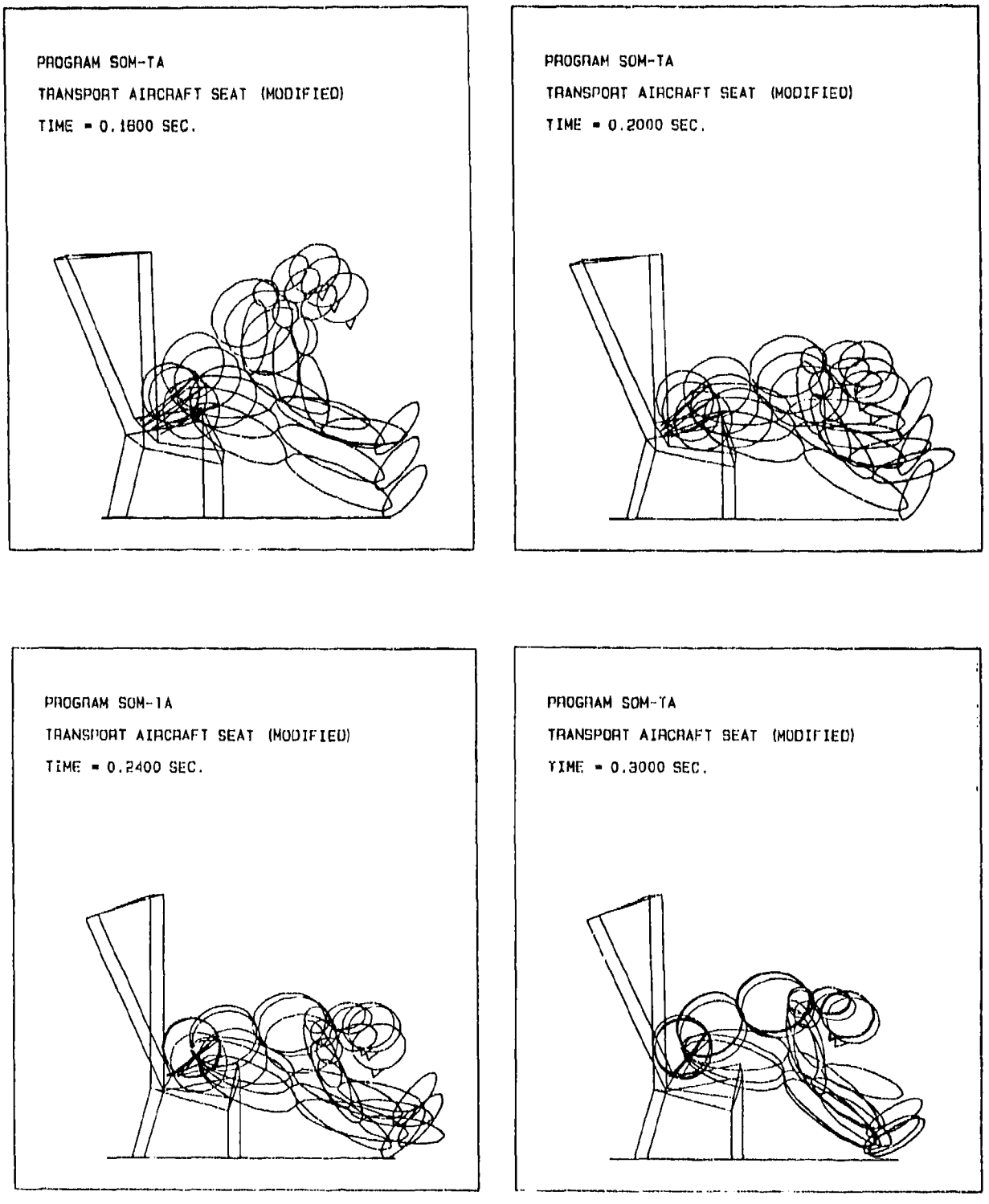

Figure 45 (contd). Program SOM-TA-predicted occupant positions for modified transport aircraft seat (CAMI Test A83-085).

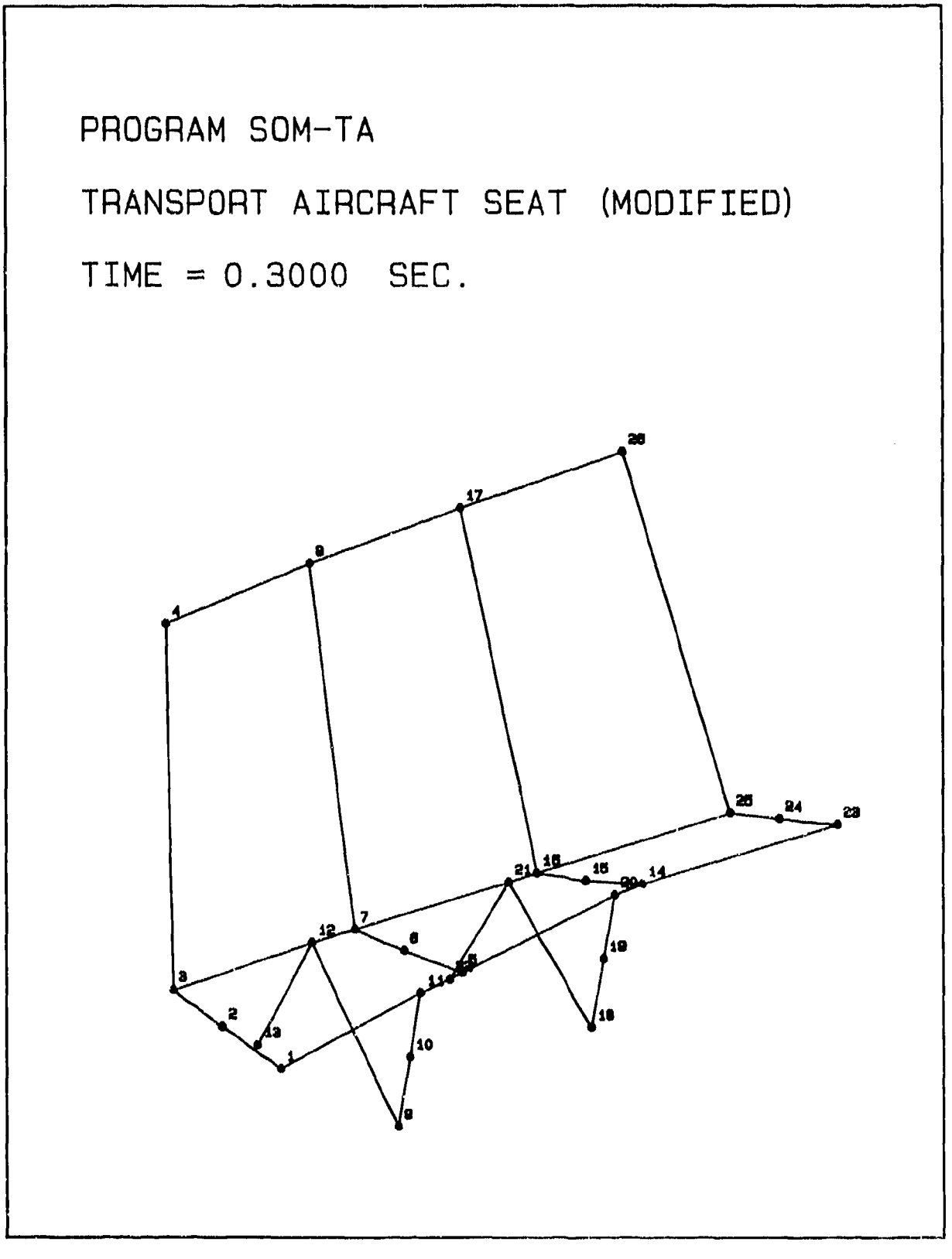

Figure 46. Program SOM-TA-predicted seat displacements for modified transport aircraft seat (CAMI Test A83-085).

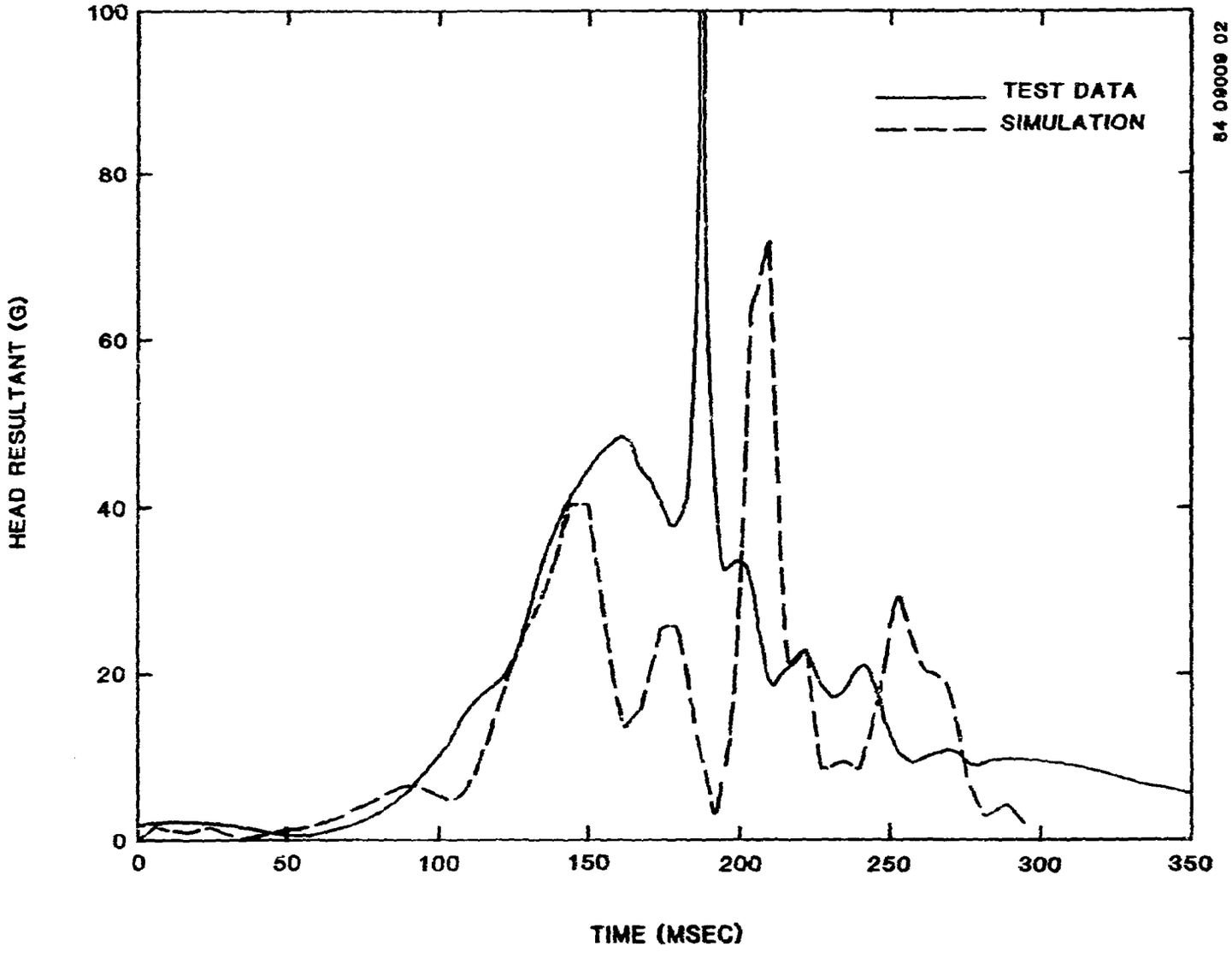

Figure 47. Modified transport aircraft seat, CAMI Test A83-085, head (resultant) acceleration.

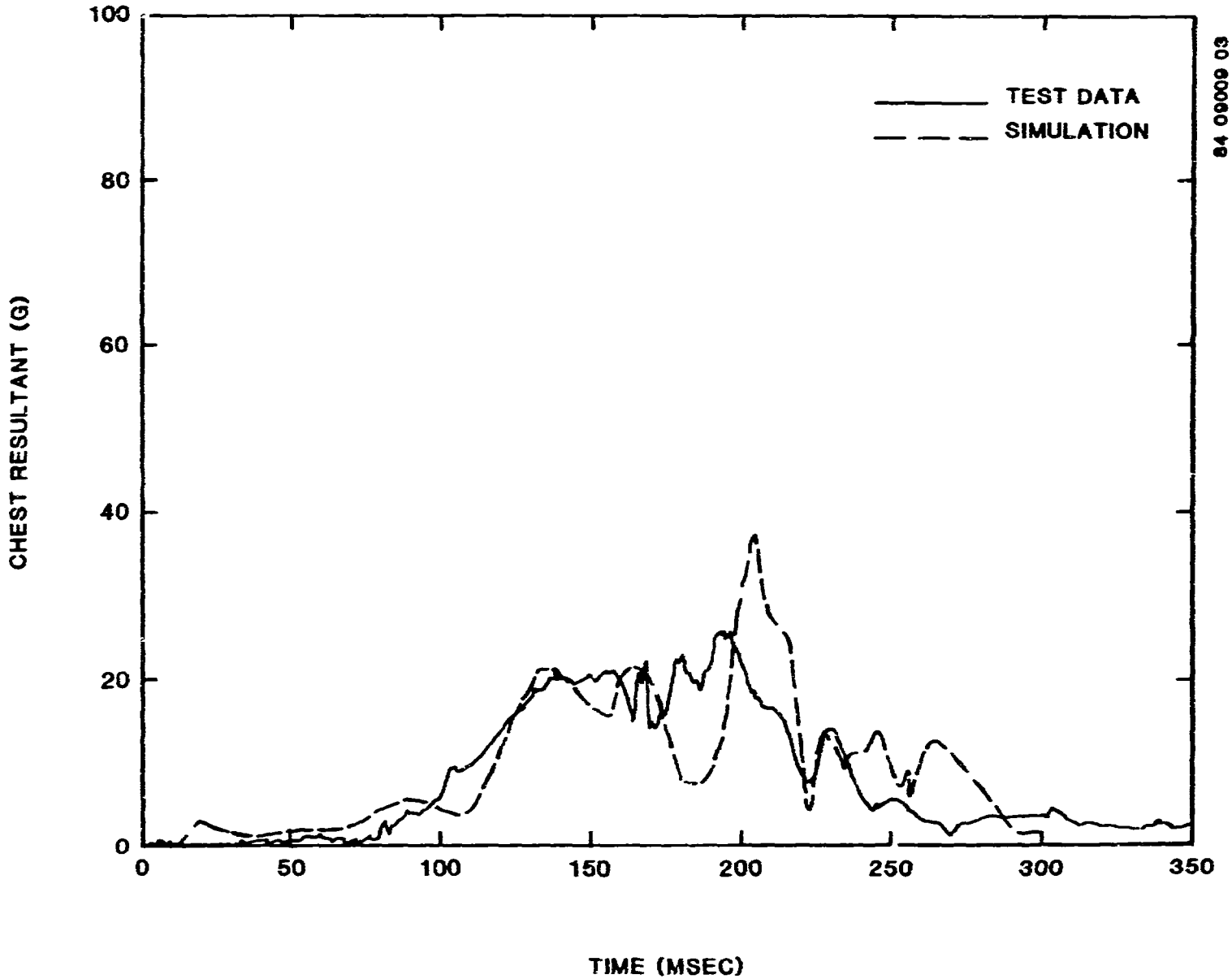

Figure 48. Modified transport aircraft seat, CAMI Test A83-085, chest (resultant) acceleration.

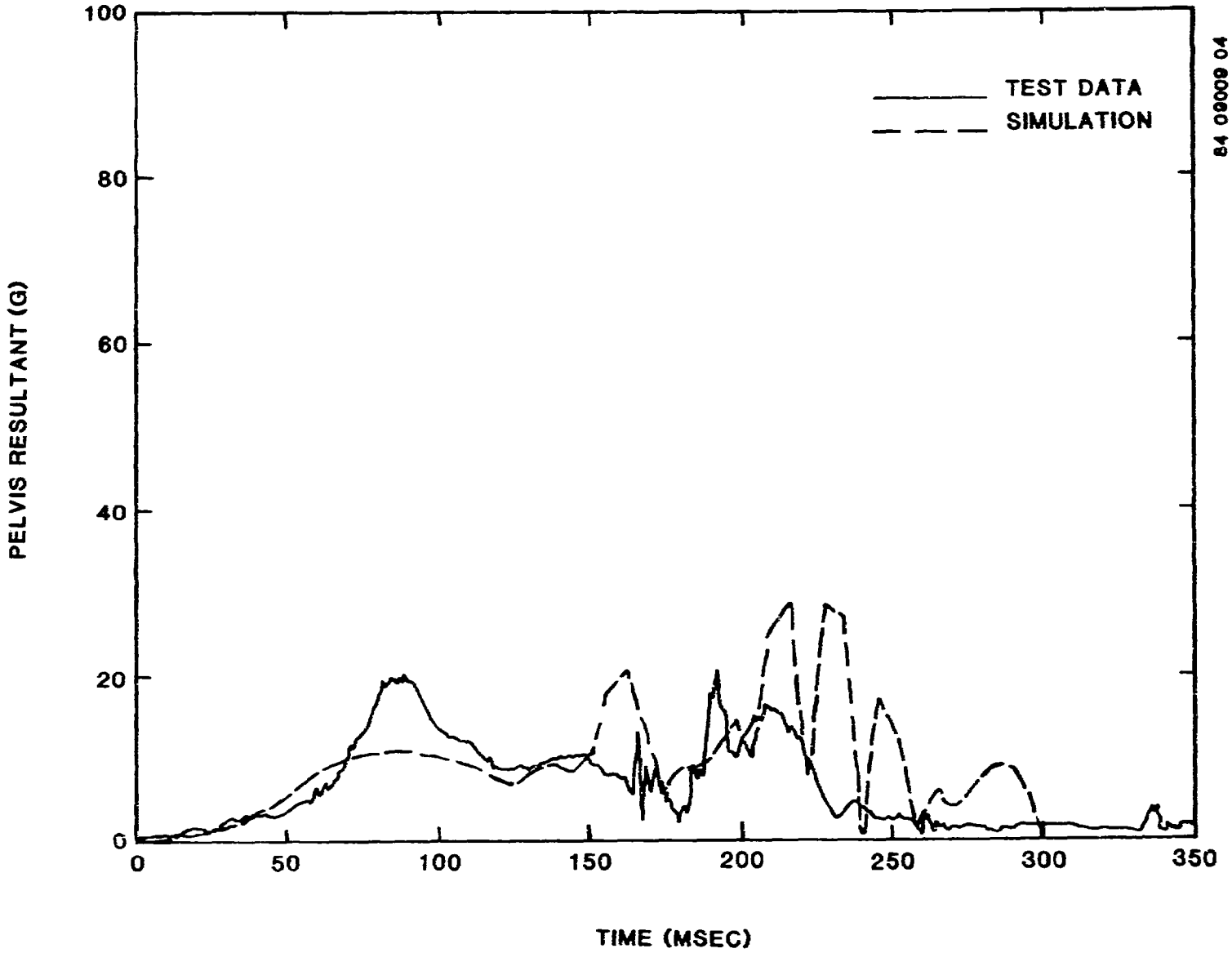

Figure 49. Modified transport aircraft seat, CAMI Test A83-085, pelvic (resultant) acceleration.

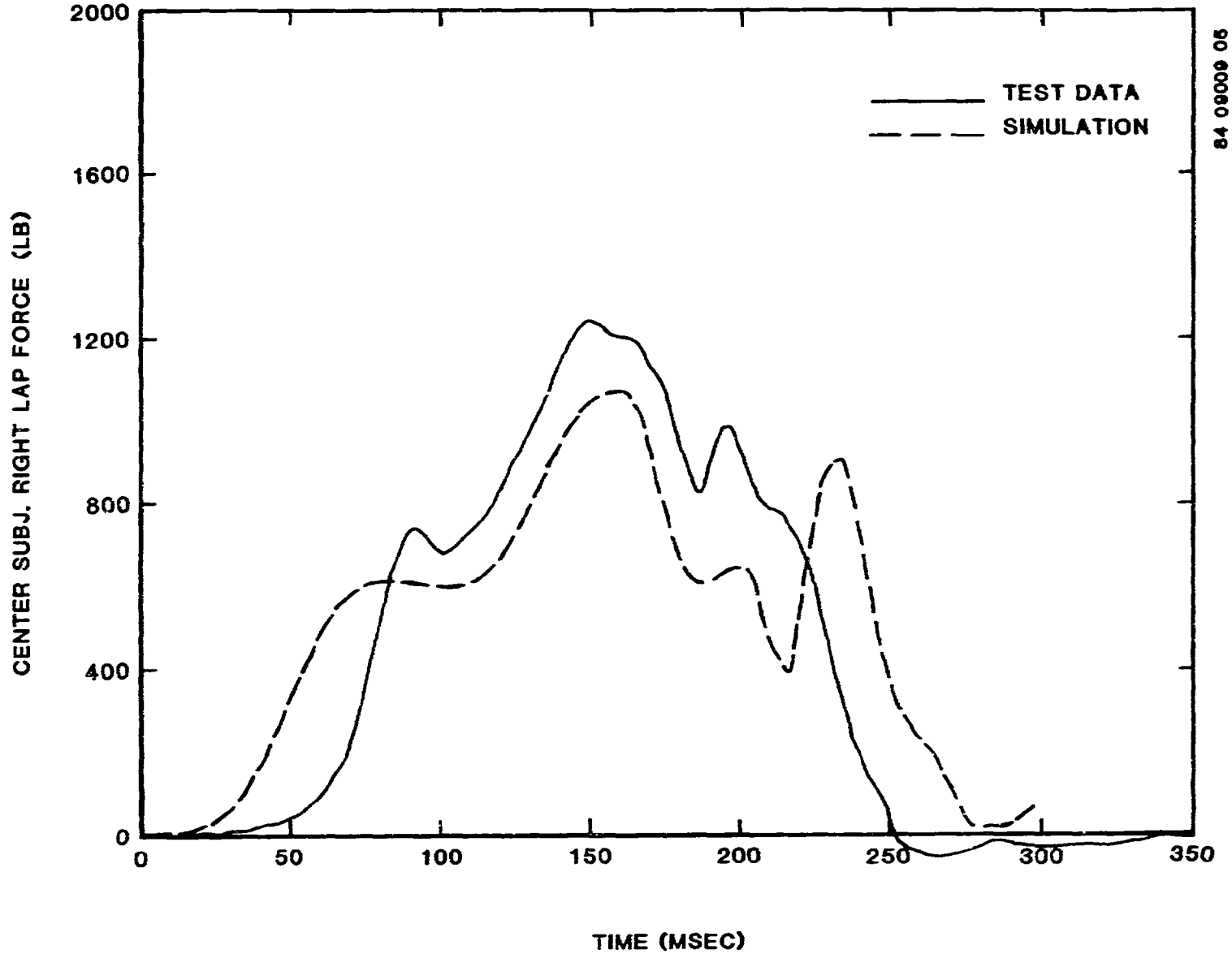

Figure 50. Modified transport aircraft seat, CAMI Test A83-085, center occupant right lap belt load.

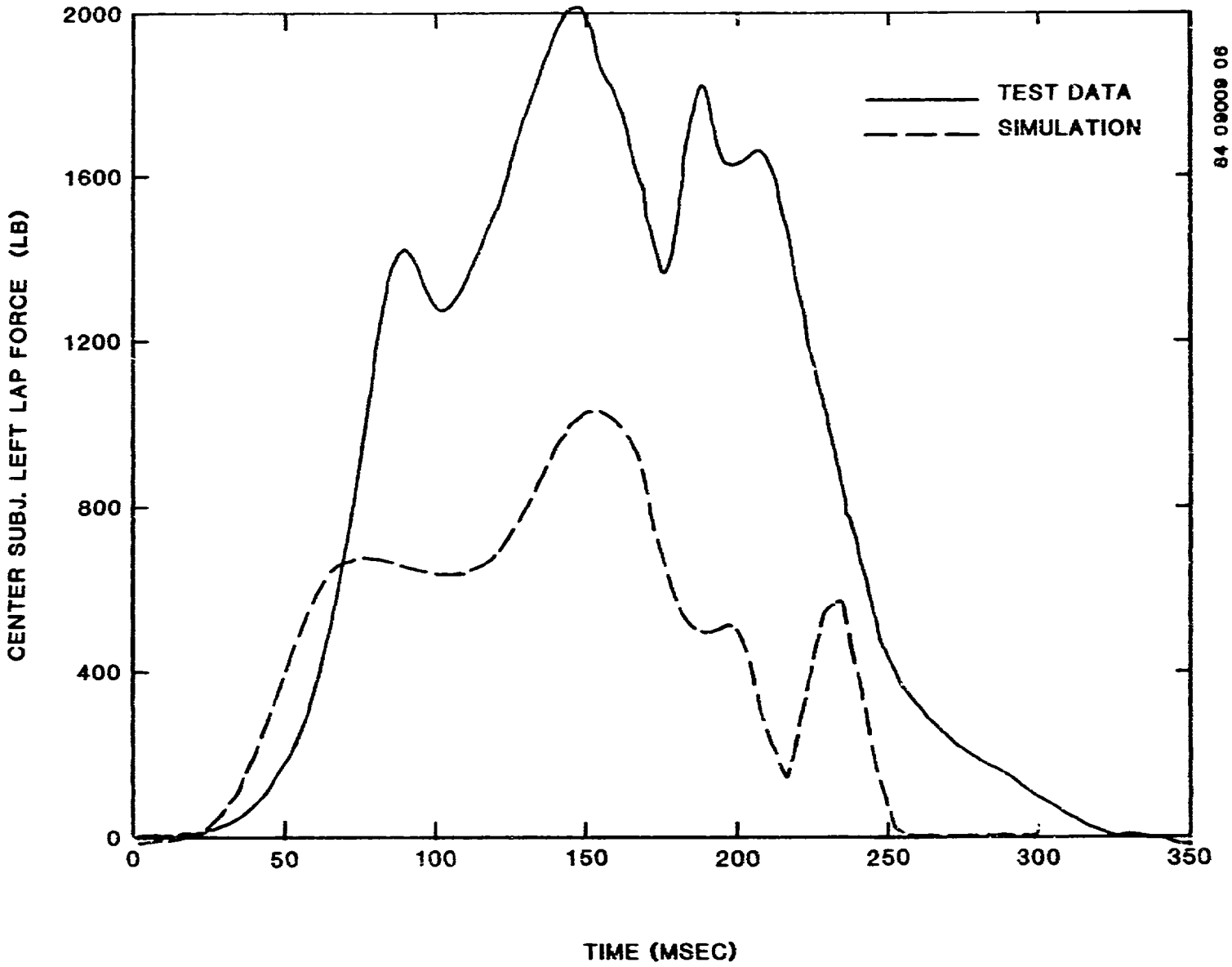

Figure 51. Modified transport aircraft seat, CAMI Test A83-085, center occupant left lap belt load.

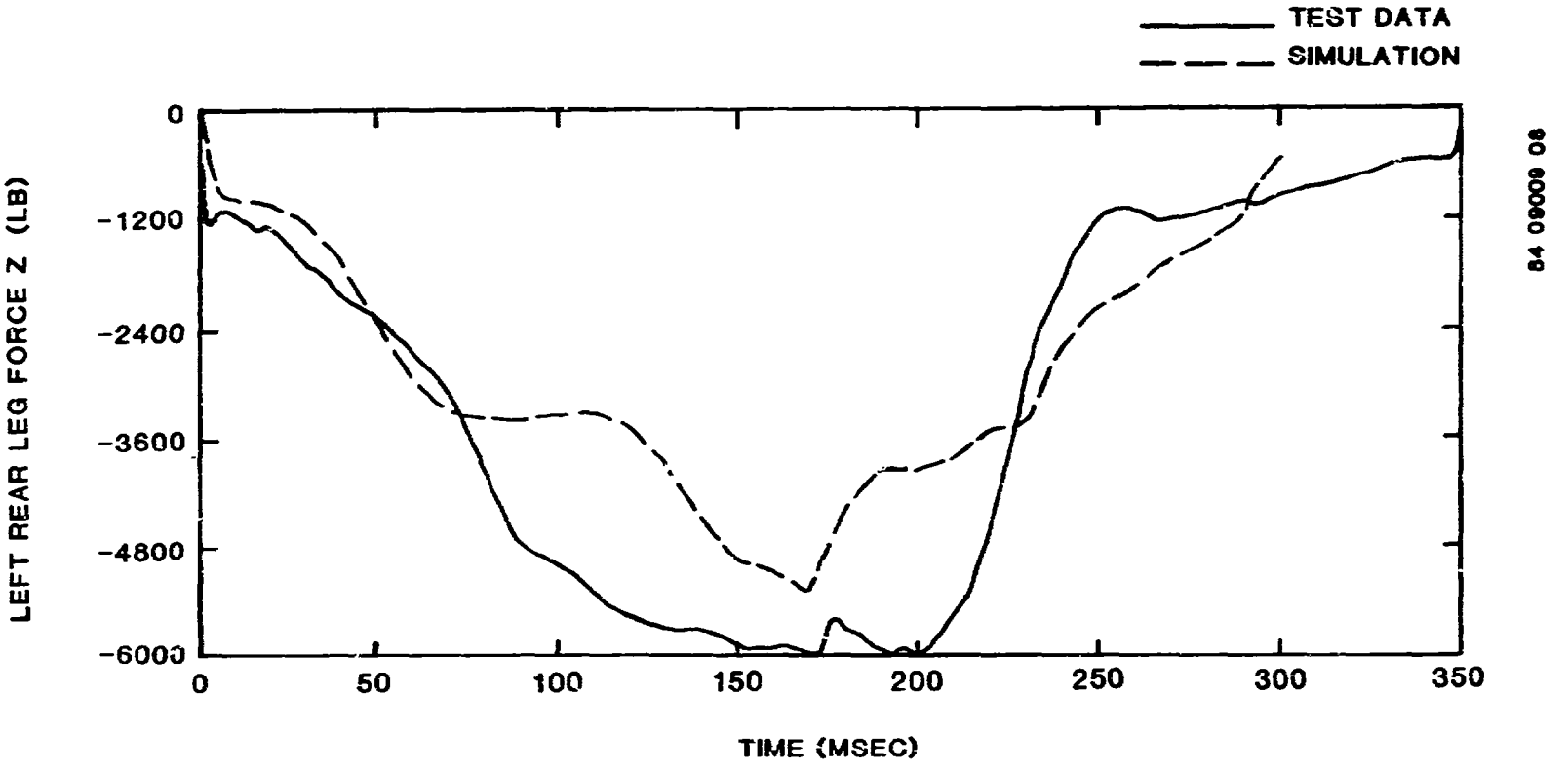

Figure 52. Modified transport aircraft seat, CAMI Test A83-085, left (underside) rear leg vertical reaction.

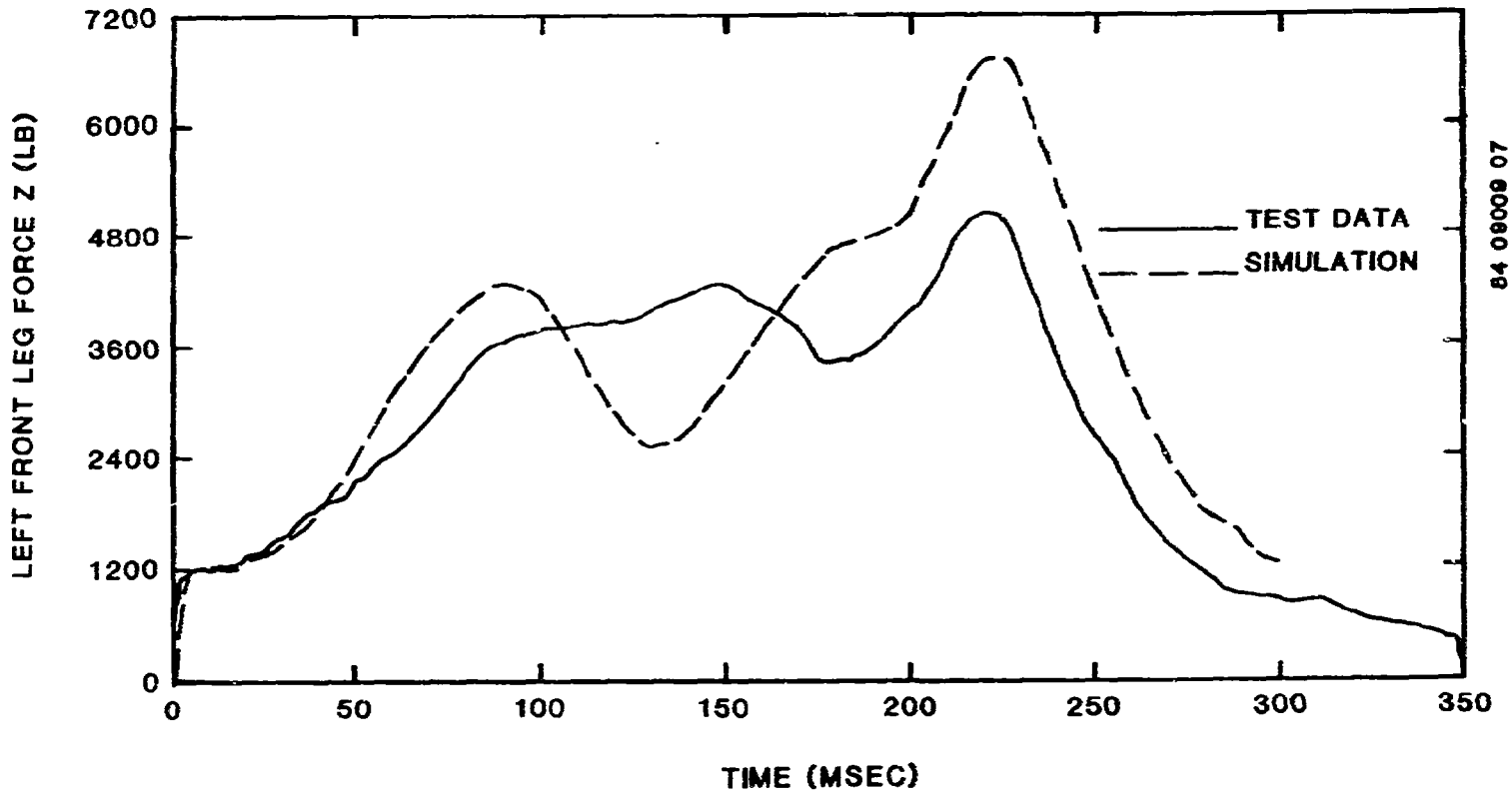

Figure 53. Modified transport aircraft seat, CAMI Test A83-085, left (underside) front leg vertical reaction.

6.0 CONCLUSIONS

The Seat/Occupant Model - Transport Aircraft (Program SOM-TA) provides a method for analyzing the performance of a seat and occupant in an aircraft crash environment. For preliminary analyses where details of the seat structure are not known, a rigid seat can be used. Otherwise, finite element modeling capability is available to model the seat structure in greater detail.

7.0 REFERENCES

1. Laananen, D. H., "Aircraft Crash Survival Design Guide, Volume II, Aircraft Crash Environment and Human Tolerance," Simula Inc.; USARTL Technical Report 79-22B, Applied Technology Laboratory, U.S. Army Research and Technology Laboratories (AVRADCOM), Fort Eustis, Virginia, January 1980.

2. Bartz, J. A., "Development and Validation of a Computer Simulation of a Crash Victim of Three Dimensions," Proceedings of the Sixteenth Stapp Car Crash Conference, Society of Automotive Engineers, New York, 1972, pp. 105-127.

3. Huston, R. L., Hessel, R., and Passerello, C., "A Three-Dimensional Vehicle-Man Model for Collision and High Acceleration Studies," SAE Paper No. 740275, Society of Automotive Engineers, 1974.

4. Robbins, D. H., Bennett, R. O., and Bowman, B. M., "User-Oriented Mathematical Crash Victim Simulator," Proceedings of the Sixteenth Stapp Car Crash Conference, Society of Automotive Engineers, New York, 1972, pp. 128-148.

5. Young, R. D., "A Three-Dimensional Mathematical Model of an Automobile Passenger," Texas Transportation Institute, College Station, Texas, Research Report 140-2, 1970.

6. Laananen, D. H., Coltman, J. W., and Bolukbasi, A. O., Computer Simulation of an Aircraft Seat and Occupant in a Crash Environment, Volume II - Program SOM-LA User Manual, Simula Inc. Tempe, Arizona; DOT/FAA/CT-82/33-II, Federal Aviation Administration, Atlantic City Airport, New Jersey, September 1982.

7. McConville, J. T., and Laubach, L. L., "Anthropometry," Anthropometric Source Book, Volume I: Anthropometry for Designers, Chapter III, NASA Reference Publication 1024, NASA Science and Technical Information Office, Houston, Texas, July 1978.

8. Chandler, R. F., and Young, J., "Uniform Mass Distribution Properties and Body Size Appropriate for the 50 Percentile Male Aircrewmember During 1980-1990," Civil Aeromedical Institute, Protection and Survival Laboratory, Memorandum Report No. AAC-119-81-4 (draft), Federal Aviation Administration, Mike Monroney Aeronautical Center, Oklahoma City, March 1981.

9. Hubbard, R. P., and McLeod, D. G., "Geometric, Inertial and Joint Characteristics of Two Part 572 Dummies for Occupant Modeling," Proceedings of the Twenty-First Stapp Car Crash Conference, SAE P-73, Society of Automotive Engineers, Inc., Warrendale, Pennsylvania, 1977, pp. 933-71.

10. Dempster, W. T., "Space Requirements of the Seated Operator," Wright Air Development Center Technical Report 55-159, Wright-Patterson Air Force Base, Ohio, July 1955.

11. Glanville, A. D., and Kreezer, G. "The Maximum Amplitude and Velocity of Joint Movements in Normal Male Human Adults," Human Biology, Vol. 9, 1937, pp. 197-211.

12. Yeung, K. S., and Welch, R. E., "Refinement of Finite Element Analysis of Automotive Structures Under Crash Loading," IIT Research Institute, Chicago, Illinois, Report No. DOT-HS-803-466, U.S. Department of Transportation, Washington, D.C., October 1977.

13. Meek, J. L., Matrix Structural Analysis, McGraw-Hill, 1971.

14. Hartzman, M., and Hutchinson, J. R., Nonlinear Dynamics of Solids by the Finite Element Method, Computers and Structures, Vol. 2, Pergamon Press, 1972, pp 47-77.

15. Pirotin, S. D., and East, G. H., "Large Deflection, Elastic-Plastic Response of Piping: Experiment, Analysis and Application," Paper F3/1, 4th SMIRT Conference, San Francisco, California, August 1977.

16. Spunt, L., Optimum Structural Design, Prentice-Hall, 1971.

17. Gadd, C. W., "Criteria for Injury Potential," Impact Acceleration Stress, Publication 977, NAS-NRC| 1962. pp. 141-45.

18. Gadd, C. W., "Use of a Weighted-Impulse Criterion for Estimating Injury Hazard," Proceedings of the Tenth Stapp Car Crash Conference, Society of Automotive Engineers, New York, 1966.

19. Gadd, C. W., "Tolerable Severity Index in Whole-Head Nonmechanical Impact," Proceedings of the Fifteenth Stapp Car Crash Conference, Society of Automotive Engineers, New York, 1971.

20. Mertz, H. J., and Patrick, L. M., "Strength and Response of the Human Neck," Proceedings of the Fifteenth Stapp Car Crash Conference, Society of Automotive Engineers, New York, 1971, pp. 207-55.

21. Mertz, H. J., and Patrick, L. M., "Investigation of the Kinematics and Kinetics of Whiplash," Proceedings of the Eleventh Stapp Car Crash Conference, Society of Automotive Engineers, New York, 1967.

22. Brinkley, J. W., "Development of Aerospace Escape Systems," Air University Review, Vol. XIX, July-August 1968, pp. 34-49.

23. Patrick, L. M., Kroell, C. K., and Mertz, H. J., Jr., "Forces on the Human Body in Simulated Crashes," Proceedings of the Ninth Stapp Car Crash Conference, Society of Automotive Engineers, New York, 1965.

24. Patrick, L. M., Mertz, H. J., Jr., and Kroell, C. K., "Cadaver Knee, Chest and Head Impact Loads," Proceedings of the Eleventh Stapp Car Crash Conference, Society of Automotive Engineers, New York, 1967.

25. Viano, D. C. and Khalil, T. B., "Investigation of Impact Response and Fracture of the Human Femur by Finite Element Modeling," SAE Paper No. 760773, Publication SP-142, Society of Automotive Engineers, Warrendale, Pennsylvania, 1976.

APPENDIX A

OCCUPANT SEGMENT POSITION:

THREE-DIMENSIONAL MODEL

Referring to figure A-1, and using $\bar{\rho}_n = L_n - \rho_n$ the absolute position of the mass center of each body segment is given below. The elements of the transformation matrices $[T^n]$ are functions of the generalized coordinates, as given by equations (6), (9), and (10).

Segment 1:

(X_1, Y_1, Z_1), the coordinates of the reference point on the body are the generalized coordinates (q_1, q_2, q_3).

Segment 2:

$$\begin{Bmatrix} X_2 \\ Y_2 \\ Z_2 \end{Bmatrix} = \begin{Bmatrix} X_1 \\ Y_1 \\ Z_1 \end{Bmatrix} + \begin{bmatrix} T^1 \end{bmatrix} \begin{Bmatrix} 0 \\ 0 \\ \bar{\rho}_1 \end{Bmatrix} + \begin{bmatrix} T^2 \end{bmatrix} \begin{Bmatrix} 0 \\ 0 \\ \rho_2 \end{Bmatrix}$$

Segment 3:

$$\begin{Bmatrix} X_3 \\ Y_3 \\ Z_3 \end{Bmatrix} = \begin{Bmatrix} X_1 \\ Y_1 \\ Z_1 \end{Bmatrix} + \begin{bmatrix} T^1 \end{bmatrix} \begin{Bmatrix} 0 \\ 0 \\ \bar{\rho}_1 \end{Bmatrix} + \begin{bmatrix} T^2 \end{bmatrix} \begin{Bmatrix} 0 \\ 0 \\ L_2 \end{Bmatrix} + \begin{bmatrix} T^{12} \end{bmatrix} \begin{Bmatrix} 0 \\ 0 \\ L_{12} \end{Bmatrix} + \begin{bmatrix} T^3 \end{bmatrix} \begin{Bmatrix} e_3 \\ 0 \\ \rho_3 \end{Bmatrix}$$

Segment 4:

$$\begin{Bmatrix} X_4 \\ Y_4 \\ Z_4 \end{Bmatrix} = \begin{Bmatrix} X_1 \\ Y_1 \\ Z_1 \end{Bmatrix} + \begin{bmatrix} T^1 \end{bmatrix} \begin{Bmatrix} 0 \\ 0 \\ \bar{\rho}_1 \end{Bmatrix} + \begin{bmatrix} T^2 \end{bmatrix} \begin{Bmatrix} 0 \\ -L_S \\ L_2 \end{Bmatrix} + \begin{bmatrix} T^4 \end{bmatrix} \begin{Bmatrix} 0 \\ 0 \\ -\rho_4 \end{Bmatrix}$$

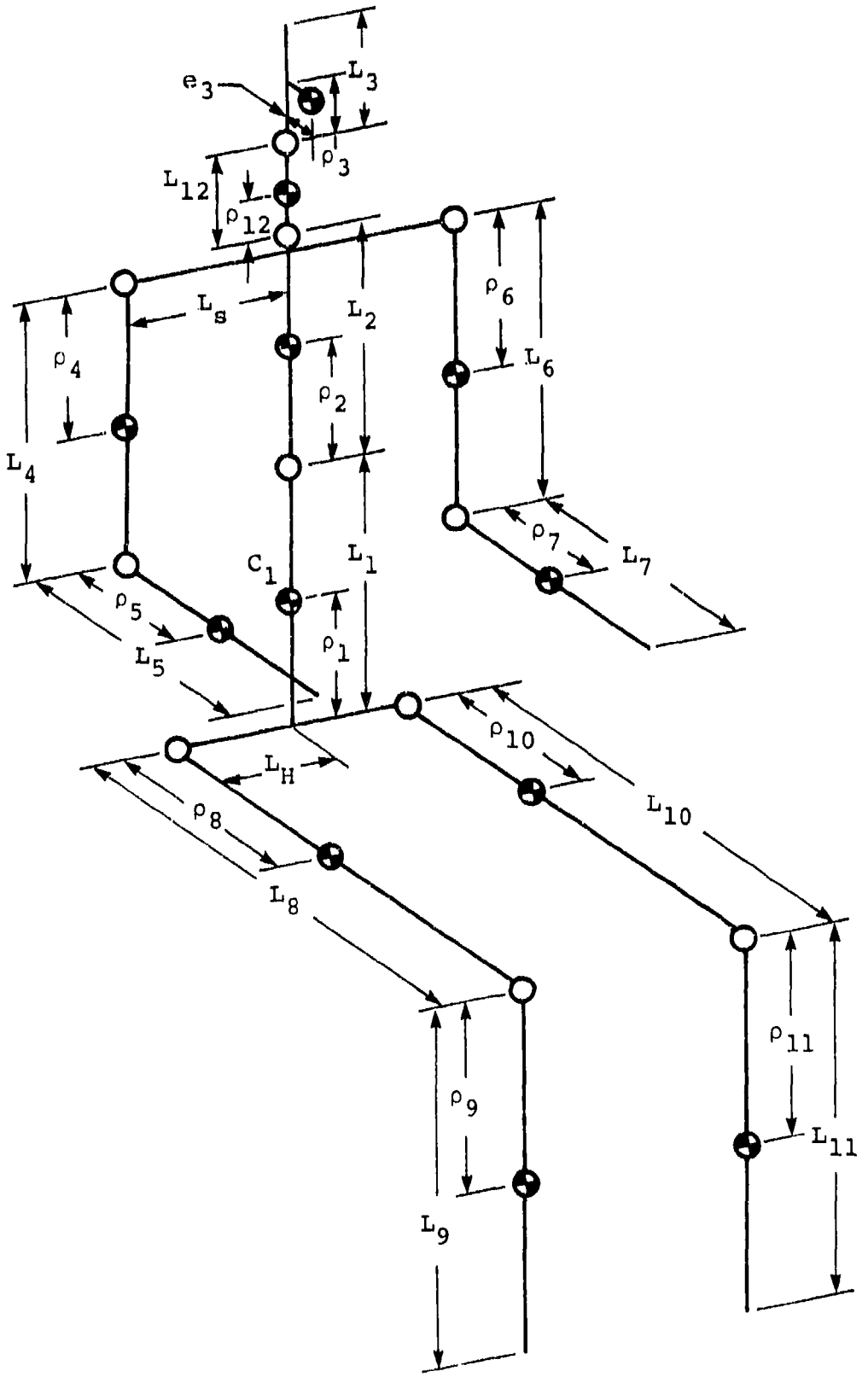

Figure A-1. Body segment lengths and mass center locations for three-dimensional model.

Segment 5:

$$\begin{Bmatrix} X_5 \\ Y_5 \\ Z_5 \end{Bmatrix} = \begin{Bmatrix} X_1 \\ Y_1 \\ Z_1 \end{Bmatrix} + \begin{bmatrix} T^1 \end{bmatrix} \begin{Bmatrix} 0 \\ 0 \\ \bar{\rho}_1 \end{Bmatrix} + \begin{bmatrix} T^2 \end{bmatrix} \begin{Bmatrix} 0 \\ -L_s \\ L_2 \end{Bmatrix} + \begin{bmatrix} T^4 \end{bmatrix} \begin{Bmatrix} 0 \\ 0 \\ -L_4 \end{Bmatrix} + \begin{bmatrix} T^5 \end{bmatrix} \begin{Bmatrix} \rho_5 \\ 0 \\ 0 \end{Bmatrix}$$

Segment 6:

$$\begin{Bmatrix} X_6 \\ Y_6 \\ Z_6 \end{Bmatrix} = \begin{Bmatrix} X_1 \\ Y_1 \\ Z_1 \end{Bmatrix} + \begin{bmatrix} T^1 \end{bmatrix} \begin{Bmatrix} 0 \\ 0 \\ \bar{\rho}_1 \end{Bmatrix} + \begin{bmatrix} T^2 \end{bmatrix} \begin{Bmatrix} 0 \\ -L_s \\ L_2 \end{Bmatrix} + \begin{bmatrix} T^6 \end{bmatrix} \begin{Bmatrix} 0 \\ 0 \\ -\rho_6 \end{Bmatrix}$$

Segment 7:

$$\begin{Bmatrix} X_7 \\ Y_7 \\ Z_7 \end{Bmatrix} = \begin{Bmatrix} X_1 \\ Y_1 \\ Z_1 \end{Bmatrix} + \begin{bmatrix} T^1 \end{bmatrix} \begin{Bmatrix} 0 \\ 0 \\ \bar{\rho}_1 \end{Bmatrix} + \begin{bmatrix} T^2 \end{bmatrix} \begin{Bmatrix} 0 \\ L_s \\ L_2 \end{Bmatrix} + \begin{bmatrix} T^6 \end{bmatrix} \begin{Bmatrix} 0 \\ 0 \\ -L_6 \end{Bmatrix} + \begin{bmatrix} T^7 \end{bmatrix} \begin{Bmatrix} \rho_7 \\ 0 \\ 0 \end{Bmatrix}$$

Segment 8:

$$\begin{Bmatrix} X_8 \\ Y_8 \\ Z_8 \end{Bmatrix} = \begin{Bmatrix} X_1 \\ Y_1 \\ Z_1 \end{Bmatrix} + \begin{bmatrix} T^1 \end{bmatrix} \begin{Bmatrix} 0 \\ -L_H \\ -\rho_1 \end{Bmatrix} + \begin{bmatrix} T^8 \end{bmatrix} \begin{Bmatrix} \rho_8 \\ 0 \\ 0 \end{Bmatrix}$$

Segment 9:

$$\begin{Bmatrix} X_9 \\ Y_9 \\ Z_9 \end{Bmatrix} = \begin{Bmatrix} X_1 \\ Y_1 \\ Z_1 \end{Bmatrix} + \begin{bmatrix} T^1 \end{bmatrix} \begin{Bmatrix} 0 \\ -L_H \\ -\rho_1 \end{Bmatrix} + \begin{bmatrix} T^8 \end{bmatrix} \begin{Bmatrix} L_8 \\ 0 \\ 0 \end{Bmatrix} + \begin{bmatrix} T^9 \end{bmatrix} \begin{Bmatrix} 0 \\ 0 \\ -\rho_9 \end{Bmatrix}$$

Segment 10:

$$\begin{Bmatrix} X_{10} \\ Y_{10} \\ Z_{10} \end{Bmatrix} = \begin{Bmatrix} X_1 \\ Y_1 \\ Z_1 \end{Bmatrix} + \begin{bmatrix} T^1 \end{bmatrix} \begin{Bmatrix} 0 \\ L_H \\ -\rho_1 \end{Bmatrix} + \begin{bmatrix} T^{10} \end{bmatrix} \begin{Bmatrix} \rho_{10} \\ 0 \\ 0 \end{Bmatrix}$$

Segment 11:

$$\begin{Bmatrix} X_{11} \\ Y_{11} \\ Z_{11} \end{Bmatrix} = \begin{Bmatrix} X_1 \\ Y_1 \\ Z_1 \end{Bmatrix} + \begin{bmatrix} T^1 \end{bmatrix} \begin{Bmatrix} 0 \\ L_H \\ -\rho_1 \end{Bmatrix} + \begin{bmatrix} T^{10} \end{bmatrix} \begin{Bmatrix} L_{10} \\ 0 \\ 0 \end{Bmatrix} + \begin{bmatrix} T^{11} \end{bmatrix} \begin{Bmatrix} 0 \\ 0 \\ -\rho_{11} \end{Bmatrix}$$

Segment 12:

$$\begin{Bmatrix} X_{12} \\ Y_{12} \\ Z_{12} \end{Bmatrix} = \begin{Bmatrix} X_1 \\ Y_1 \\ Z_1 \end{Bmatrix} + \begin{bmatrix} T^1 \end{bmatrix} \begin{Bmatrix} 0 \\ 0 \\ \overline{\rho}_1 \end{Bmatrix} + \begin{bmatrix} T^2 \end{bmatrix} \begin{Bmatrix} 0 \\ 0 \\ L_2 \end{Bmatrix} + \begin{bmatrix} T^{12} \end{bmatrix} \begin{Bmatrix} 0 \\ 0 \\ \rho_{12} \end{Bmatrix}$$

APPENDIX B

OCCUPANT SEGMENT POSITION: TWO-DIMENSIONAL MODEL

Referring to figure 6, the absolute position of the mass center of each body segment is given below. L_S and L_H are the lateral distances from the mid-saggital plane to the shoulder and hip joints, respectively.

Segment 1:

(X_1, Y_1, Z_1), the coordinates of the reference point on the body. X_1 and Z_1 are the generalized coordinates q_1 and q_2.

Segment 2:

$$X_2 = X_1 - e_1 \cos \theta_1 + \frac{S (\cos \theta_1 - \cos \theta_2)}{\theta_2 - \theta_1} + e_2 \cos \theta_2$$

$$Y_2 = Y_1$$

$$Z_2 = Z_1 + e_1 \sin \theta_1 + \frac{S (\sin \theta_2 - \sin \theta_1)}{\theta_2 - \theta_1} - e_2 \sin \theta_2$$

Segment 3:

$$X_3 = X_1 - e_1 \cos \theta_1 + \frac{S (\cos \theta_1 - \cos \theta_2)}{\theta_2 - \theta_1} + \rho_2 \sin \theta_2$$

$$+ \frac{\rho_3(\cos \theta_2 - \cos \theta_3)}{\theta_3 - \theta_2} + e_3 \cos \theta_3$$

$$Y_3 = Y_1$$

$$Z_3 = Z_1 + e_1 \sin \theta_1 + \frac{S (\sin \theta_2 - \sin \theta_1)}{\theta_2 - \theta_1} + \rho_2 \cos \theta_2$$

$$+ \frac{\rho_3(\sin \theta_3 - \sin \theta_2)}{\theta_3 - \theta_2} - e_3 \sin \theta_3$$

Segment 4:

$$X_4 = X_1 - e_1 \cos\theta_1 + \frac{S(\cos\theta_1 - \cos\theta_2)}{\theta_2 - \theta_1} + \rho_2 \sin\theta_2 - \rho_4 \sin\theta_4$$

$$Y_4 = Y_1 - L_s$$

$$Z_4 = Z_1 + e_1 \sin\theta_1 + \frac{S(\sin\theta_2 - \sin\theta_1)}{\theta_2 - \theta_1} + \rho_2 \cos\theta_2 - \rho_4 \cos\theta_4$$

Segment 5:

$$X_5 = X_1 - e_1 \cos\theta_1 + \frac{S(\cos\theta_1 - \cos\theta_2)}{\theta_2 - \theta_1} + \rho_2 \sin\theta_2$$

$$- L_4 \sin\theta_4 + \rho_5 \cos\theta_5$$

$$Y_5 = Y_1 - L_s$$

$$Z_5 = Z_1 + e_1 \sin\theta_1 + \frac{S(\sin\theta_2 - \sin\theta_1)}{\theta_2 - \theta_1} + \rho_2 \cos\theta_2$$

$$- L_4 \cos\theta_4 - \rho_5 \sin\theta_5$$

Segment 6:

$$X_6 = X_4$$
$$Y_6 = Y_1 + L_s$$
$$Z_6 = Z_4$$

Segment 7:

$$X_7 = X_5$$
$$Y_7 = Y_1 + L_s$$
$$Z_7 = Z_5$$

Segment 8:

$$X_8 = X_1 - \rho_1 \sin \theta_1 + \rho_8 \cos \theta_8$$
$$Y_8 = Y_1 - L_H$$
$$Z_8 = Z_1 - \rho_1 \cos \theta_1 - \rho_8 \sin \theta_8$$

Segment 9:

$$X_9 = X_1 - \rho_1 \sin \theta_1 + L_8 \cos \theta_8 - \rho_9 \sin \theta_9$$
$$Y_9 = Y_1 - L_H$$
$$Z_9 = Z_1 - \rho_1 \cos \theta_1 - L_8 \sin \theta_8 - \rho_9 \cos \theta_9$$

Segment 10:

$$X_{10} = X_8$$
$$Y_{10} = Y_1 + L_H$$
$$Z_{10} = Z_8$$

Segment 11:

$$X_{11} = X_9$$
$$Y_{11} = Y_1 + L_H$$
$$Z_{11} = Z_9$$

APPENDIX C

DISTRIBUTION LIST

Civil Aviation Authority (5)
Aviation House
129 Kingsway
London WC2B 6NN England

DOT-FAA AEU-500 (5)
American Embassy
APO New York, NY 09667

Embassy of Australia (1)
Civil Air Attache
1601 Mass. Ave. NW
Washington, DC 20036

University of California (1)
Service Dept Institute of
Transportation Standard Lib
412 McLaughlin Hall
Berkely, CA 94720

Scientific & Tech. Info FAC (1)
ATTN: NASA Rep.
P.O. Box 8757 BWI Airport
Baltimore, MD 21240

British Embassy (1)
Civil Air Attache ATS
3100 Mass Ave. NW
Washington, DC 20008

Northwestern University (1)
Trisnet Repository
Transportation Center Library
Evanston, ILL 60201

Director DuCentre Exp DE LA (1)
Navigation Aerineene
9141 Orly, France

ANE-40	(2)	ACT-624	(2)	ASW-53B	(2)
ASW-52C4	(2)	AAL-62	(2)	AAC-44.4	(2)
APM-13 Nigro	(2)	M-493.2 Bldg. 10A	(5)	ACE-66	(2)
AEA-66.1	(3)			ADL-1	(1)
ADL-32 North	(1)	APM-1	(1)	ALG-300	(1)
AES-3	(1)	APA-300	(1)	ACT-8	(1)
ANM-60	(2)	AGL-60	(2)		

FAA, Chief, Civil Aviation Assistance Group (1)
Madrid, Spain
c/o American Embassy
APO New York 09285-0001

Al Astorga (1)
Federal Aviation
Administration (CAAG)
American Embassy, Box 38
APO New York 09285-0001

Dick Tobiason (1)
ATA of America
1709 New York Avenue, NW
Washington, DC 20006

Government Activities

FAA, Washington, DC 20591
(Attn: Harold W. Becker, ASF-300;
Thomas McSweeny, AWS-100) (2)

FAA, 4344 Donald Douglas Drive,
Long Beach, CA 90808
(Attn: Stephen Soltis, ANW-102N) (1)

FAA, Central Region Headquarters,
601 East 12th Street, Federal Building,
Kansas City, Missouri, 64106
(Attn: Earsa Tunkesley, ACE-100) (1)

FAA, Southwest Region Headquarters,
4400 Blue Mound Road,
P.O. Box 1689
Fort Worth, Texas 76101
(Attn:: John Shapley, ASW-110) (1)

FAA, Northwest Mountain Region
Headquarters,
17900 Pacific Highway South, C-68966,
Seattle, Washington 98168
(Attn: Steven Wallace, ANW-110) (1)

FAA, Mike Monroney Aeronautical Center,
P.O. Box 25082,
Oaklonoma City, OK 73125
(Attn: Richard Chandler, AAM-119) (1)

NASA, Langley Research Center,
Hampton, VA 23365
(Attn: Emilio Alfaro-Bou, MA-495;
Huey Cardin, MS-495) (2)

U.S. Army Aviation Applics Technology
Directorate, USAARTA, (AVSCOM),
Fort Eustis, VA 23604
(Attn: Roy Burrows, Code SAVRT-TY-ASV) (2)

U.S. Navy Naval Air Development Center,
Warminister, PA 18974
(Attn: Leon Domzalski, Code 60322) (1)

NTSB, 800 Independence Ave. S.E.,
Washington, DC 20594
(Attn: John C. Clark, TE 60) (1)

Non-Government Activities

Beech Aircraft Corp.,
P.O. Box 85,
Wichita, KS 67201
(Attn: Dayton L. Hartley;
James E. Terry; William Schultz) (3)

Bell Helicopter Co.,
P.O. Box 482,
Fort Worth, TX 76101
(Attn: James Cronkite, Dept. 81,
MS 11; Roy G. Fox) (2)

Boeing Airplane Co.,
P.O. Box 3707,
Seattle, WA 98124
(Attn: Edward Widmayer, MC-9W-22) (1)

Boeing Co., Vertol Division,
P.O. Box 16858,
Philadelphia, PA 91942
(Attn: Denise Vassilakos, MS P30-27) (1)

Cessna Aircraft Co.,
P.O. Box 7704,
Wichita, KS 67277
(Attn: John Berwick; Robert Held;
Richard Soloski) (3)

Fairchild Aircraft Corp.,
P.O. Box 3246,
San Antonio, TX 78284
(Attn: Walt Dwyer) (1)

General Dynamics/Convair,
P.O. Box 80847,
San Diego, CA 92138
(Attn: L. Mastay, MA 80-6030) (1)

Grumman Aerospace Corp.,
So. Oyster Bay Road,, Bethpage,
L.I., NY 11714
(Attn: Robert Winter, A08-35;
Allan B. Difko, A08-35) (2)

Gulfstream Aerospace Corp.,
P.O. Box 2206,
Savannah, GA 31402
(Attn: George Westphal) (1)

Non-Government Activities (Continued)

Gulfstream Aerospace Corp.,
P.O. Box 22500,
Oklhoma City, OK 73123
(Attn: Richard Southard) (1)

Lockheed-California Co.,
Burbank, CA 91503
(Attn: Gil Wittlin, D 76-12,
B 63G, PLT A-1) (1)

McDonnell Douglas Corp.,
3855 Lakewood Drive,
Long Beach, CA 90846
(Attn: J. Webster;
John L. Galligher) (2)

McDonnell Douglas Helicopter,
4645 S. Ash Ave.,
Tempe, AZ 85182
(Attn: Lyndon Landborne;
J.K. Sen) (2)

Piper Aircraft Corp.,
2925 Piper Drive,
Vero Beach, FL 32960
(Attn: Marion Dees) (1)

Sikorsky Aircraft,
North Maint Street,
Stratford, CT 06601
(Attn: Brain Cornell, MS 5207A;
Pramonik Mukunda, MS 5207A) (2)

☆ U.S. COVERNMENT PRINTING OFFICE:1986-705-122